DESIGN OPTIMIZATION FOR AN ACTIVE IN-CORE NUCLEAR HEAT CALORIMETER: A PARAMETRIC STUDY

A Thesis

Submitted to the Graduate Faculty of the
Louisiana State University and
Agricultural and Mechanical College
in partial fulfillment of the
requirements for the degree of
Master of Science

in

The Department of Nuclear Engineering

by

Paul Nelson English
B.S., Louisiana State University, 1972
August, 1977

Dedicated to my wife, Leslie,
my daughter, Elayne,
my child to be, and Mom

ACKNOWLEDGMENTS

In the normal course of events leading to the successful completion of a degree program there are many persons who teach, support, guide, push, prod, prompt, humor and cajole the candidate as he pursues his goal. At this time, I would like to acknowledge and thank those individuals who aided me as I plodded along my way.

My thanks to my wife for her support and inexhaustible patience.

I would like to thank my parents for instilling within me the motivation and desire to achieve.

I would like to express my sincere gratitude to Dr. Robert C. McIlhenny for being my stellar protagonist. He inspired me in the classroom and had faith in me when others did not.

I would like to thank Dr. Frank A. Iddings for the wealth of knowledge imparted to me within the formal classroom and without. Special thanks for teaching me to work "within" the system.

I was fortunate to have not one, but three excellent advisors for my thesis research. Special recognition is due each of them. Sincere thanks to Dr. C. C. Price of Argonne National Laboratory. Dr. Price supplied the basic thesis problem and intelligently guided the major portion of my research. I appreciate his amazingly vast knowledge of many subjects, his assistance, his willingness, and his patience.

Sincere thanks to Dr. John C. Courtney for his role as committee chairman, his industrious imparting of knowledge in the classroom, and his assistance in preparing the thesis manuscript.

To my remaining co-advisor, Dr. Ozer Arnas, I offer sincere thanks for assistance in the performance of my research and preparation of this thesis. More importantly however, I wish to thank Dr. Arnas for what he did for me in the classroom. Dr. Arnas is the finest and most inspiring instructor I have had the pleasure of studying under.

I am deeply indebted to Dr. Howard A. Larson of Argonne National Laboratory for his assistance in numerical analysis and other areas of mathematical information. Unfortunately for me, I did not have the opportunity to study under Dr. Larson in the formal classroom....; he is, I think, another of the ultimate pedagogues.

A special thanks to Mrs. Priscilla Milligan for the typing and retyping of the thesis manuscript.

In conclusion I would like to thank Gene Pool. Without Genes' contribution this thesis would not be what it is.

TABLE OF CONTENTS

LIST OF TABLES (CONTINUED)

LIST OF FIGURES

LIST OF FIGURES (CONTINUED)

ABSTRACT

To characterize the EBR-II system as an irradiation facility, there are many parameters which must be identified and quantified. One such parameter is the nuclear heating rate as it occurs in structural materials. The nuclear heating rate in structural materials is induced by the interaction of components of the reactor radiation environment, with the atomic environment of structural materials within the core.

The focus of this work is the optimization of a design for an active nuclear heat calorimeter, the use of which will provide a more accurate measurement of the nuclear heating rate. Ideally, such an active calorimeter will serve as a bench mark and calibration device for passive nuclear heat calorimeters. Scoping work has been done for in-core calorimetry from which basic design criteria have been established and evaluated. These criteria and the results of early scoping studies have led to the basic design choice which emphasizes axial conduction heat transfer.

The analysis of this study consists of a parametric study to evaluate certain proposed calorimeter concepts. The proposed calorimeter configurations are mathematically modeled and the analysis has resulted in a quantitative evaluation of several points.

First, comparisons are made of the relative ability of a calorimeter, utilizing a susceptor surrounded by a heat shield versus a calorimeter employing a solid susceptor of outer dimensions equal to those of the heat shield, to minimize radiation heat transfer.

Minimization of heat lost by thermal radiation minimizes calorimeter error due to the uncertainty inherent in the characterization of material thermal emissivities.

Second, an analysis is performed to study the effect of different heating rates upon the performance of the potential optimized designs identified in the preceding analysis.

The third and final part of the composite study consists of an error analysis to estimate the accuracy with which the potentially optimized design can measure the in-core nuclear heating rates.

The information gathered and collated from this study results in a fully optimized design to be included in a proposal for an active nuclear heat calorimeter. The proposed calorimeter will be used for core characterization in the EBR-II test facility.

Preface

In the United States today there is an ubiquitous air of public concern for the safety and viability of present and potential energy sources. Nuclear energy in general and nuclear fission in particular is one such source that is undergoing close public scrutiny. With such close apprasial, fastidious attention to design considerations, as pertain to safety of operation and accurate characterization of facility operation, is required for political as well as technical reasons.

The number of different configurations for fission reactor design, while not limitless, is certainly vast. One type of reactor, the breeder, can have an important impact on the economics of power production. The breeder is a reactor in which nuclear transmutations produce more fissile nuclei than are consumed in the fission process. Two main types of breeding cycles are possible, one of which is based upon a fast reactor using plutonium-239 as the fissile species and uranium-238 as the fissionable and fertile species; the other is based upon either thermal or fast reactors utilizing uranium-233 and thorium-232 as the fissile and fissionable-fertile species, respectively. The fissionable-fertile species is employed in the form of a blanket surrounding the core. So in principle, a large portion of the neutrons escaping from the core are captured in the blanket where fissile material is formed. The balanced nuclear reactions for breeding are:

$$^{238}_{92}U + ^{1}_{0}n \rightarrow ^{239}_{92}U + ^{0}_{0}\gamma$$

$$^{239}_{92}U \rightarrow ^{0}_{-1}\beta + ^{239}_{93}Np$$

$$^{239}_{93}Np \rightarrow ^{0}_{-1}\beta + ^{239}_{94}Pu$$

and

$$^{232}_{90}Th + ^{1}_{0}n \rightarrow ^{233}_{90}Th + ^{0}_{0}\gamma$$

$$^{233}_{90}Th \rightarrow ^{0}_{-1}\beta + ^{233}_{91}Pa$$

$$^{233}_{91}Pa \rightarrow ^{0}_{-1}\beta + ^{233}_{92}U$$

In some designs, especially for fast reactors, fertile material is included in the core loading so that fissile nuclei are formed both in the core and in the blanket. The fissile material produced in the core is useful as fuel "in situ" where as that generated in the blanket must be appropriately processed for installation in the core proper as "fuel".

In a fast reactor, no attempt is made to slow down the neutrons before they are captured in the fission process. To the contrary, with the principal objective of such a reactor being the production of Pu-239 from fertile U-238, the aforementioned fissile-fertile scheme is most efficient only in a fast neutron spectrum. This is because fission neutron production is increased with increasing energy of the neutron that causes the fission. Consequently, materials

are selected to minimize the moderation of neutrons. For example, liquid metals can be used for coolant instead of light water.

The only presently operating Liquid Metal Cooled Fast Breeder Reactor (LMFBR) in the United States is the Experimental Breeder Reactor II (EBR-II) located at the Idaho National Engineering Laboratory (INEL) near Idaho Falls, Idaho, and operated by the western branch of Argonne National Laboratories (ANL-W). EBR-II is a liquid metal cooled fast breeder reactor (LMFBR), with its primary coolant being liquid sodium. The liquid metal coolant is a high heat capacity, thermally efficient, heat transport medium which has a low elastic scatter cross section. This promotes the hardened or more energetic spectrum as required along with the proper fuel combination for enhancing the breeding capability. This reactor is a pool type reactor with stainless steel core internals and neutron reflector surrounding the core. The nuclear fuel is typically uranium that is nominally fifty percent enriched in U-235 (pseudo-breeder). The fuel is arranged in a hexagonal array consisting of 637 subassemblies. Each subassembly is a stainless steel clad bundle of fuel pins, with each bundle having passages to permit flow of the liquid metal coolant. The fission process occurs mainly in the driver region at or near the center of the core, while the major portion of breeding occurs in the inner blanket section.

EBR-II has an approximate thermal power rating of 62.5 Mw and an electrical rating of 20 Mw (gross) or 16.5 Mw (net). Initially, the mission of the reactor was to demonstrate high thermal performance, efficient breeding, and the use of prototype components for later

incorporation in central-station power plants. The mission profile of EBR-II has since evolved through stages of fuel irradiation, and coolant flow studies. Its projected mission is as a safety test facility.

Fast reactors have a number of unique characteristics which have bearing upon the interests of the ensuing study. Because of the absence of moderator, the core is generally small and the power density is high. As a consequence, careful design of heat removal systems is mandatory. Special attention must be given to the occurrence of large temperature gradients and their causes. Because of the high concentration of fissile material in a fast reactor core, a compaction promoted by core melting might result in a large increase in reactivity. The designer must take extraordinary precautions to prevent loss of cooling during operation at power, and make suitable arrangements for removal of fission product decay heat when the reactor is shut down. The preceding requirements dictate accurate quantification of the thermal hydraulic environment parameters existent in fast reactor cores.

Introduction

The focus of this work is upon optimization of a design for an active (instrumented) nuclear heat calorimeter, the use of which will provide a more accurate quantification of the nuclear heating rate in structural materials. In particular, the desire is to quantify and strip away the heating components contributed by local activation product betas, inelastic and elastic neutron recoil interactions and be left with the pure gamma heating rate. Ideally, such an active calorimeter will serve as a benchmark and calibration device for passive (uninstrumented) calorimeters. In addition, normalization data can be provided for analytic determinations.

The nuclear heating rate in reactor structural materials is induced by (1) fission fragment recoil; (2) degradation in energy of recoiling nuclei, these nuclei having received their energy in previous neutron interactions, elastic and inelastic scattering; (3) degradation in the energy of traversing beta particles; (4) material interaction with prompt fission gammas, inelastic scattering gammas, radiative capture gammas, and radioactive activation product and fission product decay gammas. Of primary concern to this study is the latter, namely (4), primary and secondary gamma heating interactions in structural materials. Scoping work and analytic analysis have been done for in core calorimetry[1, 2, 3]. An examination of some of this work will be detailed in a later portion of this chapter.

The fission of a single U-235 nucleus (or a similar fissile heavy nucleus) is found to be accompanied by the release of approximately 200-212 MeV of energy[4]. Over 80% of this energy is carried away as kinetic energy of the fission fragments, which produces local heating. The remaining 20 percent is liberated as prompt gamma rays, kinetic energy of the fission neutrons, beta particles, and gamma rays from the radioactive fission products as they decay over a period of time. Eventually this energy appears in the form of heat as the various radiations interact with and are absorbed by matter. The approximate distribution of fission energy is given by Table 1-1.

The heating effects of the gamma rays, both primary and secondary are significant, and as previously indicated are of major concern in reactor design and operation in general, and in fast reactor design and operation in particular. The impetus for this work derives from this concern.

The energies of the fast neutrons released cover a considerable range, i.e., $0 \leq E \leq 17$ MeV. The prompt fission gamma rays have a continuous energy spectrum from about 0.5 MeV to 10 MeV where the intensity for $E \leq 7$ MeV is quite small. With the exception of ordinary hydrogen, which has a single capture gamma, most other common elements exhibit a complex gamma emission spectrum with an upper limit of about 8 MeV. Decay gammas have energies generally less than 5.5 MeV.

Design optimization in LMFBR systems is a nontrivial task which is a function of many parameters. For example, structural

Table 1-1

	MeV	Disposition of Energy
1. Kinetic energy of fission fragments	165	local heating
2. Instantaneous gammary energy (prompt gammas)	7	local and dispersed heating
3. Kinetic energy of fission neutrons	5	local and dispersed heating
4. Radiative capture gamma rays	9	local and dispersed heating
5. Beta particles from fission products	7	local heating
6. Gamma rays from fission products	6	local and dispersed heating
7. Neutrinos	10	escape and therefore are not recoverable as heat
Total energy released ≃	209 MeV	

components must be provided with adequate cooling owing to the thermal gradients induced by gamma heating. If ignored and/or not properly accounted for, these thermal gradients may promote excessive thermal expansion and creep phenomenon, thus causing distortion of in-core internals. As a result, neutronics behavior may be drastically affected. Structural deformation is therefore an important design consideration and is necessarily a function of the gamma heating environment. Specifically then, gamma heating plays a major role in the design of LMFBR fuel subassemblies, control rods and safety rods. The need for such gamma heating information, as briefly delineated in the preceding, discussion has supplied some of the specific impetus for the present study.

Additionally, the accurate gamma environment characterization is important and inseparable from considerations in shielding design as well as, and importantly so, the coolant system design requirements for after shutdown decay heat.

Looking beyond the reactor proper design considerations, are the needs of the experimenter who will utilize the facility. He is interested in the nuclear heating environment in general and the gamma heating environment in particular, in order to accurately establish the nature of the thermal hydraulic environment as influences the design and interpretation of his in-core (near core, etc.) experiments. Consequently, since temperature is of paramount interest to the experimenter (materials experimenter), gamma heating is again an indispensable adjunct in many experiment design considerations.

Efforts to define and quantify gamma-ray heating in LMFBR environments are being emphasized; this emphasis is based upon the current needs and requirements of the EBR-II systems as well as concern for future fast reactor systems. An extensive effort to characterize the neutron environment in reactor systems has been actively supported over the years. As a result, estimates of the "state of the art" accuracy readily achievable is approximately 5-10% for a 2 σ or 95.0% confidence interval. The future requirements entail needs for accuracies in the 1-3% range. The general feeling is, however, that the 2-5% level is more realistically achievable in the near future.[5]

An interesting contrast with neutronics characterization accuracies are accuracies in the characterization of the gamma-ray environment. Both effort and support have been severely lacking, and as a consequence, serious deficiencies exist in the overall body of knowledge in this area. "State of the art" accuracy in gamma ray heating is currently listed as being an approximate 10% uncertainty in quantification for a 2 σ or 95.0% confidence interval. The immediate goal is a reduction of this value to less than 5% and a future goal of less than 3% uncertainty.[5]

Some early work[6, 7, 8, 9] was performed for defining the in-core gamma-ray heating and temperature distributions for the Materials Test Reactor (early 1950's) to satisfy the requirements for accurate temperature profiles utilized for in-core thermal neutron materials irradiation experiments. The next stimulus for information arose from the needs of the EBR-II system as it evolved from a demonstration facility into its present role as an irradiation facility (high fluence test experiments). Again, the primary motivation was to

more accurately characterize and define the in-core materials test environment. EBR-II characterization capabilities are representative, in the U. S. at least, of presently achievable state-of-the art description as pertains to in-reactor gamma heating.

Following is a brief review of some of the calculational and experimental efforts engaged in to date, namely those with the attendant goal and probability of improving the nuclear (gamma) heating environment detail, and accuracy. This is not intended to be a comprehensive review of all efforts presently being engaged in nor even a detailed examination of those efforts cited. Information related is intended to lend scope and background to the study hereinafter presented.

From a literature examination it is obvious that the most serious and comprehensive analytical efforts for calculating gamma heating effects, especially in LMFBR environments[10], have been initiated within the last 5 years[11, 12]. Motivation of the efforts seems to have arisen from a number of important concerns:

1) transition of EBR-II from a demonstration plant to an irradiation facility;
2) evaluation and comparison of potential LMFBR control rod materials;
3) evaluation of safety related phenomena, such as gamma heating in structural components and cooling requirements for after shutdown decay heat; and
4) shielding.

The overall approach used for calculating gamma spectra and related phenomenon is generally the same in all of the efforts cited. In general, ANL analyses are based upon the two-dimensional[13] discrete ordinate transport theory utilizing the computer code DOT, whereas Hanford Engineering Development Laboratory (HEDL) has employed two and three dimensional diffusion theory using the computer codes 2DBS and 3DB.[14, 15, 16, 17, 18]

In all these computer codes, U-235 fission product decay gammas are used discounting any differences which exist among fissile nuclides formed in an LMFBR. In the absence of actual observations and data for these nuclides, this assumption is necessary. It does, however, serve as a particularly good illustration of the need for an expanded nuclear data base for gamma calculations. While all reactor calculations suffer from this data insufficiency, gamma-ray computations possess even greater shortcomings in this regard. Gamma calculations must apriori possess all existing inadequacies of neutron calculations and in addition suffer from important deficiencies in basic data for the following gamma-ray production modes: fission product decay, prompt fission, neutron capture, and inelastic neutron scattering.

Gamma heating measurements can be carried out in high power environments with a number of calorimetric devices or experiments. From the basis of calorimetric devices there are, in general, two broad classes, passive and active monitors.

Passive monitors are those which do not have implanted instrumentation requiring continuous monitoring and hence, do not

require instrument leads; the result of this characteristic is greater flexibility of potential locations within the reactor. Many concepts have been proposed for passive in-core temperature monitoring, an overview of which comprises;

1) melt wires are perhaps the earliest passive temperature monitors for restricted environments. This type device provides discrete range temperature estimates according to the melting points of various metals[5].
2) the phase transition principle is utilized in a device based upon the temperature sensitive phase transition phenomenon exhibited by suitably chosen materials[5].
3) a vapor pressure monitor is a device which utilizes the temperature dependent vapor pressure sensitivity of certain elements in a precipitation trap to relate the maximum temperature to which it has been subjected[19].
4) Thermal Expansion Difference Monitors (TED) and Gamma Expansion Difference Monitors (GEDM) comprise a class of devices whose principle of operation relies upon the differential dimension change (volumetric expansion) of two different materials as a function of temperature[5].

Active monitors are those monitors which contain continuously monitorable instrumentation and thus have instrument leads which must

be routed from their place of implantation. Within this broad class are two specific examples:

1) electrical heaters are placed in certain instrumented subassemblies to infer temperature increase in test specimen vs input power, and[13]

2) temperature monitoring thermocouples are implanted or imbedded in a suitable susceptor material for inducing radiation interactions and consequently measure temperature gradients.[2]

In the main, active devices are more desirable in that they indicate time dependent functionality; that is for example, the time dependent temperature history T(t) or the time dependent heat generation rate $\dot{Q}(t)$ can be provided.

Several devices have been considered for the EBR-II system. An evaluation of the above concepts has shown that complicated heat transfer analyses are required to deduce gamma heating rates using data from the electrical heater experiments; while neither the thermocouple containing calorimeter nor either of the passive devices (Thermal Expansion Difference principle) require as complex a heat transfer analysis. Evaluation of the above concepts by the EBR-II Project, resulted in a choice of the active calorimeter[2] and the passive calorimeter, TED-GEDM[5] for continued development and use.

In core temperature measurements are routinely and accurately carried out with active thermocouple devices. In the temperature

range of interest, namely 600-1400°F, chromel-alumel thermocouples work reliably and accurately. A point worth noting is that this accuracy is not maintained for temperatures beyond the upper limit cited because of electrical shunting in the insulating material surrounding the current carrying thermocouple leads. In core nuclear heating rates can also be measured with thermocouple imbedded, temperature monitoring calorimeters. One such device was recently employed in scoping experiments by J. F. Koenig, R. G. Matlock, and C. C. Ford[2].

Consequently, state-of-the-art information concerning active nuclear calorimetry for gamma heating is at present well represented by the experiments of Koenig et al., at the EBR-II facility. The design configuration for the calorimeter used is shown in Figure 1-1. The device consists of an insulated cylinderical radiation susceptor with a thermocouple imbedded near the insulated end. Components of the reactor radiation environment interact with the susceptor atoms and thus deposit locally some or all of their incident energy. An equilibrium condition is reached when a balance is achieved, such that the rate of heat generation in each differential susceptor volume is equal to the combined rate(s) of heat removal from the same volume by conduction, convection and radiation.

Energy input and efflux is evidenced by a temperature change in the susceptor material, thus reflecting the acquisition of energy by the susceptor atoms. A complex functional relationship exists among the associated phenomenon. A qualitative description of the existent functionality may be written as:

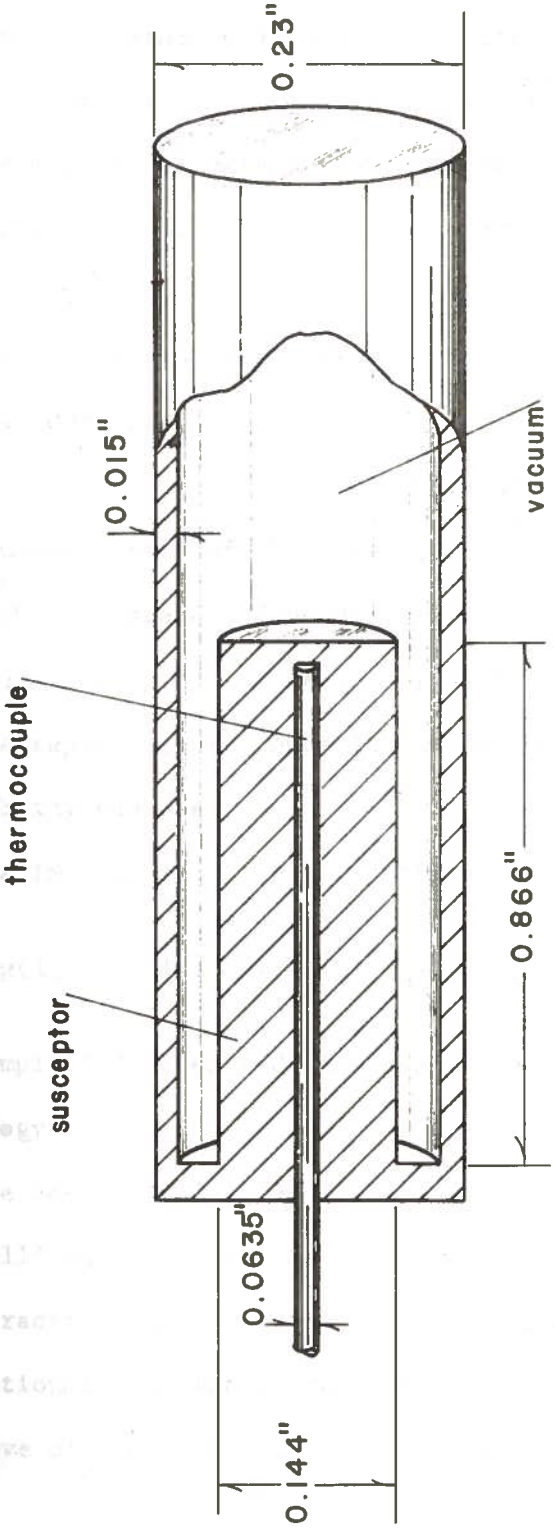

Koenig experiment calorimeter

FIGURE I-1

$$T = f\left(\dot{Q}, \rho, k(T), \varepsilon(T), \vec{R}, \ldots.\right) \qquad (1\text{-}1)$$

where:

T = the temperature at a general point in the medium being described as a function of relevant parameters and/or variables,

$\dot{Q}$ = the internal heat generation rate/volume or mass,

ρ = a representative material property such as density,

$k(T)$ = the temperature dependent thermal conductivity of the medium,

$\varepsilon(T)$ = the temperature dependent thermal radiation emissivity of the medium present, and

$\vec{R}$ = a representative location in the medium being examined.

From (1-1) is implied a relationship of the form

$$\dot{Q} = g(T, \rho, k(T), \varepsilon(T), \vec{R}, \ldots.) \qquad (1\text{-}1')$$

A simplified model and expression will serve to illustrate the methodology of the Koenig et al. experimental analysis as well as particularize Equation (1-1) and (1-1') for a one-dimensional geometry. For the simplified model examination of the Figure 1-2 geometry, heat transfer by radiation and/or convection is neglected giving rise to the aforementioned one-dimensional relationship. Equation (1-2) is representative of the qualitative relationship of Equation (1-1):

$$T(z) = T_o + \frac{\dot{Q}\rho}{k}\left(L\,z - \frac{z^2}{2}\right) \qquad (1\text{-}2)$$

where:

$T(z)$ = temperature at location z,

$\dot{Q}$ = the uniform internal heat generation,

k = thermal conductivity of the material,

L = length of the calorimeter,

z = axial distance of a general point as measured from the cold or zero end of the calorimeter, and

T_o = typically the cold end or base temperature.

To describe the system then, the energy deposited is conducted along the axis of the susceptor to the coolant heat sink at the zero end. In EBR-II this heat sink is the ambient sodium environment surrounding the calorimeter. Conductive and convective losses from the sides and top of the susceptor are neglected in the analysis from which Equation (1-2) arises. In reality conduction is minimized by a vacuum in the annular space between the susceptor and the containment tube walls. Radiation heat transfer is reduced by conditioning the surfaces of the susceptor and tube. With the simplified example above it can be seen that, knowing precisely the values of ε and k and an accurate measurement of T_o, and $T(z)$ for some z, will allow calculation of $\dot{Q}$, the overall internal heat generation rate. Actually a closed form expression for the internal heat generation rate may be obtained from Equation (1-2) by rearrangement of terms to obtain

$$\dot{Q} = \frac{k}{\rho} [T(z) - T_o] \; / \; (Lz - \frac{z^2}{2}) \qquad (1\text{-}2')$$

The preceding equations and explanations are illustrative in considering the calorimeter's operation. Actual analysis of the calorimeter data for the Koenig experiment was performed with the Transient Heat Transfer Big (THTB) heat transfer computer code[20, Appendix D]. THTB was used to allow accounting for the complex nature of the non-zero radiation heat transfer, the temperature dependence of the thermal conductivity, and the perturbation of the susceptor heat transfer by the imbedded thermocouple. Conduction and convection across the evacuated annulus were shown to be insignificant.

From an examination of Figure 1-1, it is immediately recognized that radiation heat transfer exists for the configuration utilized and furthermore it is found to account for a considerable portion of energy transferred in the system. Precise quantification of the radiation heat transfer thus presents a serious obstacle to ultimate calorimeter accuracy based upon the proposed design, Figure 1-1. The major fault lies in the fact that the radiation component cannot be accurately quantified owing to rather severe inaccuracies inherent in the knowledge and quantification of the thermal emissive properties of the engineering materials of interest. In all probability, regardless of the basic design, there will be characterization inaccuracies derived from material properties uncertainties. Knowing in advance then, that any design will have to contend with the presence of such inaccuracies, it will be necessary to "minimize the effect" of any such inaccuracy upon data analysis. For the case in point, this basically means that the relative amount of energy transferred by

radiation must be reduced to as low a level as possible within the limits of the remaining design requirements, hoping all the while that no combination of those requirements engenders complete and mutual exclusivity.

Radiation heat transfer in the above configuration is a significant mode of heat dissipation for the susceptor due to the relatively small susceptor radius, the cause for which will be examined and explained in the design parameter section of Chapter 2. It is felt however, that minor modifications of the system may result in a substantial reduction in the relative amount of energy transfer by radiation.

The Koenig experiment is significant for at least 4 reasons:

1) it established a viable basic design configuration worthy of considerable additional study; such design apparently offers the potential for a significant increase in accuracy over previous or contemporary contiguous designs;
2) it identified certain shortcomings in present design parameters and afforded basic information concerning the elimination of the shortcomings;
3) it aroused sufficient interest and demonstrated enough potential to supply the impetus for its inclusion in future evaluations of means for more accurate determinations of nuclear heat generation rates;

4) the overall experimental error of the calorimetry measurements was judged to be less than 10%. This error was determined to be dominated by uncertainties in the quantification of thermal conductivities (k), and uncertainties in the emissivity, ε, of the material of interest, stainless steel.

It is however felt[21] that improved accuracy may be obtained with adequate attention to design details, proper material evaluation, and congnizance of experiment requirements.

Chapter 2

PROBLEM DELINEATION

The design configuration for the proposed calorimeter was established based upon the following "basic design criteria":

1) limitations in available instrument irradiation space;
2) necessity for the calorimeter to approximate a point detector;
3) a desire to take advantage of the natural axial geometry of the EBR-II core and design;
4) relative completeness and accuracy in the characterization and quantification of conduction heat transfer, hence the desire that the primary mode of heat transfer be conduction;
5) accurate and precise modelability of any chosen design with respect to characterizing the radiation heat transfer; and
6) a desire for a calorimeter with maximized accuracy.

The calorimeter used by J. F. Koenig, Figure 1-1, satisfies the preceding criteria with the exception of (5) and (6). Preliminary analysis[21] indicates that the calorimeter may be fabricated to rather small dimensions relative to EBR-II core and flux profile dimensions. This satisfies criteria (1) and (2). The

configuration depends upon uniaxial conduction heat transfer in a cylindrical calorimeter as the primary mode of energy transport, thus satisfying (3) and (4). Dr. C. C. Price has suggested a modification which assists in satisfying the requirements[5] of (5). The proposal envisions a calorimeter of the basic Koenig type, but with the addition of a mirror image susceptor opposing the primary susceptor, and heat shields to isolate both susceptors from the containment tube wall. The final configuration would be somewhat as shown in Figure 2-1. The advantage over the design in Figure 1-1 is that it will minimize heat loss by radiation and lead to a smaller overall calorimeter uncertainty; this uncertainty is fostered by the rather large uncertainties in calorimeter material emissivities. With this design relatively large uncertainties in the surface emissivities can be tolerated because the temperature differences between the emitting surfaces is forced to be small.

As stated in the preceding Chapter, the Koenig et al. experiment identified a relatively large source of error in a basic design with otherwise desirable properties. Accuracy of this basic calorimeter design may be enhanced if it is possible to provide a system for which the uncertainties in the characterization of radiation heat transfer are minimized. Three basic concepts have been proposed as means for supressing radiation heat transfer in the calorimeter thus reducing error engendered by material properties uncertainties.

The ensuing analysis will consist in part of an evaluation of these three "base line parameters" as means for accomplishing a significant reduction in the relative amount of energy transported by the radiation mechanism. Table 2-1 identifies and briefly defines the

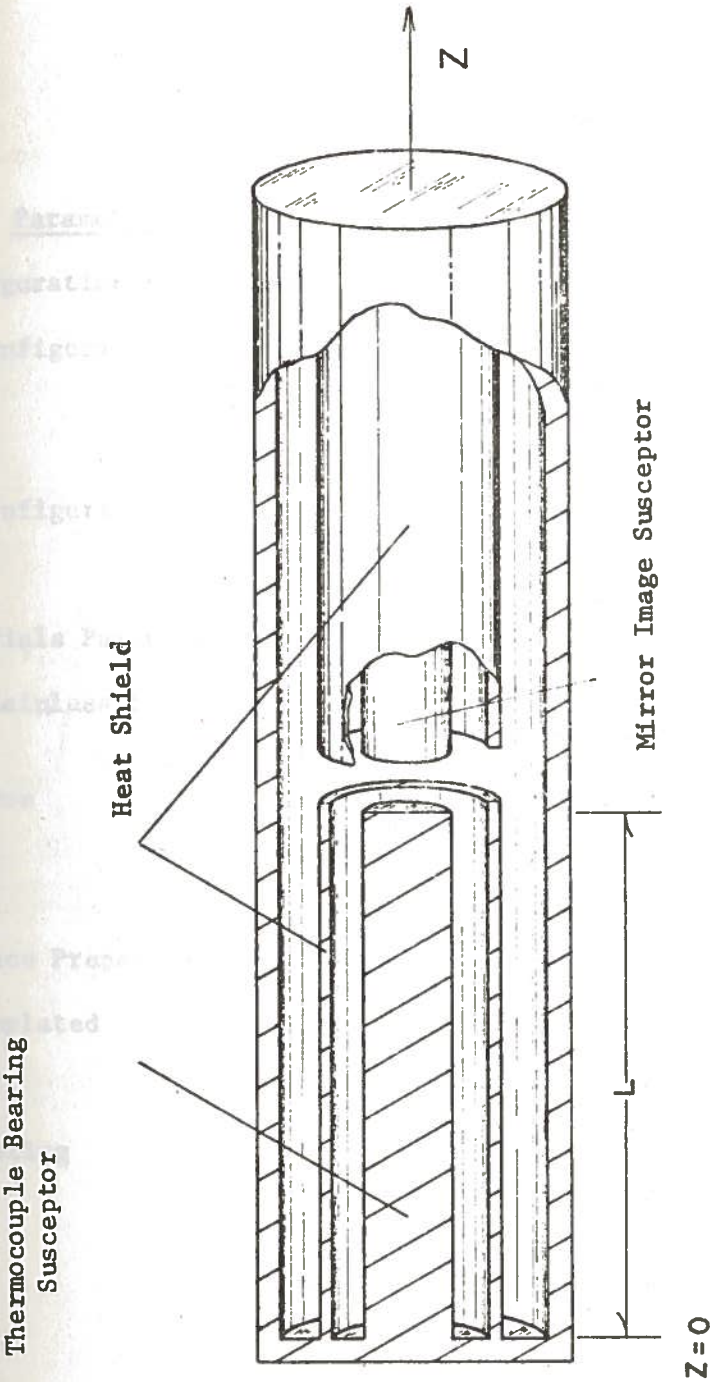

Price Modification
Figure 2-1

Table 2-1

Baseline Parameters

Parameters	Description
Configuration Parameters:	
Configuration A	Calorimeter employing a solid susceptor, Figure 2-3 of increased outer dimensions equal to those of the heat shield in Configuration B.
Configuration B	Calorimeter with its susceptor surrounded by a heat shield, Figure 2-4.
Materials Parameters:	
Stainless Steel	The material which is most representative of EBR-II structural material
Iron	A material which presents a similar radiation interaction environment and has more accurately characterized thermal properties.
Surface Preparation Parameters:	
Unplated	Relying upon mechanical or chemical surface conditioning to promote radiation reduction.
Plating	Plating the calorimeter internals with a material for which there is an accurate characterization of thermal emissive properties, and which additionally reduces the surface emissivity of the calorimeter internals.

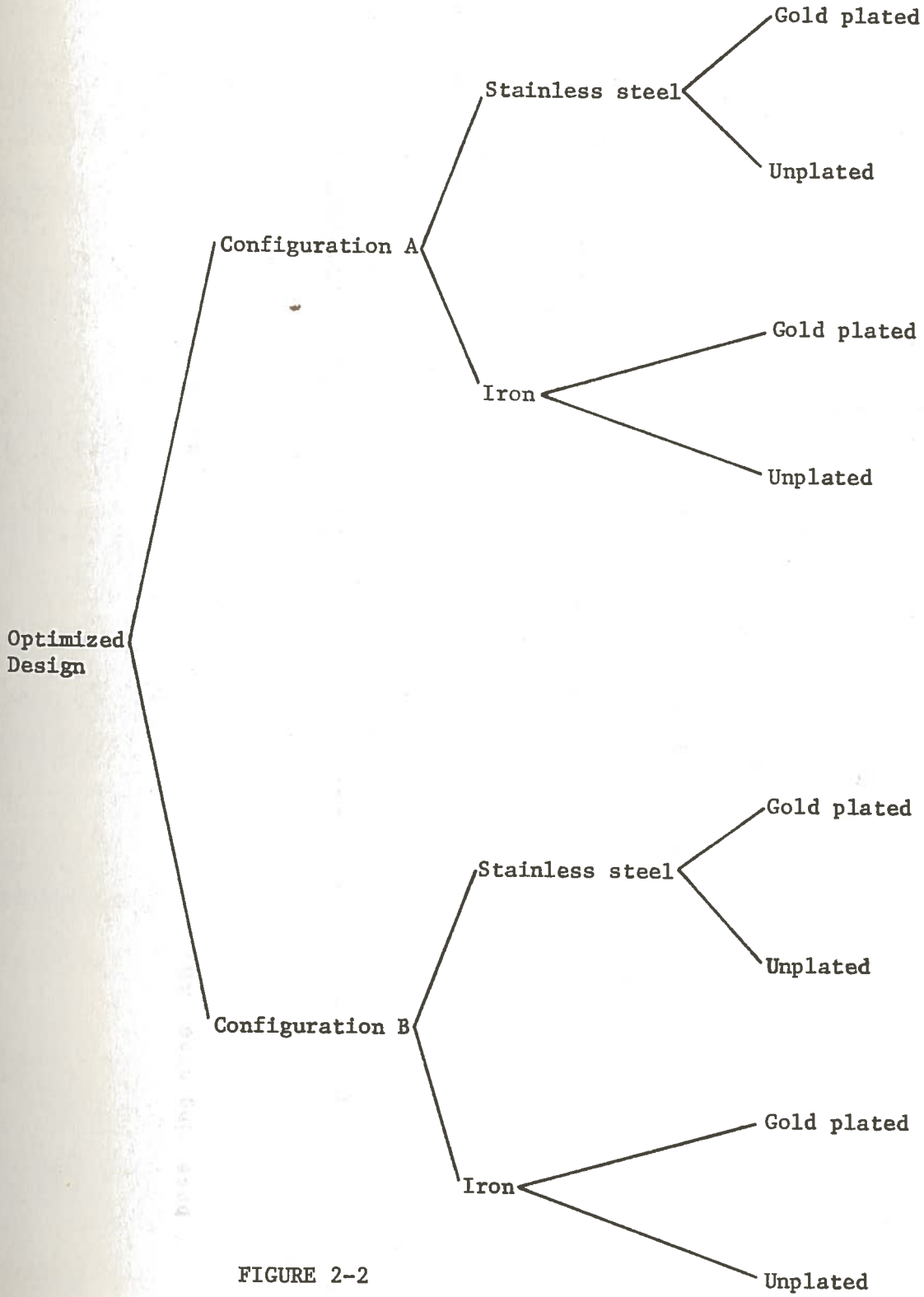

FIGURE 2-2

Parametric Study Tree

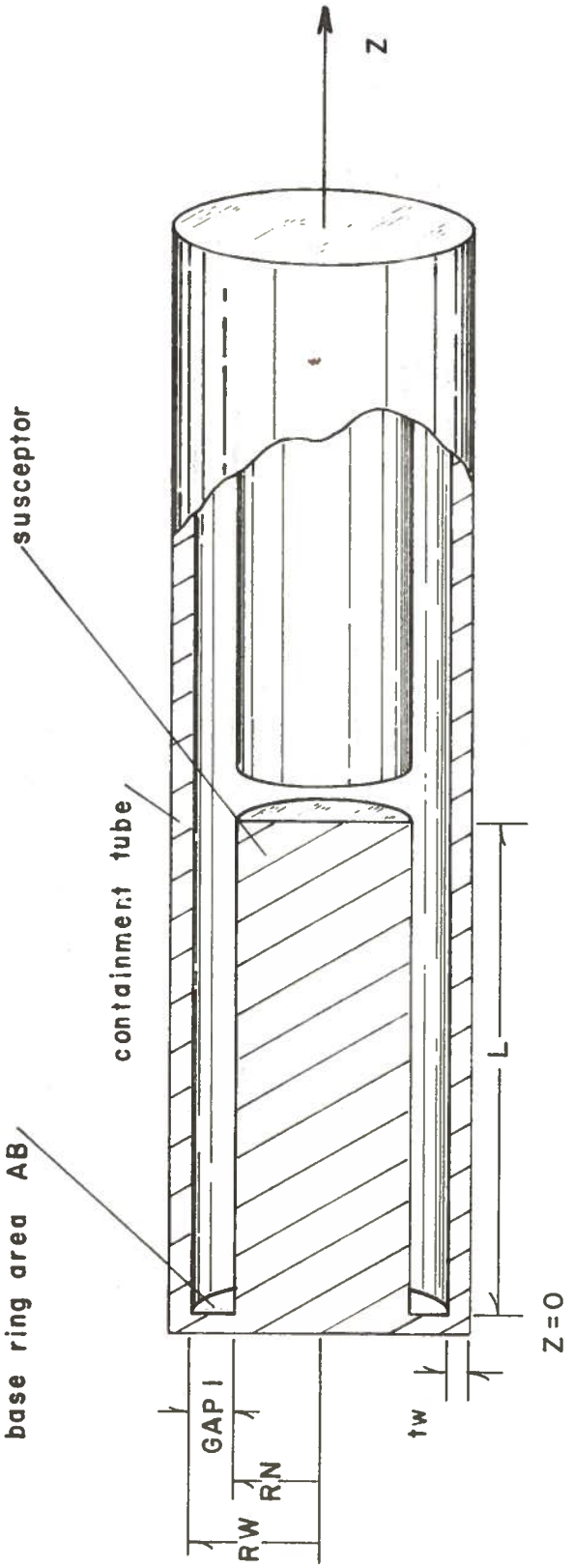

Configuration A solid susceptor

FIGURE 2-3

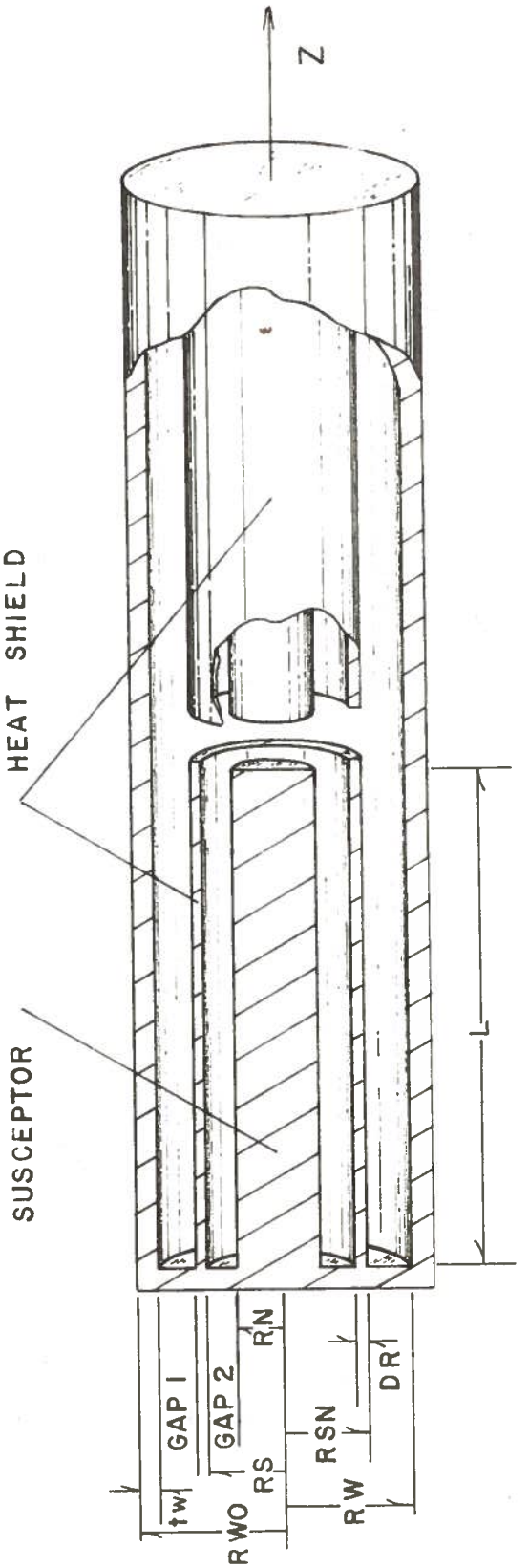

FIGURE 2-4

Configuration B heat shielded susceptor

aforementioned base line parameters. The analysis suggested in the preceding will employ a parametric study of the base line parameters identified; their relationships to the study and to one another are best described through the use of the "parametric study tree" shown in Figure 2-2.

Considerable amplification is necessary to provide a more complete understanding of the base line parameters and their significance.

The configuration parameter will be resolved in terms of a choice between the solid susceptor of Configuration A. Figure 2-3 and the heat shielded susceptor of Configuration B, Figure 2-4. As previously stated, the desire is to reduce the energy transfer by radiation relative to the total energy transferred within the system, as this will suppress the relative error in characterization of the system. Two means are identified for reducing the relative amount of radiation. They are:

1) utilizing a calorimeter with a larger susceptor radius; and/or
2) interposing a thin heat shield, Figure 2-4 between the susceptor and the sink to which radiation would normally take place, the containment tube wall.

A justification of 1) above proceeds from the following heuristic analysis. The two modes of heat transfer from the susceptor body, Figure 2-3, are conduction and radiation. Qualitatively the heat transferred by conduction from the susceptor is given by the Fourier Law[22,23].

$$\dot{q}_{cond} = -k\, A_k \frac{\Delta T}{\Delta z} \qquad (2\text{-}1)$$

where

$$A_k = \pi r^2$$

and

r = susceptor radius,

The heat transferred by radiation is given by the Stefan-Boltzmann Law for finite black bodies:[22,23,24]

$$\dot{q}_{rad} = F_{1-2}\, \sigma A_1 \, (T_1^4 - T_2^4) \tag{2-2}$$

where T_1 = calorimeter susceptor temperature

T_2 = containment tube wall temperature

$A_1 = 2\,\pi rL$

and

L = the susceptor length

The ratio of the heat transferred by radiation to the heat transferred by conduction is then given by

$$\dot{q}_{rad}/\dot{q}_{cond} = \frac{F_{1-2}\, \sigma\, A_1 (T_1^4 - T_2^4)}{-k\, A_k\, \Delta T/\Delta z} \tag{2-3}$$

$$= \frac{F_{1-2}\, \sigma\, (T_1^4 - T_2^4)\, 2\,\pi rL}{-k\, \Delta T/\Delta z\, \pi r^2} \tag{2-4}$$

$$= \frac{2F_{1-2}\, \sigma\, (T_1^4 - T_2^4)}{-k\, \Delta T/\Delta z} (L) \cdot \frac{1}{r} \tag{2-5}$$

and

$$\dot{q}_{rad}/\dot{q}_{cond} \propto \frac{1}{r} \tag{2-6}$$

Qualitatively at least, it is suggested that the relative contribution by radiation can be reduced by increasing the susceptor radius. Relative radiation reduction by alternative means 2), use of heat shield, may be explained in terms of the basic heat shield principle[22,23,24]. In terms of the "shielding" effect, the heat shield assumes a temperature intermediate to the two bodies between which it is interposed, thus offering an elevated sink temperature. Furthermore, the heat shield is itself a "susceptor" for the nuclear heating radiation. Therefore in addition to acquiring a temperature elevation due to radiation heating equilibration, it simultaneously receives an input of energy from nuclear interactions, as does the calorimeter susceptor. The net effect is an increase in the shield temperature above the idealized equilibrium value. The calorimeter susceptor instead of "seeing" and hence radiating to the lower sink or containment tube wall temperature, in effect, "sees" a temperature profile near that of its own, and as a consequence radiates less.

With respect to the two basic calorimeter configurations, Figures 2-3 and 2-4, the solid susceptor versus the heat shielded susceptor, there are two overlapping reasons for wanting to minimize the calorimeter size. First is the point detector requirement, because the properties which are desirable for measurement are generally required at a point inasmuch as the property of interest may be spatially dependent, and may vary greatly over short distances; second is the desire to have the detector locally perturb the system as little as possible.

In a reactor core any irradiation space, the volume set aside for experiments, necessarily eliminates fuel unless the experiment happens to contain fuel. This volume, depleted of fuel as it is, changes the criticality requirements of the system and locally perturbs conditions such as the radiation environment. It is necessary therefore to minimize the local volume of non-fueled regions in the core as any large perturbation therefrom destroys the validity of the measurement.

Concisely then, it is desirable to minimize the experiment volume, which in this case is the calorimeter volume. An examination of Figure 2-3 of the solid susceptor geometry and Figure 2-4 for the heat shielded geometry clearly shows that the containment tube wall thickness and the immediately adjacent evacuated annular space volume requirements are the same for both calorimeter configurations. The remaining internal volume of the calorimeters is, in the case of the solid susceptor, the volume occupied by the susceptor proper, and in the case of the heat shielded susceptor, the combined volume of the heat shield, evacuated annular space, and susceptor. For future reference this volume will be classified the "active" or "working" volume of the calorimeter.

For the solid susceptor, Figure 2-3, this volume is contained within the cylindrical boundaries defined by the susceptor length L and the susceptor radius RN. The working volume of the heat shielded susceptor, Figure 2-4, is contained within the boundaries defined by the susceptor length L, and the outside radius of the heat shield RSN = RS + DR. Subsequent analysis and comparison can be easily

accomplished in terms of RN, RSN = RWK; wherein RWK is defined as the "working radius" or the radius of the working volume of the calorimeter.

One object of this study is, by some combination of parameters relating the geometry and operation, to minimize the working volume which is required to reduce the radiation heat transfer influence on calorimeter characterization. In the case of the two calorimeter designs, it reduces to making the most efficient use of the working volume by either filling the entire volume with susceptor mass, or filling the volume with some judiciously chosen combination of mass of heat shield material, evacuated space and susceptor mass. "Efficiency" applies to the ability to reduce the relative heat transfer by radiation from the susceptor as a percentage of the total heat conducted or generated in the susceptor.

The susceptor material parameter has been reduced to a choice of either stainless steel or iron. The basis of the design, to reiterate, is to permit the measurement of the gamma heating or energy deposition rate in "structural material". Stainless steel is that "structural material", however, there is the inherent disadvantage to fabrication from stainless steel due to uncertainties in quantification of thermal properties, primarily thermal conductivity with $2\sigma = \pm 5\%$, for the material. Iron on the other hand has thermal properties which are more accurately quantified, $2\sigma = \pm 2\%$ for iron thermal conductivity. Iron is not the exact structural material generally utilized in terms of constituents; however, it does present essentially the same interaction environment to incident gammas. Basically speaking,

the gamma ray interaction probability is a strong function of the atomic number $Z^{(4)}$ of the interaction medium; iron presents essentially the environment of elemental iron, Z = 26. Stainless steel 304 and 316 present, respectively, an average value of atomic number $\bar{Z}$ = 25.799 and $\bar{Z}$ = 26.39. This is because of the presence of considerable quantities of Cr, Z = 24 and Ni, Z = 28 as primary constituents. Therefore, if iron affords a clear advantage in terms of the characterization of its thermal properties, it should be strongly considered.

The susceptor Surface Preparation Parameter entails an examination and quantification of any numerical, as opposed to mechanical, advantage resulting from plating the calorimeter internals with a material which has:

a) an extremely low value for total hemispherical emissivity, and

b) accurately characterized thermal properties.

Gold is most suitable in terms of the above requirements, however at elevated temperatures there is a problem. Above approximately 800°F, gold rapidly diffuses into stainless steel. This diffusivity at high temperatures will necessarily prohibit its use with stainless steel calorimeters for the purpose of establishing a quantified standard for comparison the emissivity reduction for gold plated calorimeter internals will be examined.

The base line parameters (Table 2-1) are considered the primary variables of the analysis; in addition to these three, there is another group of parameters, for future reference to be called, secondary parameters. Table 2-2 identifies these secondary, though no less important variables. These parameters will be further defined

Table 2-2

Secondary Parameters

Parameter	Description
Operating Parameters:	
1. Maximum Temperature	Maximum temperature attained by the body of the susceptor.
2. Temperature Profile	Temperature profile attained by the body of the susceptor.
3. Internal heat generation rate	Rate with which energy is imparted to the calorimeter susceptor by interacting nuclear radiation.
Geometric Parameters:	
4. Susceptor length	See Figures 2-3 and 2-4
5. Susceptor radius	
6. Outside calorimeter diameter	
7. Containment tube wall thickness	
8. Gap spacing	
9. Heat shield thickness	
Error Parameter:	
10. Propogated error in heat generation rate	Estimation of the accuracy with which the fully optimized design can measure in-core nuclear heating rates, hopefully $\leq$ 5%.

and described herein but in some cases left without numerical values until further analysis. It is, however, the task of this study to impart specificity to these important parameters.

The operating parameter, maximum susceptor temperature is best explained with an examination of the simplified model of Figure 1-2 and Equation (1-2) repeated here for convenience:

$$T(z) - T_o = \frac{\dot{Q}_\phi}{K} (Lz - z^2/2) \qquad (1\text{-}2)$$

As indicated the temperature increases monotonically from a minimum value of T_o which, in the configuration to be employed, is the base temperature of the susceptor, to some relative maximum at the end of the susceptor. The base temperature is controlled by the ambient sodium coolant temperature. It is desirable to have the temperature at and near the other end of the susceptor to be:

1) within the accurate operating range of the imbedded thermocouple, that is, less than approximately 1400°F;
2) within the range for which the thermal properties of iron, gold, and stainless steel are accurately quantified, that is, less than approximately 1500°F; and
3) at such a value as to promote the most "accurate" performance of the calorimeter as relates to propagation of error contributions from temperature measurement.

Suffice it to say at present that "for reasons of accuracy" it is desirable to have the highest possible maximum temperature

within the limits of constraints imposed by other considerations, hence the maximum operating temperature increment $\Delta T = T_{max} - T_o$. Justification for this requirement will be explained in Chapter 5, Error Analysis. It was decided that in view of the preceding requirements, a mean operating temperature of approximately 1350°F would be suitable inasmuch as it would satisfy the above requirements while providing an adequate operating range above and below. An operating range of 1350 ± 50°F will be henceforth designated as Range A.

The next operating parameter is the internal heat generation rate. This parameter, that which we hope the calorimeter to measure, is a reactor system dependent quantity; it is not, in general, a constant but rather it exhibits strong spatial dependence. The optimized design, with some limitations, will hopefully be able to accommodate accurate measurements regardless of location or heating rate at a particular location. An understanding of this concern can best be gained through Equation (1-2) and noting that once the calorimeter is fabricated (i.e., material and length determined), the operating temperature profile and maximum value are functions of the heating rate at a particular location. It is desirable that the calorimeter be able to, at all times, operate within Range A in order to insure accuracy of measurements. An analysis will therefore be made to determine the range of heating rates for which this desire is accommodated. This range, when determined, will be operating Range C.

The geometric parameter, susceptor length, can also be examined with reference to Equation (1-2). It is noted that with the other parameters constant the maximum temperature, T_{max} is a strong function of the length of the susceptor. That is, T_{max} will be

proportional to the square of the length L. The choice of length will be an open design parameter to be determined during the parametric study. In general, concern will be toward preservation of a point dimensioned detector with respect to axial gamma flux profile and core axial dimension as well as minimizing volume requirements. Furthermore, stainless steel and iron possess considerably different coefficients of thermal conductivity, thereby necessitating different lengths to achieve operation within Range A.

The geometric parameter susceptor radius can be examined through inference from Equation (1-2). The maximum temperature achieved by the calorimeter is directly proportional to the volumetric or mass internal heat generation rate. As the susceptor radius increases so will the total internal heat generated and concomitantly the temperature profile is expected to be perturbed upward. There is the additional concern for limited available space for instrumented experiments in the core of EBR-II, as well as the point detector requirement, both of which dictate choice in favor of as small a calorimeter as possible. Recall that the Koenig experiment, however, indicated that smaller radii calorimeters enhance radiation heat transfer at the expense of conduction, thus engendering an overall error in subsequent calculations. An optimized calorimeter susceptor radius is another parameter to be determined through this study. In general, it is felt that the susceptor radius, RN must be within the following range, $0.08" \leq RN_{max} \leq 0.335"$. RN_{max} = RWO - (Gap 1 + tw).

The geometric parameter, overall calorimeter diameter is next explained. The primary concern in terms of the overall calorimeter diameter of radius RWO, Figure 2-3, is dependent upon the needs of the preceding related parameters in terms of permitting sufficient internal volume to accomplish the objectives of efficient radiation reduction with as small a volume as possible. Available instrumentable volume within the core of EBR-II dictates that the outside diameter of the calorimeter be less than 0.75 inches therefore the outer radius, RWO, of the calorimeter will be the optimized value from the range:

$$0.125'' \leq RWO \leq 0.375''$$

The geometric parameter containment tube wall thickness, tw, Figure 2-3 and 2-4, should be thin to preserve as much working volume as possible, yet be sufficiently thick to be rigid and machinable without great difficulty. A readily accomplishable value for the containment tube wall thickness, tw, is tw = 0.020".

The geometric parameters, Gap 1 of Figure 2-3 and Gaps 1 and 2 Figure 2-4 serve to isolate calorimeter internals. The annular space must be easily controlled and accomplished while at the same time require as small a volume as possible in light of preceeding considerations. A probable value for each of the gap spaces is 0.020". It is felt that this value may be easily controlled and accomplished during fabrication.

The last geometric parameter is the heat shield thickness DR. The behavior of a heat shielded susceptor is to be analyzed

and evaluated as a facet of the parametric study. Fabrication requirements specify that the heat shield be of sufficient thickness, DR, to permit ease of fabrication while being relatively rigid when assembled. For these reasons a minimum value of DR will be approximately 0.010", and the optimized value is to determined during the study.

The error parameter will result from a study of the contribution to overall error in implicit calculations of heat generation rate, as a function of the inherent errors in the other parameters. The analysis will be described and performed as a propogation of error evaluation in Chapter 5, Error Analysis.

An optimized design will be the result of conjoining desirable factors identified in an analysis of the preceding parameters.

Chapter 3

Configuration Modeling

With the Koenig design as a basis for extrapolation, the Price modification to simplify the boundary conditions, and the set of areas of investigation identified (Tables 2-1 and 2-2), the next step is to model, for analysis, the configurations of interest. Analytic methods treat the conduction medium as a continuum and yield a great deal of information of a general nature. When successfully applied, an analytic solution allows the determination of the temperature at any point, within the body at anytime. Since the results are in general given in closed analytic form, it is possible to ascertain the effect of changing various parameters, such as the effect of altering the body geometry.

A great number of problems can and have been solved analytically; these however, are usually restricted to rather simple geometrical shapes such as cylinders, spheres, and infinite slabs. In addition there is generally the necessity to provide boundary conditions which are simple to express mathematically. There are expected to be many general conduction problems of considerable practical value then, which because of the geometry or complex nature of the boundary conditions, have no analytical solution. The absence of an analytical solution will not however, obviate the necessity of a solution. Numerical techniques exist which allow the treatment of quite complex problems to the degree of accuracy desired;

in cases of this nature the effort required is directly proportional to the accuracy demanded of the solution.

Throughout the present chapter continued reference will be made to the collective body of knowledge generally known as "Heat Transfer"[22,23,24]. For immediate use and convenience, several basic constructs of this science will be related herein. Most readers will be familiar with the terms used to denote the three modes of heat transfer; conduction, convection, and radiation, as outlined below:

1. Conduction: (Fourier's Law)[22,23]

$$\dot{q}_{cond} = -k_k A_k \frac{dT}{dz} \qquad (3\text{-}1)$$

$$\approx -kA_k \frac{\Delta T}{\Delta z} \qquad (3\text{-}1')$$

where

$\dot{q}_{cond}$ = heat transfer rate, e.g., BTU/hr;

k = thermal conductivity, e.g., BTU/hr-ft°F;

A_k = area through which heat transfer takes place, e.g., ft^2;

$dT, \Delta T$ = differential, incremental temperature existent between regions exchanging energy by conduction; and

$dz, \Delta z$ = differential, incremental spatical separation between regions exchanging energy by conduction.

2. Convection: (Newton's Law)[22,23]

where

$$\dot{q}_{conv} = h_c A_c (T - T_\infty) \qquad (3\text{-}2)$$

where

$\dot{q}_{conv}$ = heat transfer rate by convection, e.g., BTU/hr;

h_c = convection heat transfer coefficient, e.g., BTU/hr $ft^2°F$;

T = temperature of body surface from or to which convection takes place;

A_c = area through which heat transfer by convection takes place; and

T_∞ = bulk temperature of the medium or fluid from or to which convection takes place.

Radiation: (Stefan-Boltzmann Law for Finite Black Bodies)[22, 23, 24]

$$\dot{q}_{rad} = F_{1-2}A_1 \sigma (T_1^4 - T_2^4) \qquad (3\text{-}3)$$

from which comes (Stefan-Boltzmann Law for Finite Gray Bodies)[22, 23, 24]

$$\dot{q}_{rad} = F'_{1-2}A_1 \sigma (T_1^4 - T_2^4) \qquad (3\text{-}3')$$

where

$\dot{q}_{rad}$ = heat transfer rate by radiation, e.g., BTU/hr;

F_{1-2} = radiation "shape or view factor" representing the fraction of the energy which leaves body 1 and is received directly by body 2;

A_1 = surface of body one (1) at temperature T_1;

σ = Stephan Boltzman constant with the value 0.1714×10^{-8} BTU/hr $ft^2°R^4$;

T_1 = temperature of body 1, e.g., °Rankine;

T_2 = temperature of body 2, e.g., °Rankine; and

F'_{1-2} = radiation "exchange factor" for two gray bodies which is generally a function of F_{1-2}, ε_1, and ε_2.

From Equation (3-1) comes the general three dimensional heat conduction equation:[22,23]

$$\text{div } [k(T) \text{ Grad } T(R)] + \dot{q} = \rho c \frac{\partial T}{\partial \tau} \tag{3.4}$$

$$\nabla \cdot [k(T) \nabla T(R)] + \dot{q} = \rho c \frac{\partial T}{\partial \tau} \tag{3-4'}$$

The ideal analysis for the thesis problem is to solve Equation (3-4) while modeling the radiation boundary condition(s) in terms of some form of Equation (3-3) or (3-3'). The resulting equation is a general Poisson type differential equation with at least one non-linear boundary condition. Formulation of the problem in terms of the radiation boundary condition is difficult for the solid susceptor geometry, and even more so for the heat shielded geometry. The heat shielded geometry requires "two" coupled equations of the general type (3-4), one for the susceptor and one for the heat shield.

Existence of a closed form analytic solution of the form:

$$\dot{q}(r, \theta, z) = f(T(r, \theta, z)), k(T), \varepsilon_1(T), \varepsilon_2(T), F_{1-2}(r, \theta, z)) \tag{3-5}$$

where in general,

$\dot{q}(r, \theta, z)$ = the internal heat generation rate per unit volume at a general point in the susceptor medium,

$T(r, \theta, z)$ = the temperature at a general point in the susceptor medium,

$k(T)$ = the temperature dependent thermal conductivity of the susceptor medium,

$\varepsilon_1(T)$, $\varepsilon_2(T)$ = the temperature dependent hemispherical emissivities of the two bodies exchanging energy by thermal radiation, and

$F_{1-2}(r, \theta, z)$ = the radiation "shape or view factor",

is not guaranteed in either case. It is felt, therefore, unwise to devote a major effort to an attempted solution of this type, one with so little chance for success, when more expedient means are already available in the form of the general heat transfer computer code THTB[20].

The semi-quantitative analysis of Equation (1-2) did arise from a simplification and solution of Equation (3-4). The simplifying assumptions which permitted solving Equation (3-4) were:

1) uniaxial conduction of one-dimensional analysis,
2) constant thermal conductivity,
3) zero surface radiation, and
4) steady state conditions.

Equation (3-4) for the exist nt geometry then becomes:

$$k \frac{d^2T}{dz^2} + \dot{q} = 0 \qquad (3\text{-}6)$$

with attendant boundary conditions:

1. at $z = 0$, $T = T_o$
2. at $z = L$, $dT/dz = 0$.

The solution of Equation (3-6) is then,

$$T(z) = T_o + \frac{\dot{q}}{k} (Lz - \frac{z^2}{2}) \qquad (3\text{-}7)$$

and Equation (3-7) may be transformed to Equation (1-2) if the simple adjustment is made that

$$\dot{Q} = \frac{\dot{q}}{\rho}$$

where

ρ = the susceptor material density so that

$$T(z) = T_o + \frac{\dot{Q}\rho}{K} (Lz - \frac{z^2}{2}) \qquad (1\text{-}2)$$

for which it is recalled that,

$T(z)$ = the temperature at any axial location z,

T_o = the susceptor base temperature,

$\dot{Q}$ = the internal heat generation rate within the susceptor medium in terms of energy/mass,

ρ = the susceptor material density,

z = the axial coordinate of a general point.

For the purpose of this study then it has been useful to re-arrange Equation (1-2) in order to be explicit in the variable of interest;

$$\dot{Q} = \frac{k}{\rho} \cdot \frac{(T(z) - T_o))}{(Lz - z^2/2)} \qquad (1\text{-}2')$$

Equations (1-2) and (1-2') are approximations to the more complex solutions which would define conditions in the actual calorimeter. The equations do, however, relate the qualitative behavior of the system and additionally yield quantitative information concerning the limiting case of suppressed radiation from the susceptor surface.

Figure 3-1 is a plot of this limiting case temperature profile for a one inch long calorimeter susceptor fabricated from stainless steel. The internal heat generation rate is 3 watts per gram.

As has been acknowledged, radiation makes a non-zero contribution to the total heat transferred from the calorimeter susceptor. An attempt was made to modify the one-dimensional convection cooled fin[23,25] with internal heat generation to accommodate the non-zero radiation factor and obtain a closed form analytic solution. The general fin equation is:

$$\frac{d^2\theta}{dz^2} - \frac{1}{k} \cdot \frac{1}{A(z)} \cdot \frac{d\theta}{dz} - \frac{h_r}{k} \cdot \frac{1}{A(z)} \cdot \frac{dS(z)}{dz} \cdot \theta + \frac{\dot{q}}{k} = 0 \qquad (3\text{-}9)$$

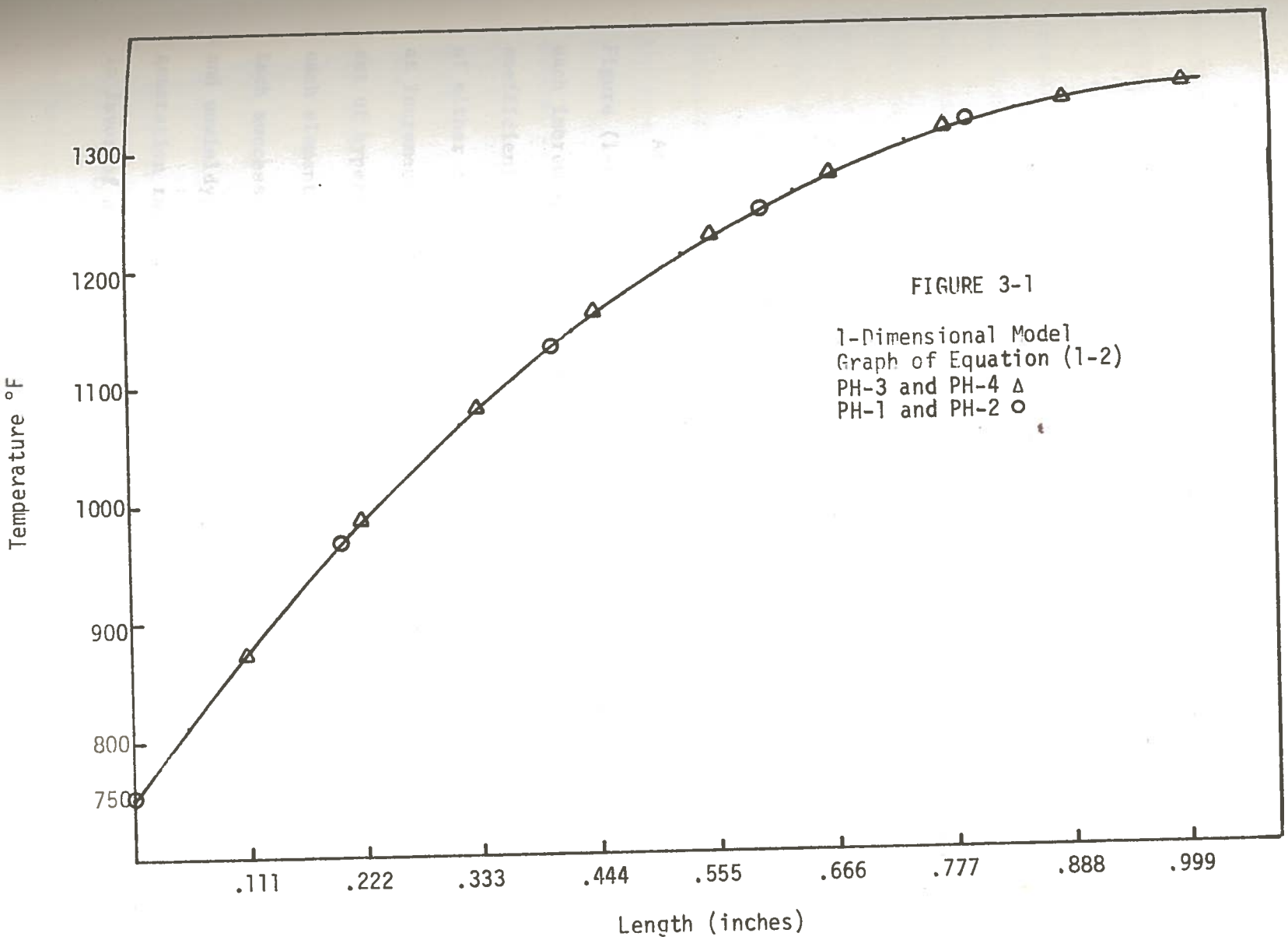

FIGURE 3-1

1-Dimensional Model
Graph of Equation (1-2)
PH-3 and PH-4 Δ
PH-1 and PH-2 O

where

$\theta = T(z) - T_f$

$T(z)$ = the axial temperature profile of the fin (susceptor);

T_f = the bulk temperature of the fluid to or from which convection takes place (modified herein to be the characterization temperature of the body(s) to which radiation takes place);

$A(z)$ = the cross sectional area of the fin (susceptor) as a function of axial position z;

$S(z)$ = the surface area per unit length of the fin (susceptor) as a function of axial position z; and

h_r = convection like radiation coefficient.

Attempts were made to solve this equation for the geometry of Figure (1-1) over incremental lengths of the "fin" or susceptor with each increment having a characteristic convection-like radiation coefficient h_r. In addition, there were provided boundary conditions, of either continuity of temperature or continuity of heat conducted at increment interfaces. The result in each case was a complicated set of hyperbolic functions with temperature as the dependent variable, each element of which applied to an increment of the susceptor. Each successive increment after the first became more complicated and unwieldy. A closed form solution for $\dot{q}$ or $\dot{Q}$, the internal heat generation rate, was not obvious, therefore the effort was abandoned in favor of a numerical analysis approach.

Initially this project was envisioned to be a parametric study using exclusively THTB[20], a sophisticated, three-dimensional, finite difference, heat transfer program to model the proposed calorimeter configurations. It was felt that in order to obtain a more thorough understanding of the problem and subsequent analysis, a general survey or qualitative investigation of configuration parameters would be self educating. Following the preceding simple analysis is an examination of finite difference modeling techniques to facilitate a better understanding of parameter interaction and permit more efficient utilization of program THTB. To that end, a study of simple numerical methods of heat conduction is undertaken. Following are some of the highlights of this study.

Descriptively speaking, numerical methods yield "numerical" values for temperatures, for example, at pre-selected, discrete points. Any generality as would be obtained from an analytical solution must be foregone. The finite difference approximations, upon which all general numerical methods are based, is used to render an algorithm for solving differential equations such as the general heat conduction equation with the radiation boundary condition. There are of course other methods of solving differential equations in general and the heat conduction equation in particular.

The basic principle of the numerical approach to a heat conduction problem is the replacement of the differential equation for the continuous temperature distribution in a heat conducting medium by a finite difference equation, which must be satisfied only at certain points in the field. Recall that for cartesian coordinates the general steady-state conduction equation is given by:

$$\frac{\partial}{\partial x}\left[k(T)\frac{\partial T}{\partial x}\right) + \frac{\partial}{\partial y}\left(k(T)\frac{\partial T}{\partial y}\right) + \frac{\partial}{\partial z}\left(k(T)\frac{\partial T}{\partial z}\right)\Big] + \dot{q} = 0 \qquad (3\text{-}10)$$

from Equation (3-4).

Within a volume chosen, if the temperature throughout is not subject to large variation, it is justifiable to assume that k(T) = constant = k. The general Equation (3-10) then becomes:

$$\frac{d^2T}{\partial x^2} + \frac{d^2T}{\partial y^2} + \frac{d^2T}{\partial z^2} + \frac{\dot{q}}{k} = 0. \qquad (3\text{-}11)$$

The relationship of the finite difference expression to the differential equation can be understood best by deriving the latter from the former using the Taylor Series expansion of a function of 3 variables, i.e.,

$$f = f(x, y, z)$$

Let h, m, and J > 0 represent increments in the variables x_o, y_o, z_o respectively. In general then, a forward expansion of the function to $x_o + h$, in terms of its value at x_o, y_o, z_o, a general point, is:[8]

$$f(x_o+h, y_o, z_o) = f(x_o, y_o, z_o) + h\frac{\partial f}{\partial x}(x_o, y_o, z_o) + \frac{h^2}{2}\frac{\partial^2 f}{\partial x^2}(x_o, y_o, z_o) + \frac{h^3}{3!}\frac{d^3 f}{\partial x^3}(x_o, y_o, z_o) + \sum_{i=4}^{n}\frac{h^i}{i!}\frac{\partial^i f}{\partial x^i}(x_o, y_o, z_o) . \qquad (3\text{-}12)$$

And similarly then a backward expansion of f yields

$$f(x_o - h, y_o, z_o) = f(x_o, y_o, z_o) - h \frac{\partial f}{\partial x}(x_o, y_o, z_o) + \frac{h^2}{2} \frac{\partial^2 f}{\partial x^2}(x_o, y_o, z_o) - \frac{h^3}{3!} \frac{\partial^3 f}{\partial x^3}(x_o, y_o, z_o) + (-1)^{n-1} \sum_{i=4}^{n} \frac{h^i}{i!} \frac{\partial^i f}{\partial x^i}(x_o, y_o, z_o) \qquad (3\text{-}13)$$

To obtain a central difference approximation to the second partial derivative it is necessary to add (3-12) and (3-13) while neglecting terms of order 4 and greater, therefore:

$$f(x_o+h, y_o, z_o) + f(x_o - h, y_o, z_o) \simeq 2 f(x_o, y_o, z_o) + h^2 \frac{\partial^2 f}{\partial x^2}(x_o, y_o, z_o) \qquad (3\text{-}14)$$

or the desired second derivative approximation is

$$\frac{\partial^2 f}{\partial x^2}(x_o, y_o, z_o) \simeq \frac{1}{h^2} [f(x_o + h, y_o, z_o) - 2 f(x_o, y_o, z_o) + f(x_o - h, y_o, z_o)] \qquad (3\text{-}15)$$

Similar expressions may be derived for the partial derivatives in terms of the other variables. If then $f(x, y, z) = T(x, y, z)$ and it is assumed that x_o, y_o, z_o is a general point we may write:

$$\frac{\partial^2 T}{\partial x^2} \simeq \frac{1}{h^2} [T(x + h, y, z) - 2\, T(x, y, z) + T(x - h, y, z)\ ] \tag{3-16}$$

$$\frac{\partial^2 T}{\partial y^2} \simeq \frac{1}{k^2} [T(x, y + k, z) - 2\, T(x, y, z) + T(x, y - k, z)\ ] \tag{3-17}$$

$$\frac{\partial^2 T}{\partial z^2} \simeq \frac{1}{J^2} [T(x, y, z + J) - 2\, T(x, y, z) + T(x, y, z - J)\ ] \tag{3-18}$$

Consider Equation (3-11) and its finite difference approximation letting $h = \Delta x$, $m = \Delta y$, $J = \Delta z$ which becomes:

$$\frac{k}{(\Delta x)^2} [T(x + \Delta x, y, z) - 2\, T(x, y, z) + T(x - \Delta x, y, z)\ ] +$$

$$\frac{k}{(\Delta y)^2} [T(x, y + \Delta y, z) - 2\, T(x, y, z) + T(x, y - \Delta y, z)\ ] +$$

$$\frac{k}{(\Delta z)^2} [T(x, y, z + \Delta z) - 2\, T(x, y, z) + T(x, y, z - \Delta z)\ ] + \dot{q} = 0. \tag{3-19}$$

The above expression (3-19) can be interpreted as representing the temperature at a point x in a medium, that is, T(x, y, z) in terms of the temperature at neighboring points $(x + \Delta x, y, z)$; $(x - \Delta x, y, z)$; $(x, y + \Delta y, z)$; $(x, y - \Delta y, z)$; $(x, y, z + \Delta z)$; $(x, y, z - \Delta z)$. Thus, if a body is divided into n distinct points, n distinct equations may be written; and this set of equations can be solved uniquely for the temperatures at the n points. This can be done without consideration for the temperature between said points. From the development of Equation (3-19) it is obvious that increased accuracy can be obtained

by decreasing Δx, Δy, and Δz (i.e., increasing the number of points). In fact the error will in general be on the order of $(\Delta x)^4$.

Consider the one-dimensional finite difference approximation which may be reduced from Equation (3-19) to yield:

$$\frac{k}{\Delta z^2}\left[T(z + \Delta z) - 2\,T(z) + T(z - \Delta z)\right] + \dot{q} = 0 \tag{3-20}$$

Convenient generalizations can be deduced from Equation (3-20) if consideration is given to the following:

Recall Equation (3-1')

$$\dot{q}_{cond} = -kA_k \frac{\Delta T}{\Delta z} = -\frac{\Delta T}{\Delta z/kA_k} \tag{3-21}$$

and we can define a total thermal conductive resistance R_k as,

$$R_k = \frac{\Delta z}{kA_k} \tag{3-22}$$

Suppose now for the one-dimensional case, the temperature profile under study is that in a bar of constant cross section Figure 3-2

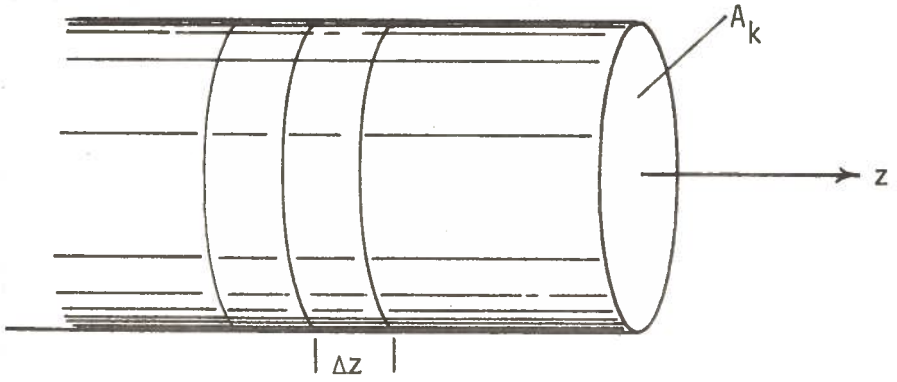

Bar of Constant Cross Section

FIGURE 3-2

Multiply Equation (3-20) by the volume of a bar increment, that is, $A_k \Delta z$ to obtain

$$A_k \Delta z \left(\frac{k}{\Delta z^2}\right) [T(z + \Delta z) - 2\, T(z) + T(z - \Delta z)] + \dot{q} A_k \Delta z = 0 \quad (3\text{-}23)$$

and the result is

$$\frac{kA_k}{\Delta z} [T(x + \Delta z) - 2\, T(z) + T(z - \Delta z)] + q = 0 \quad (3\text{-}24)$$

where $q = \dot{q}\, A_k\, \Delta z$

and it is seen

$$\frac{\Delta z}{kA_k} = R_k$$

constitutes a thermal resistance term as in Equation (3-22) and further it is possible to write Equation (3-24) in the form

$$\frac{T(z + \Delta z) - T(z)}{R_k} + \frac{T(z - \Delta z) - T(z)}{R_k} + q = 0 \quad (3\text{-}25)$$

In this form the expression suggests the electrical network analogy whereby:

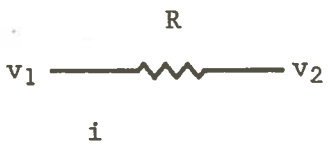

$$i = \frac{v_1 - v_2}{R} \quad (3\text{-}26)$$

Equation (3-25) suggests a summation of heat flow (energy balance) into point z a nodal point, from point, $z + \Delta z$, $z - \Delta z$ and internal

generation q (BTU/hr) at z. Therefore for a given node point i the net energy flow into i is given by:

$$\sum_{j=1}^{n} \frac{T_j - T_i}{R_{kij}} + q = 0 \qquad (3\text{-}27)$$

where,

T_j = temperature at nearest neighbor point to point i,

j = number of nearest neighbor nodes to node i,

T_i = temperature at i, and

R_{kij} = thermal conductive resistance between any nearest neighbor point j and point i, and in general

$$R_{kij} = \frac{\Delta_{ij}}{k_{ij} A_{kij}} .$$

Note that,

k_{ij} = the thermal conductivity of the material medium between point i and point j,

Δ_{ij} = the conduction distance between point i and point j, and

A_{kij} = the area normal to Δ_{ij} through which conduction between point i and point j takes place.

For a general node i, surrounded by 9 "nearest" neighbor nodes, Figure 3-3 is appropriate and Equation (3-27) becomes,

$$\sum_{j=1}^{9} \frac{T_j - T_i}{R_{kij}} + q = 0 \qquad (3\text{-}27')$$

or,

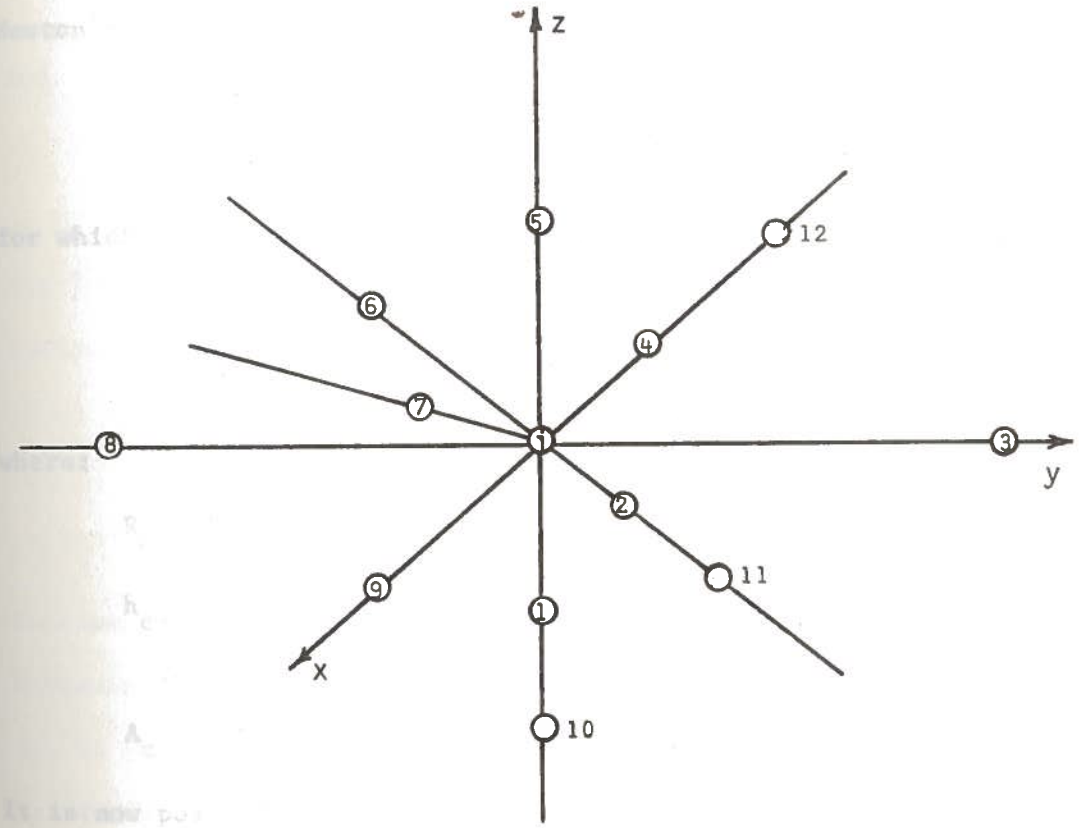

Multi-node Connection

FIGURE 3-3

$$\frac{T_1 - T_i}{R_{ki_1}} + \frac{T_2 - T_i}{R_{ki_2}} + \frac{T_3 - T_i}{R_{ki_3}} + \ldots + \frac{T_9 - T_i}{R_{ki_9}} + \dot{q} = 0$$

The energy balance interpretation of Equation (3-27) implies the viability of a more generalized extension to writing an energy balance for a surface point at which convection takes place. Recall Newton's Law of cooling,

$$\dot{q}_{conv} = h_c A_c (T_1 - T_\infty) = (T_1 - T_\infty)/(1/h_c A_c) \qquad (3\text{-}2)$$

for which it is reasonable to define a convective resistance, R_c

$$R_c = \frac{1}{h_c A_c}$$

where:

R_c = thermal convective resistance,

h_c = film coefficient for the fluid in contact with the medium surface, and

A_c = surface area from which convection takes place.

It is now possible to handle a convection boundary condition.

The boundary condition of interest, however, is a result of radiation. Use was made of the immediately preceding technique in order to extend the boundary point energy balance equation to include convection-like radiation heat transfer. Recall Equation (3-3') which gives an expression for two body radiation exchange between ideal gray bodies:

$$\dot{q}_{rad} = F'_{1-2} A_1 \sigma(T_1^4 - T_2^4). \qquad (3\text{-}3')$$

In order to obtain a useful form then, the following definition is derived

$$h_r A_1 (T_1 - T_2) = F'_{1-2}\, A_1\, \sigma(T_1^4 - T_2^4) \tag{3-28}$$

where

h_r = convection like radiation coefficient,

and

$$h_r = \frac{F'_{1-2}\, A_1\, \sigma(T_1^4 - T_2^4)}{A_1(T_1 - T_2)} \tag{3-29}$$

The "exchange factor" for a complete enclosure formed by two gray bodies is given by:[6,8]

$$F'_{1-2} = \frac{1}{\frac{1}{F_{1-2}} + \frac{A_1}{A_2}\left(\frac{1}{\varepsilon_2} - 1\right) + \left(\frac{1}{\varepsilon_1} - 1\right)} \tag{3-30}$$

In summary then, the energy balance for a general point in a one-dimensional bar can be treated with the aspects of the preceding, that is, an expression for the temperature at a general point i can be written in terms of the following energy balance:

$$\sum_{j=1}^{n} \frac{T_j - T_i}{R_{ij}} + q = 0 \tag{3-31}$$

Conductive resistance: $$R_{kij} = \frac{\Delta_{ij}}{k_{ij} A_{kij}} \tag{3-32}$$

Convective resistance: $$R_{cij} = \frac{1}{h_{cij} A_{cij}} \tag{3-33}$$

Radiative resistance: $$R_{rij} = \frac{1}{h_{rij} A_{ij}} \qquad (3\text{-}34)$$

The preceding abbreviated analysis was used to develop the finite difference approximations to the heat conduction equation, and necessary boundary conditions for treatment of the problem at hand. The resulting expressions allow the replacement of the differential equation for heat conduction in a body with an algebraic expression which applies at a nodal point and over an incremental region. As previously stated, the application of Equation (3-24) or (3-31) involves dividing the body of interest into incremental regions with nodal points at their respective centers. This division does not require symmetry. For each node then, an expression for its temperature in terms of its nearest neighbors' temperatures can be written. The resulting system of equations can be solved in an iterative fashion by the method of successive approximations. For ease of adaptation to a scheme amenable to digital computer solution, it is useful to rewrite Equation (3-31) in the following form:

$$T_i = \frac{\sum_{j=1}^{n} T_j/R_{ij} + q_i}{\sum_{j=1}^{n} 1/R_{ij}} \qquad (3\text{-}35)$$

for the temperature T_i at nodal point i. Recall that j is indicative of properties such as temperature at nearest neighbor points denoted by their indices.

The Gauss-Seidel iteration method is used for solution of the n point system.[26] The method consists of assuming an initial set of nodal temperatures $(T_i)_1$ (where the nodal temperatures are unknown), then using the n equations generated to calculate a new set of temperatures $(T_i)_2$ for each point, i. The set $(T_i)_2$ is used to calculate a third set $(T_i)_3$. The iterative generation is continued until there is an acceptably small difference between successive values of the temperature at each node. Satisfaction of this condition is generally expressed as

$$\left| [T_i]_{n+1} - [T_i]_n \right| \leq \varepsilon \tag{3-36}$$

where ε is a predetermined convergence criteria, for example $\varepsilon = 0.1$, and n and n + 1 indicate the n^{th} and $n + 1^{st}$ iterative calculations respectively.

Convergence is assured since the equation yields a system included in which is a known condition(s), temperature(s), and/or heat generation rate(s), at some point(s). Thus, the iterative solution consists of a weighted averaging process.[23] At the point in the network where conditions are known their values are continually averaged in with the incorrect values of the unknowns. The rate of convergence is difficult to ascertain; accuracy depends upon the node point spacing and the convergence criteria, ε. Improved accuracy can be obtained by using more node points and smaller values of ε. This increased accuracy is obtained at the expense of requiring a larger number of iterations, hence longer computing time. Rapidity of convergence will be enhanced by the closeness of the initial guesses to the actual temperatures.

Calorimeter determinations of the type in which this study is interested are made on an inferred or implicit basis, i.e., the program algorithms define a relationship of the form (qualitatively).

$$T = f_1(\dot{Q}, K, \varepsilon_1, \varepsilon_2, z, \ldots.) \tag{3-37}$$

There is no explicit relationship readily definable therefrom as:

$$\dot{Q} = f_2(T(z), K, \varepsilon_1, \varepsilon_2, z, \ldots.) \tag{3-38}$$

The implicit functionality is therefore defined by evaluating f_1 for a particular domain, e.g., $3.0 \leq \dot{Q} \leq 4.0$ watts/gm with the remaining variables constant, (Figure 3-4).

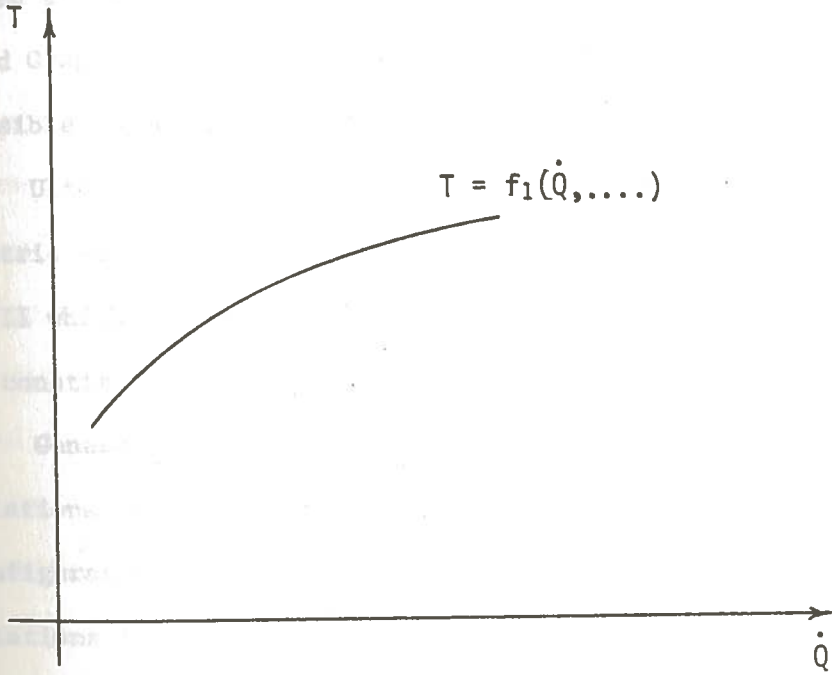

Qualitative Graph of $T = f_1(\dot{Q},\ldots.)$

FIGURE 3-4

By inference then $\dot{Q} = f_1^{-1} = T^{-1}$ is obtained.

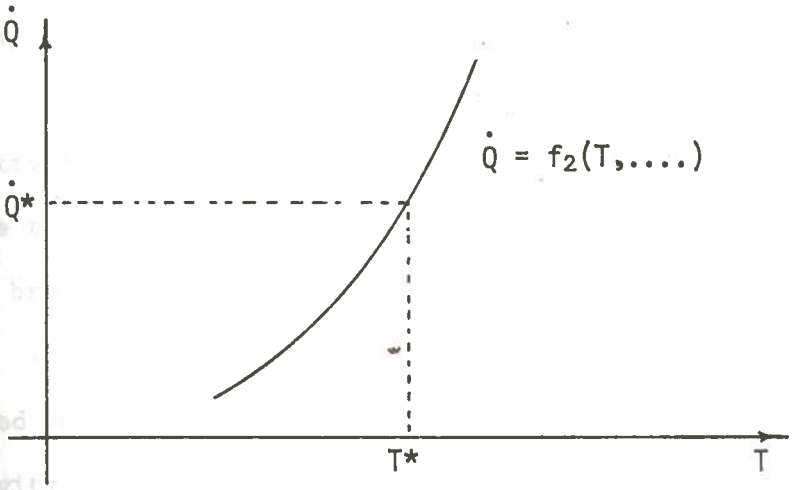

Qualitative Graph of $\dot{Q} = T^{-1}$
FIGURE 3-5

From such a relationship calorimetry measurements are made, for example: The temperature in the calorimeter characterized by f_2 is measured at Z* and denoted T* measured, then going to the previously defined Graph for $\dot{Q} = T^{-1}$, Figure 3-5, the heat generation rate responsible for causing T* at location Z* is determined to be $\dot{Q}^*$.

Ultimately three generations of computer codes, for the parametric study, have been developed; they are Generation I and Generation II which are described in this chapter, while the modification which constitutes Generation III is explained in Chapter 5, Error Analysis.

Generation I possesses two programs, PH-1 which handles calculations for the solid susceptor, unshielded calorimeter envisioned in Configuration A, shown in Figure 2-3, and PH-2 which handles calculations for the heat shielded susceptor of Configuration B, shown in Figure 2-4. Both programs are listed in Appendix B and utilize the basic algorithms of Equations (3-30), (3-32), (3-33), (3-34), and (3-35), to accommodate the heat transfer modes existent in the

configurations previously described. Uniaxial conduction is assumed for simplicity and a six susceptor node network (as shown in Figures 3-6 or 3-7) is used in each case. Program PH-1 and PH-2 solve respectively the electrical analogy networks of Figures 3-6 and 3-7 for the temperatures at the nodal points and the thermal currents in the branches.

Thermal properties are assumed to be constants, with properly averaged values for the thermal conductivity and total hemispherical emissivity calculated for the temperature range applicable and utilized in the algorithms.

It should be noted that a subroutine HIGH uses Equations (3-30) and (3-34) in PH-1 and PH-2 to model the radiation heat transfer mechanism.

The radiation interaction is treated as a one to one exchange, between a susceptor node and a containment tube node, Figure 3-6, in the case of the solid susceptor of Configuration A. In the case of the heat shielded susceptor of Configuration B, Figure 3-7, one-to-one exchange is assumed between a susceptor node and a heat shield node or a heat shield node and a containment tube node. Expression (3-30) defines the exchange relationship with the assumption that $F_{1-2} = 1$, which implies that "all" radiation leaving the transmitting node is intercepted by the receiving node. This one to one transfer is not the actual mechanism of radiation in such a system, however, it is an assumption which facilitates obtaining a solution to the overall system. The disadvantages, to this assumption are analyzed and quantified in Chapter 5. Radiation from the end of the susceptor is

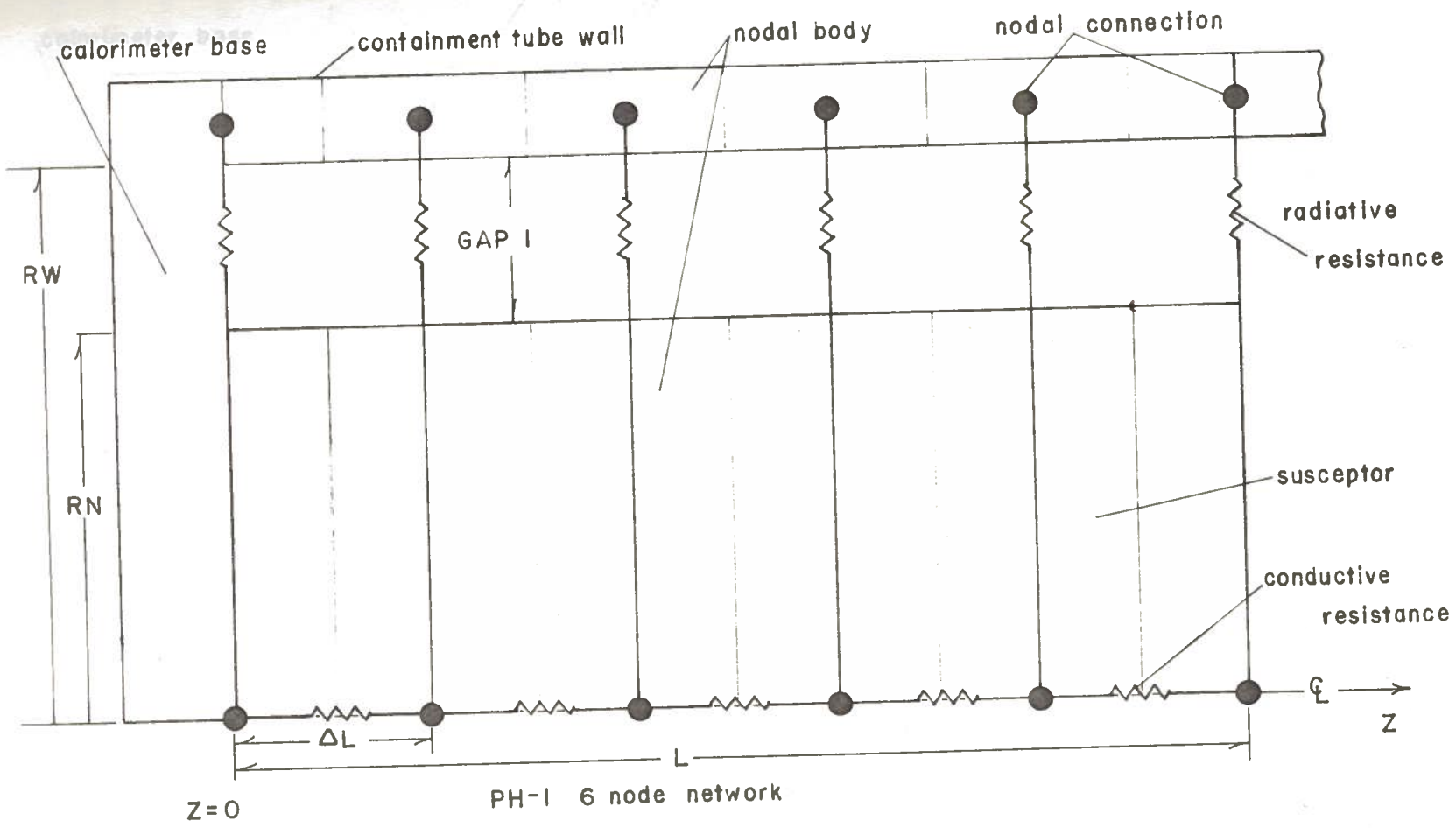
calorimeter base
containment tube wall
nodal body
nodal connection
GAP I
RW
RN
radiative
resistance
susceptor
conductive
resistance
ΔL
L
Z=0
PH-I 6 node network
Z

FIGURE 3-6

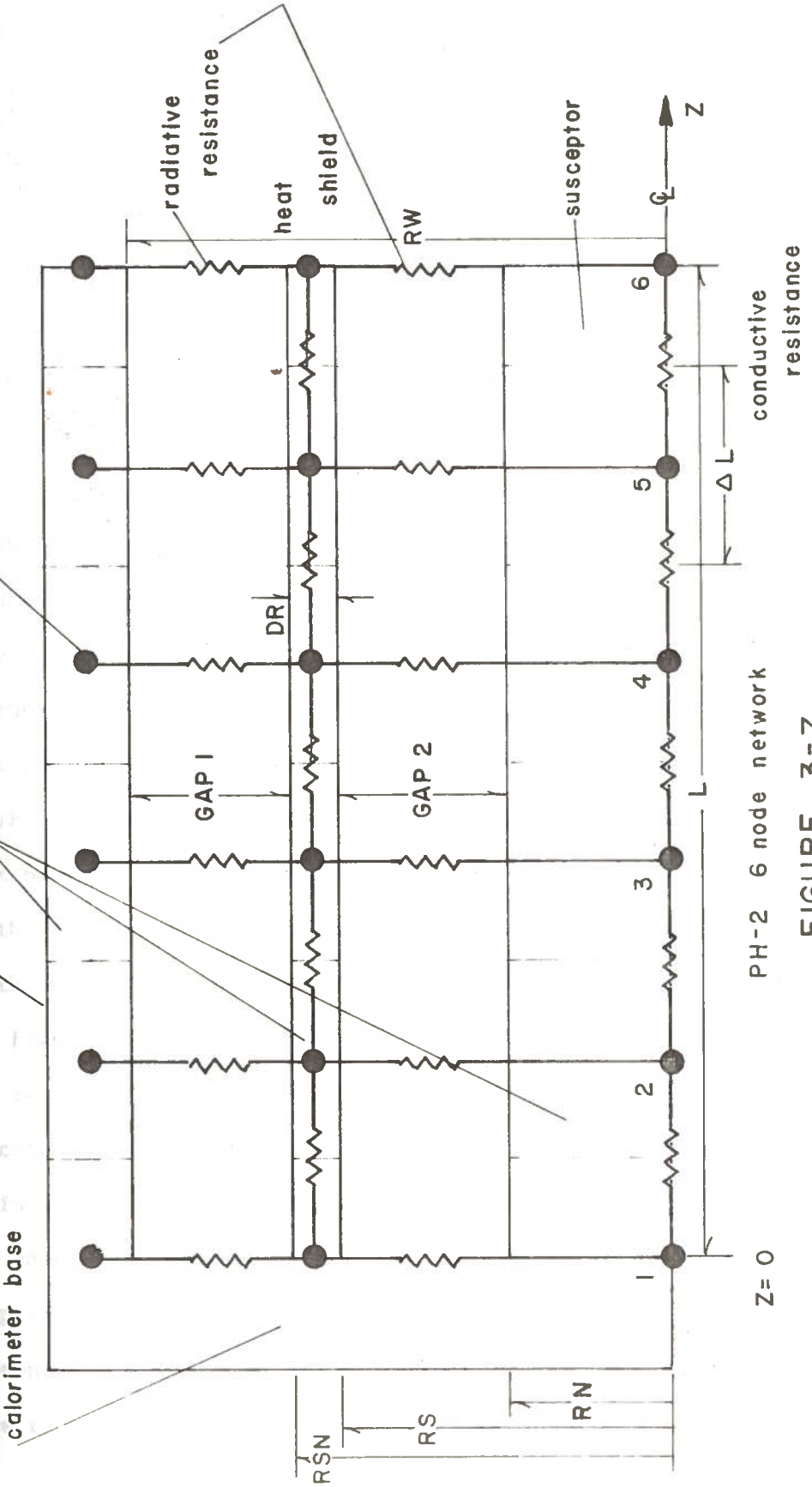

PH-2 6 node network

FIGURE 3-7

neglected by virtue of the simplifying assumption of mirror image susceptors previously described in Figures 2-3 or 2-4.

Two trial runs are used for performance evaluation. The first run for each program is to compare the limiting case of zero radiation as described by Equation (1-2) with the computer code calculations for a similar configuration with emissivities reduced to a value of 1×10^{-36}. The parameters used for the evaluation are summarized in Table G-1 of Appendix G.

Figure 3-1 illustrates that both PH-1 and PH-2 converge to the analytically derived result for the one-dimensional geometry when the surface emissivities are reduced to a value of 1×10^{-36}.

The second set of runs compares PH-1 and PH-2 performance to identical runs for program THTB. The configuration parameters for each of the two cases are given in Tables G-2 and G-3, Appendix G.

THTB verifies the validity of the one-dimensional assumption, in that the maximum deviation of the radial temperature profile is 0.4°F for the solid susceptor of Configuration A, Figure 2-3 and 0.1°F for the heat shielded susceptor of Configuration B, Figure 2-4. Table 3-1, Figure 3-8, and Figure 3-9 summarize the comparison data. Figure 3-8 relates the temperature profile comparison between PH-1 and THTB according to the input format of Table G-2. The maximum deviation in the temperature profiles occurs at the ends of both susceptors where PH-1 predicts a temperature that is 1% lower than the value predicted by THTB. PH-1 overpredicts the rate of heat efflux by conduction from the susceptor base by 1%. Figure 3-9 relates the temperature profile comparison between PH-2 and THTB

Table 3-1

Comparison Data

Comparison Parameter	PH-1	THTB (Solid Susceptor)	PH-2	THTB (Heat Shield)
Maximum susceptor temperature, TN max	1310°F	1317.5°F	1315°F	1320.5°F
Maximum heat shield temperature, TS max	--	--	1253°F	1297.6°F
Rate of conduction from susceptor base, QCN	271 BTU/hr	268.3 BTU/hr	48.7 BTU/hr	48.34 BTU/hr

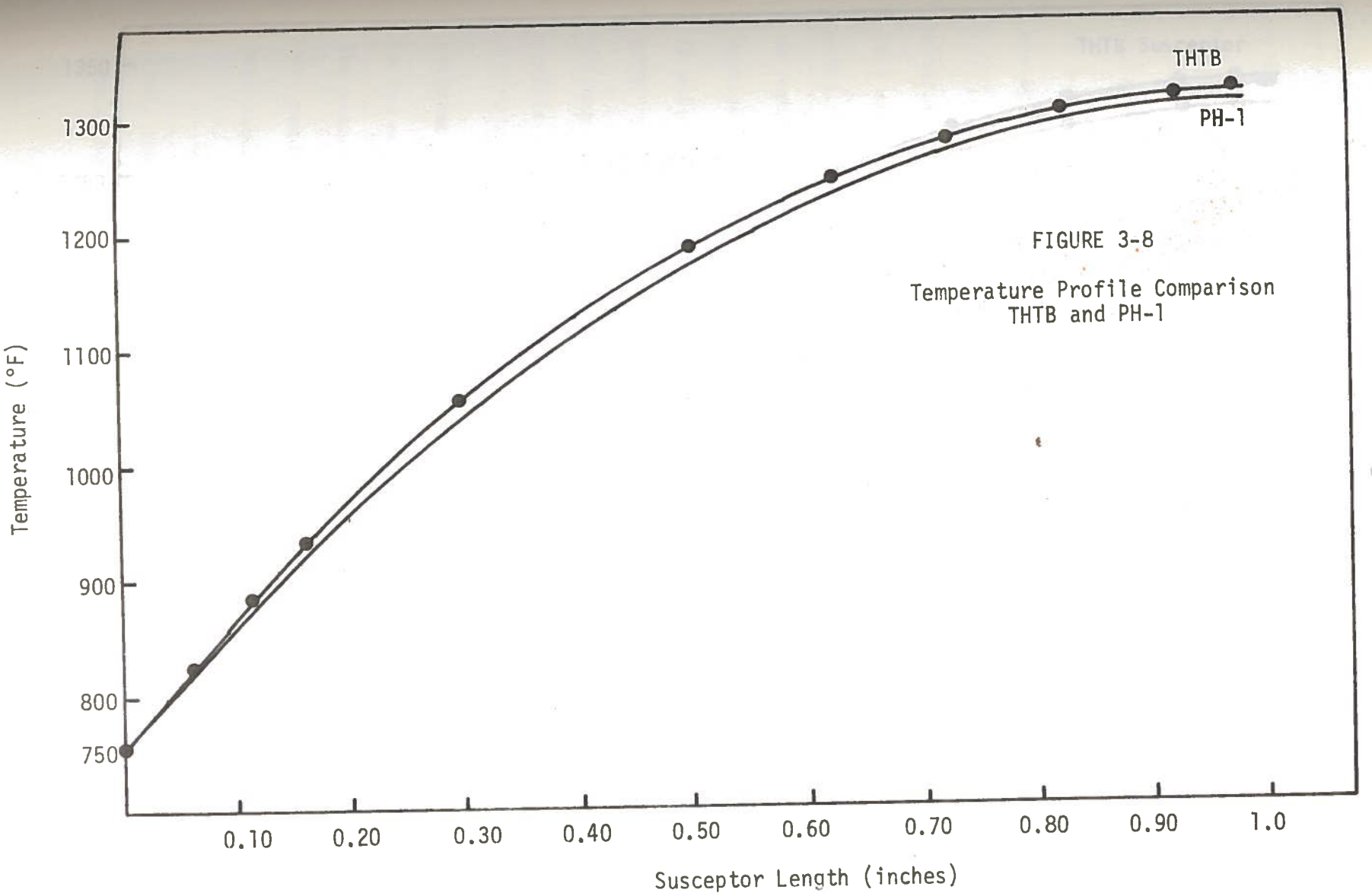

FIGURE 3-8

Temperature Profile Comparison
THTB and PH-1

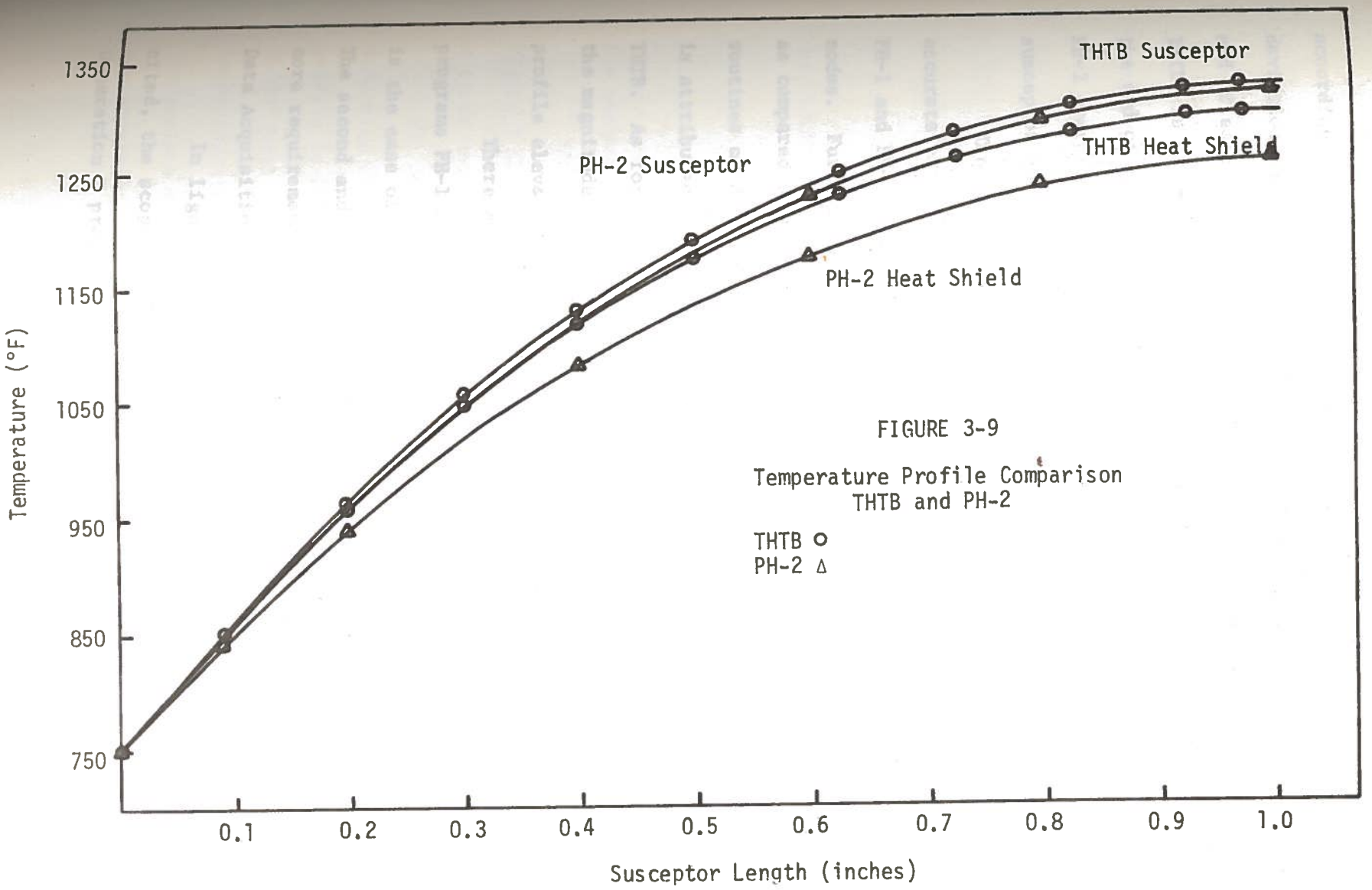

FIGURE 3-9

Temperature Profile Comparison
THTB and PH-2

THTB ○
PH-2 △

according to the input format of Table G-3. The maximum temperature deviation in the susceptors with heat shields again occurrs at the end of each. PH-2 predicts a value 0.9% lower than the value from THTB; in a similar fashion PH-2 underpredicts the temperature at the end of the heat shield by 8.1% relative to the value of THTB. PH-2 overpredicts the value of energy conduction rate from the susceptor base by 0.74%.

The comparative values from PH-1 and PH-2 are suprisingly accurate considering the relative crudeness of the approximation; PH-1 and PH-2 use the coarse 6 node network while THTB uses 20 axial nodes. Furthermore, THTB uses temperature dependent thermal properties as compared to the constant, average values used in the simple routines of PH-1 and PH-2. The relatively elevated temperature profiles is attributed to the "radiation exchange factor" algorithm used by THTB. As formulated in the reference,[13] this algorithm underestimates the magnitude of radiation heat transfer thus causing a temperature profile elevation.

There appear to be two clear-cut advantages to the simple programs PH-1 and PH-2, when compared to THTB. The first advantage is the ease of manipulation of the input data for the simple programs. The second and more important advantage is that with the more limited core requirements, PH-1 and PH-2 can be used on the more accessible Data Acquisition Systems, Sigma-5-XDS computer at ANL-W.

In light of the relative accuracy and the other advantages cited, the scoping analysis of the parametric study is done with the Generation I programs.

The validity of the qualitative proposition, Equation (2-6) can be easily verified with program PH-1. A plot of the ratio of heat transfer rate by radiation, QR to the heat transfer rate by conduction, QC, as a function susceptor radius RN can be seen in Figure 3-10. A power curve fit to the data is obtained in the form

$$y = ax^b$$

i.e.,

$$\frac{QR}{QC} = a(RN)^b \qquad (3\text{-}39)$$

for which it is found that

$$a = 7.742 \times 10^{-3}$$

$$b = -1.269$$

The qualitative assessment of $QR/QC \propto 1/RN$ is a good approximation.

Additional information is obtained by examination of Figure 3-11 for which it is noted that with a fixed susceptor radius, a fixed heat shield inside radius and a variation in shield thickness, it is the increasing shield thickness which is responsible for the reduction in radiation. The resulting perturbation in susceptor profile is from a minimum of 1316°F end point temperature with a 0.040" heat shield thickness to a maximum of 1322°F end point temperature with a 0.10" heat shield thickness. While the shield temperature profile is perturbed significantly upward, 1253°F to 1295°F the susceptor temperature profile is perturbed only slightly.

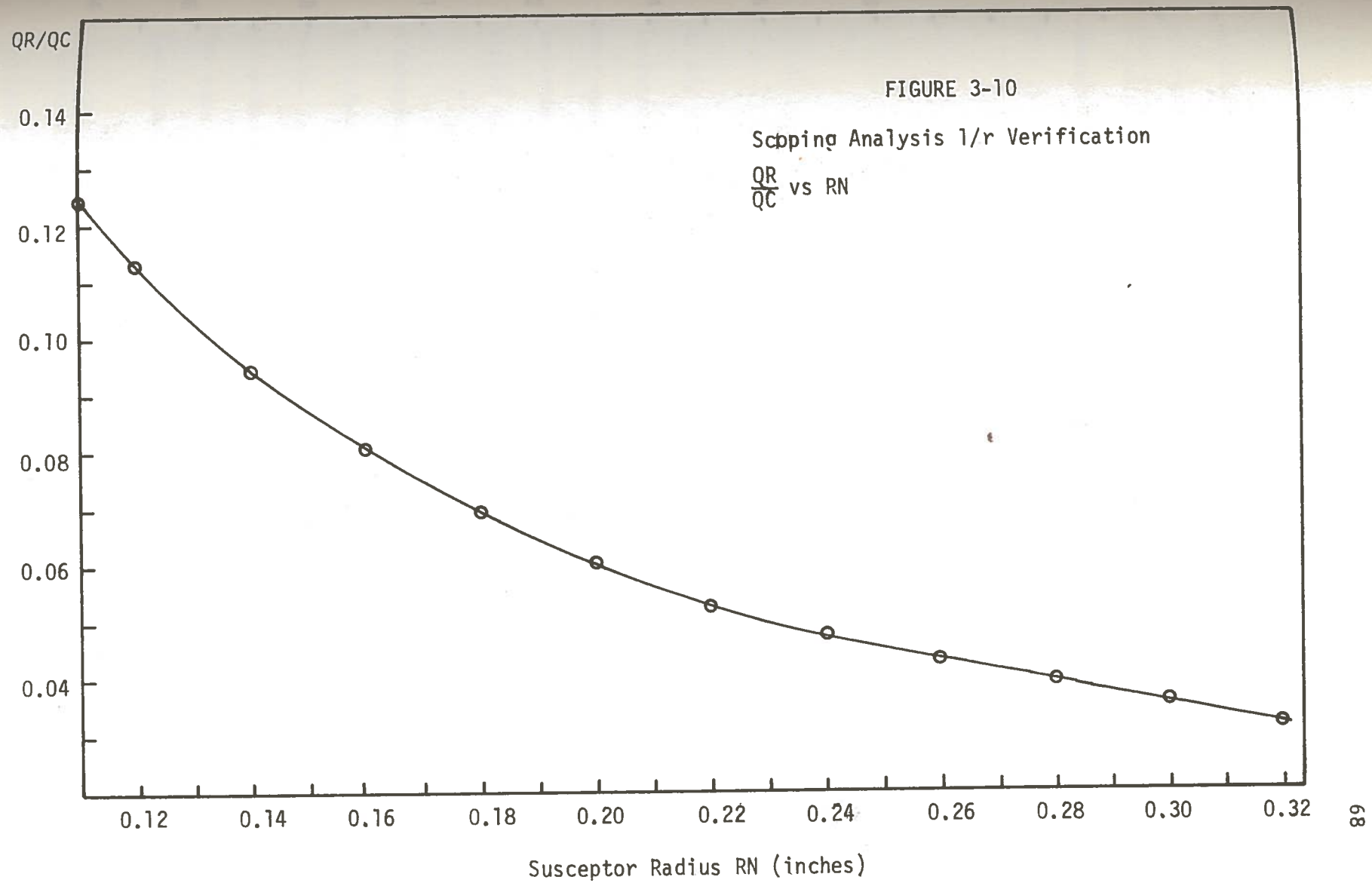

FIGURE 3-10

Scoping Analysis 1/r Verification

$\frac{QR}{QC}$ vs RN

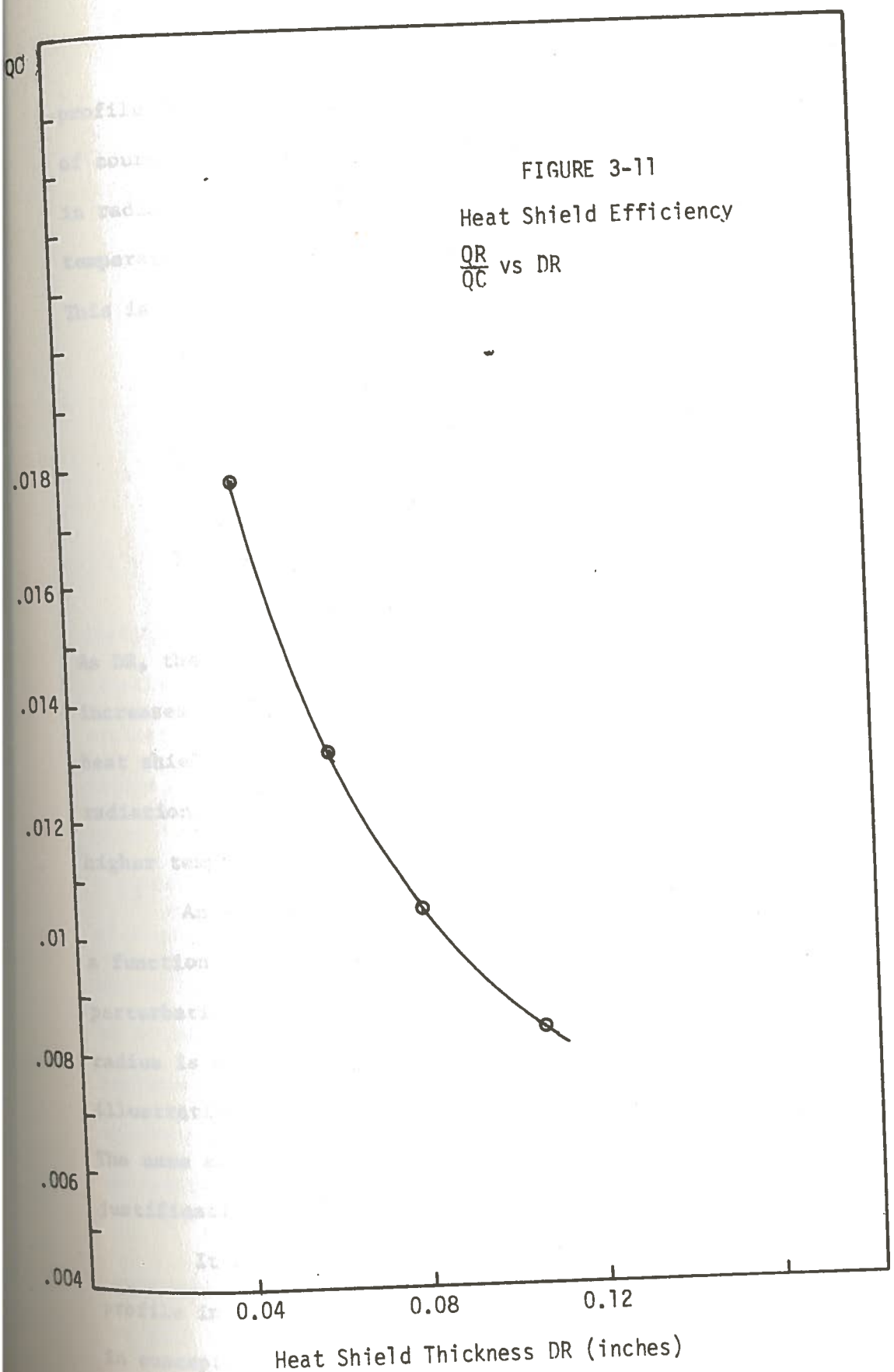

FIGURE 3-11

Heat Shield Efficiency

$\frac{QR}{QC}$ vs DR

The slight upward perturbation of the susceptor temperature profile is due to the small reduction in the heat radiation rate, and of course, the reduction in radiation rate is because of the elevation in radiation sink (heat shield) temperature. The heat shield temperature profile on the other hand is perturbed significantly upward. This is expected if it is realized that:

1) the internal heat generation rate in the shield is proportional to the shield volume (mass)
2) the shield volume (mass) increases in proportion to $L \cdot [(RS + DR)^2 - RS^2]\pi = (2RS \cdot DR + DR^2)\pi \cdot L$
3) the radiation rate from the shield increases in proportion to $2\pi\ (RS + DR)\ L$.

As DR, the heat shield thickness, increases, the ratio of 2) to 3) increases. This implies that the total heat generation rate in the heat shield is increasing faster than the heat transfer rate by radiation, thus the temperature profile equilibrates at slightly higher temperatures for thicker heat shields.

An examination of the perturbation in temperature profile as a function of susceptor radius is also made. The maximum perturbation in the temperature profiles as a function of susceptor radius is seen to occur at the susceptor end point. Table 3-2, is illustrative of end point perturbation for an unshielded susceptor. The same effect is noted for the heat shielded susceptor, and the justification follows the reasoning of the preceding paragraph.

It is concluded that generally speaking the temperature profile in the susceptor is not strongly perturbed by fluctuations in susceptor radius.

Table 3-2

End Point Perturbation for Configuration A

Susceptor radius, inches	End point temperature, °F
0.11	1280
0.13	1290
0.16	1300
0.21	1300
0.22	1310
0.31	1310

The final step of the scoping analysis is to compare the performance of the two calorimeters, Configuration A and B on some relative basis. A convenient measure of relative performance is to evaluate the ratio QR/QC as a function of RWK, the working volume radius defined in Chapter 2. Figure 3-12 is a plot of the data generated with PH-1 and PH-2. For the limited domain examined, two important facts are obtained. First, both configurations are capable of significantly reducing the relative energy radiation rate, and secondly, the heat shielded susceptor suppresses the radiation rate to a greater extent for the same working volume. The results represent qualitative behavior, because of the crudeness of the approximation, however, the relative magnitudes are expected to be maintained under finer network analysis.

Evaluation of PH-1 and PH-2 overall performance is most encouraging. Limiting case behavior is excellent, and comparison runs to THTB are very good. In fact, it is felt that in the case of

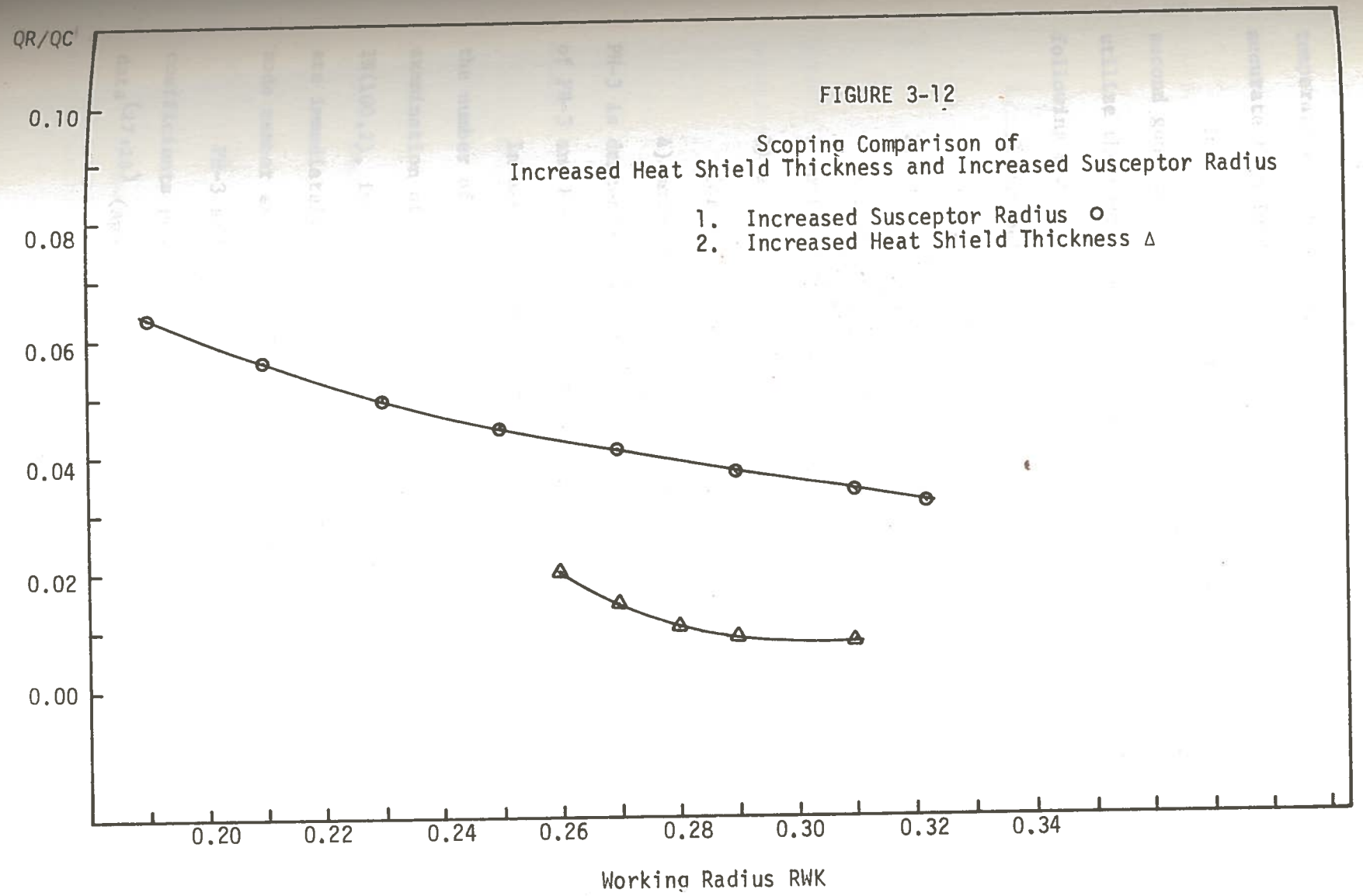

FIGURE 3-12

Scoping Comparison of
Increased Heat Shield Thickness and Increased Susceptor Radius

1. Increased Susceptor Radius o
2. Increased Heat Shield Thickness Δ

temperature profile deviations, PH-1 and PH-2 are, if anything, more accurate than THTB.

Due to the preceding evaluation, it has been decided that a second generation of programs will be written. These programs will utilize the same basic algorithms as did PH-1 and PH-2, with the following exceptions:

1) the network size will be expanded to handle a larger number of nodes to enhance accuracy;
2) temperature dependent thermal properties, that is, thermal conductivity and total hemispherical emissivity, will be incorporated;
3) a convergence acceleration routine will be added for efficiency; and
4) more efficient core storage will be provided.

PH-3 is descended from PH-1, and PH-4 is descended from PH-2. Listings of PH-3 and PH-4 are found in Appendix E.

In essence, the network size, or in the one-dimensional case, the number of axial susceptor nodes treated, is unlimited. An examination of the dimension and common statements, for example TN(100,2), implies that the number of nodes for which PH-3 and PH-4 are immediately equipped to handle is 100. (The first index denotes node number and the second denotes iteration number).

PH-3 and PH-4 use a third degree polynomial expression, with coefficients generated by least squares fitting of experimental data[27,28] (Appendix C), in subroutine THMKN, and subroutine THMKS

to calculate the temperature dependent thermal conductivities in the susceptor and shield materials, respectively.

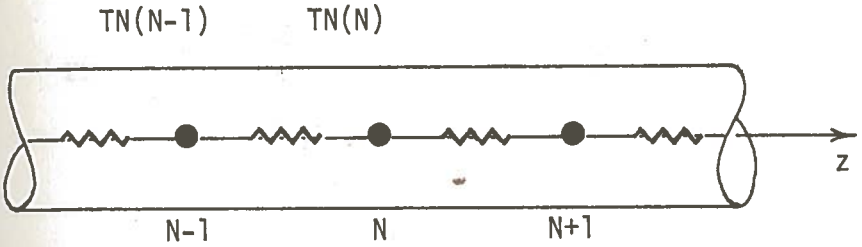

As an example the thermal conductivity used for conduction between susceptor nodes (N - 1) and (N), Figure 3-13, is generated from the following expressions.

$$KN(N) = A_3(TN(N)_{AVG})^3 + A_2(TN(N)_{AVG})^2 + A_1(TN_{AVG}) + A_o \qquad (3\text{-}40)$$

where

KN(N) = the susceptor thermal conductivity between nodes N and N - 1 with respective temperature TN(N) and TN(N - 1).

$TN(N)_{AVG} = \frac{TN(N) + TN(N-1)}{2}$.

A_o, A_1, A_2, A_3 = the polynomial coefficients generated by least squares fitting.

Temperature dependent emissivities for the susceptor, heat shield, and containment tube wall are generated by subroutine EN, ES,

and EW, respectively. A third degree polynomial expression is fit to experimentally generated data, that is:

$$EN(N, TN) = a_3TN^3 + a_2TN^2 + a_1TN + a_o \qquad (3\text{-}41)$$

EN(N, TN) = the susceptor emissivity at node N with temperature TN.

TN = the temperature of node N, and

a_o, a_1, a_2, a_3 = polynomial coefficients generated by least squares fitting.

The emissivity value is assumed to be constant over the incremental surface area assigned to each respective node.

Convergence of nodal temperatures to their true values is assured by virtue of the weighted averaging process utilized and previously described; however, the rate of convergence cannot be easily inferred beyond stating that in general, the more nodes in the network the more iterations required and hence the slower the convergence. The temperature values successively computed for a given node assymptotically approach the actual temperature. It is therefore possible, if convergence is sufficiently slow overall, that the successive temperatures at each node will be within ε, the convergence criteria, of each other, that is:

$$T_{N+1} - T_N \leq \varepsilon$$

and yet the temperatures might not have converged to their respective actual values. Care must therefore be exercised in choosing ε; in general the larger the network the smaller should be the ε. This

effect was noted on two occasions with PH-3. The limiting case of a purely one-dimensional bar Equation (1-2) with internal heat generation converges to an end point temperature of 1341°F when:

$$T_o = 752°F,$$

$$\dot{Q} = 3.75 \text{ watts/gm},$$

$$L = 1.0",$$

and

$$\bar{k} = 13.44 \text{ BTU/hr ft°F}$$

PH-3, for this geometry, independent of cross sectional area, converges to 1339°F or two degrees below the actual value with $\varepsilon = 0.1$. When ε was reduced to 0.05, PH-3 converges to the true temperature of 1341°F, a demonstration of the effect just described.

The convergence rate for this algorithm, in the form used in PH-4 does not appear to be easily accelerated as the use of a Richardson's Method[26] acceleration demonstrates. PH-4 is actually an analysis of two coupled one-dimensional configurations. Consider that the temperature at a nodal point in the susceptor is given by TN(N, I) where N equals a node number and I equals an iteration number, and similarly for TS.

In general,

$$TN(I, 2) = f(TN(I, 1)), TS(I, 1),....) \qquad (3\text{-}42)$$

and

$$TS(I, 2) = F(TN(I, 1)), TS(I, 1)....). \qquad (3\text{-}43)$$

In the normal course of calculating events the temperatures are initialized at each node point, for example, TN(N, 1), N = 1, 2.... N_{max}. N_{max} = number of nodes, in the susceptor and heat shield. Therefore, the temperatures for the respective points are recalculated from the algorithm generated in Chapter 3, Equation (3-35), so that a new set of susceptor temperatures are realized: TN(N, 2) = f(TN(N, 1), TS(N, 1),....), N = 1....N_{max}. A similar set of calculations if performed for TS, that is, a set of heat shield temperatures is calculated from the initialized values or the values from the previous iteration step. It was felt that perhaps an acceleration in convergence would be afforded by altering the values utilized in the general step 2, that is;

$$TN(N, 2) = f(TN(N, 1)), TS(N, 1)....), \quad \text{Step 1}$$

and

$$TS(N, 2) = F(TN(N, 1)), TS(N, 1)....). \quad \text{Step 2}$$

Then, by utilizing the most recently calculated value for the TN, namely, TN(N, 2) instead of TN(N, 1) to calculate TS then qualitatively there would be a new Step 2 that is Step 2':

$$TS(N, 2) = F(TN(I, 2)), TS(N, 1)....) \quad \text{Step 2'}.$$

The modification is inserted into a 20 node configuration which has previously converged in 1021 iterations; the modified routine converges in 1002, a net savings of 19 iterations:

Each of the two programs PH-3 and PH-4 is given two "trial runs" for performance evaluation. The first run for each program is to compare the limiting case of zero radiation as described by Equation (1-2) with the computer code calculations for a similar configuration with reduced emissivities. Table G-1, PH-1 and PH-2

parameter values, are the same as those used for programs PH-3 and PH-4, respectively, with the exception of the value cited for thermal conductivities; PH-3 and PH-4 instead utilize the least squares generated polynomial expression for stainless steel found in Appendix C. Figure 3-1 shows that both PH-3 and PH-4 converge to the analytically derived result if the emissivities are reduced to 1×10^{-36}.

The second set of runs is to compare PH-3 and PH-4 performance to analogous runs for program THTB. The configuration geometry is the same for PH-3 and PH-4 as was utilized in the second runs for PH-1 and PH-2 respectively. The geometry is related in Tables G-2 and G-3 with the exception that the conductivity data is temperature dependent as related by the least squares fit polynomial expression for stainless steel found in Appendix C.

Table 3-3, Figure 3-13 and 3-14 summarize the comparison data. Figure 3-13 relates the temperature profile comparison between PH-3 and THTB. The maximum deviation in temperature profiles occurs at the ends of both susceptors where PH-3 predicts a temperature 9.5°F or 1.67% lower than THTB. PH-3 overpredicts the rate of conduction from the base node by 1.3 BTU/hr or 0.48% relative to THTB. Figure 3-14 relates the temperature profile comparison between PH-4 and THTB, wherein the maximum deviation in temperature profiles in the susceptor again occurs at the end of each; PH-4 predicts a temperature value 1.5°F or 0.26% higher than THTB. PH-4 underpredicts the temperature at the end of the heat shield by 44.6°F or 8.1% relative to THTB. Finally PH-4 overpredicts the energy conduction rate

Table 3-3

Comparison Data: PH-3 and PH-4 to THTB

Comparison Parameter	PH-3 (Solid Susceptor)	THTB (Solid Susceptor)	PH-4 (Heat Shield)	THTB (Heat Shield)
Maximum susceptor temperature, TN_{max}	1308.0°F	1317.5°F	1322.0°F	1320.5°F
Maximum heat shield temperature, TS_{max}	--	--	1253.0°F	1297.6°F
Rate of conduction from susceptor base, QCN	267 BTU/hr	268.3 BTU/hr	48.9 BTU/hr	48.34 BTU/hr

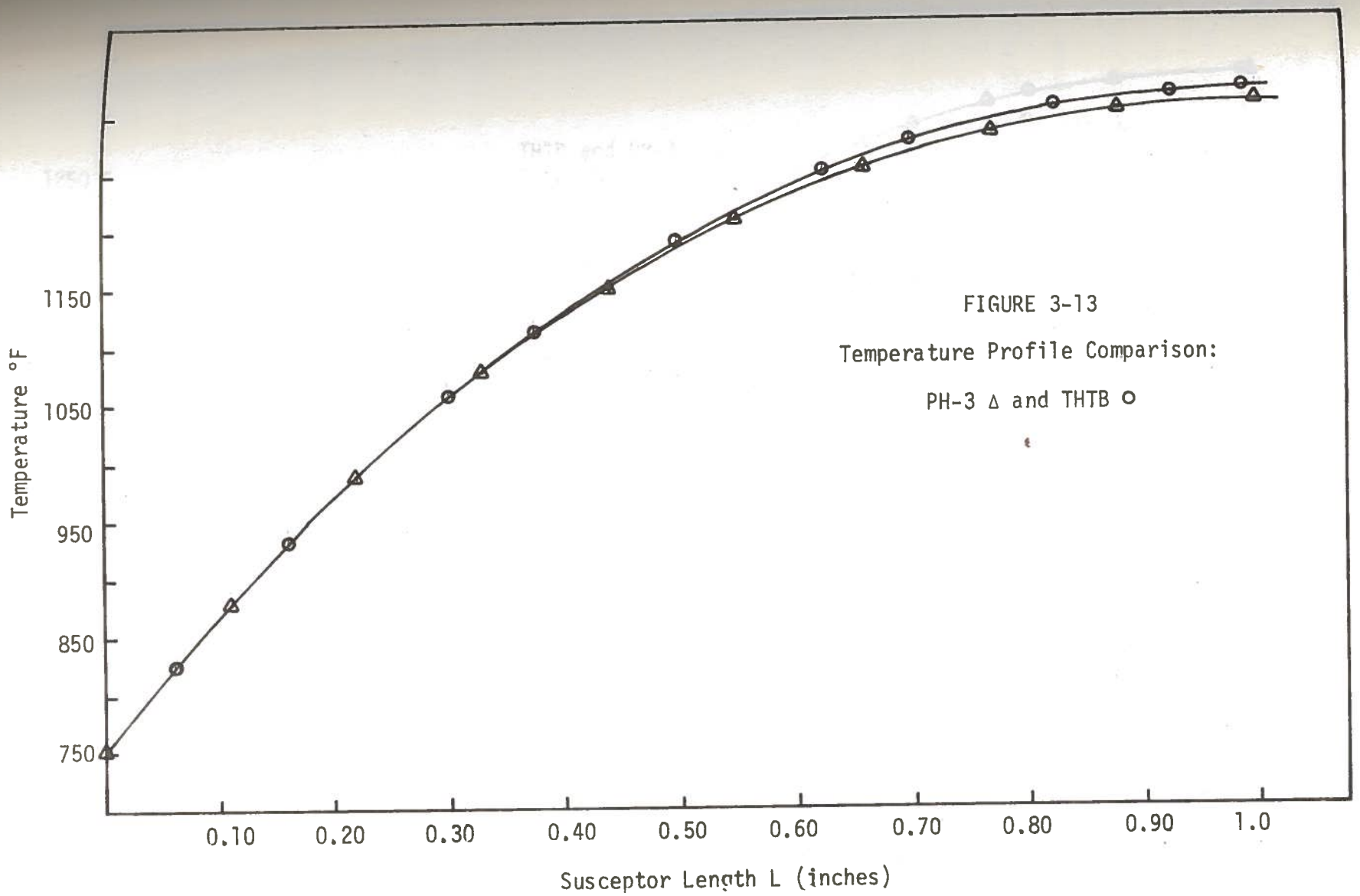

FIGURE 3-13

Temperature Profile Comparison:

PH-3 Δ and THTB O

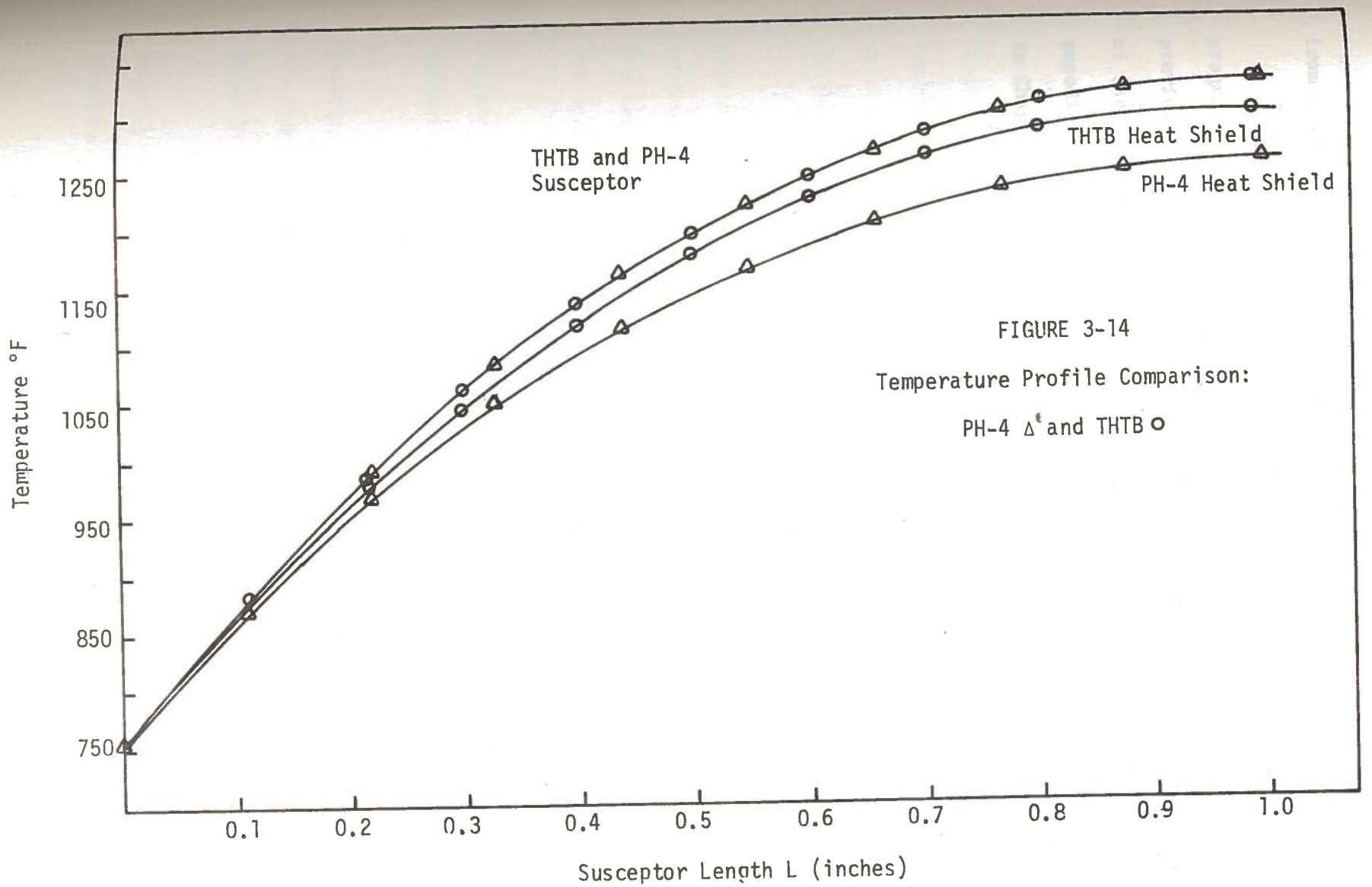

FIGURE 3-14

Temperature Profile Comparison:

PH-4 Δ and THTB O

from the susceptor base by 0.56 BTU/hr or 1.16%.

The improvements sought in the evolution to Generation II programs, PH-3 and PH-4, are realized while preserving the advantages previously cited. It is therefore felt that in view of the results of the performance evaluation, that PH-3 and PH-4 will be able to expediently and economically carry out the parametric study delineated in Chapter 2 while providing accuracy near that attainable with THTB.

Chapter 4

Parametric Study

Chapter 2 identified the parameters of consequence in Tables 2-1 and 2-2. Those parameters requiring quantification were subsequently assigned numerical values where possible; while other parameter values were deferred until the outcome of the scoping analysis of Chapter 3. Table 4-1 is a consolidated listing of all parameters to be included in the various permutations of the study. Explanation of values cited for specific parameters follows.

The scoping study of Chapter 3, performed with PH-1 and PH-2 substantiated the viability of the two opposing configurations under examination. The two concepts were demonstrated capable of reducing the relative contribution of radiation to the gross heat transfer by all mechanisms.

Range A is the primary operating range. Therefore, attention is initially directed toward adjusting the other parameter values to achieve operation within this range.

As previously stated, the susceptor length is, from qualitative analysis, expected to be the dominant parameter influencing the temperature profile. The susceptor length thus remains an open ended boundary the value of which is to be established.

Heat shield thickness is a parameter to be determined. The scoping run indicates that the lower value of 0.010" established for practical reasons is reasonable in terms of temperature insulation.

Table 4-1

Consolidation of Parameters

Parameters (Solid Susceptor)	Parameters (Heat Shielded Susceptor)
1. Configuration A (Figure 2-3)	1. Configuration B (Figure 2-4)
2. Material: (Stainless steel and Iron)	2. Material: (Stainless steel and Iron)
3. Surface preparation of calorimeter internals a) unplated b) gold plated	3. Surface preparation of calorimeter internals a) unplated b) gold plated
4. Operating T or maximum temperature allowable, Range A = 1300°F $\leq T_{max} \leq$ 1400°F	4. Operating T or maximum temperature allowable, Range A = 1300°F $\leq T_{max} \leq$ 1400°F
5. Susceptor length, L: (working volume boundary) L = open	5. Susceptor length, L: (working volume boundary) L = open
6. Calorimeter outside radius, RWO RWO $\leq$ 0.375	6. Calorimeter outside radius, RWO RWO $\leq$ 0.375
7. Containment tube thickness, tw tw = .020"	7. Containment tube thickness, tw tw = 0.020"

Table 4-1 (Continued)

Parameters (Solid Susceptor)	Parameters (Heat Shielded Susceptor)
8. Containment tube inner radius RW $\leq$ 0.355"	8. Containment tube inner radius RW $\leq$ 0.355"
9. Gap spacing: Gap 1 = 0.020"	9. Gap spacing: Gap 1 = 0.20"; Gap 2 = 0.020"
10. Susceptor radius, RN: (working volume boundary) 0.08" $\leq$ RN $\leq$ 0.355"	10. Outer radius of heat shield: (working volume boundary) RSN = RS + DR $\leq$ 0.355"
11. Containment tube wall temperature, TW: TW = 740°F	11. Heat shield thickness, DR: 0.01" $\leq$ DR $\leq$ 0.1"
12. Susceptor base temperature, TN1 TN1 = 752°F	12. Inner radius of heat shield, RS: RS = RN + 0.020"
13. Performance coefficient, PCTRQG: Range B = PCTRQG $\leq$ 1%	13. Susceptor radius, RN: 0.08" $\leq$ RN $\leq$ 0.355"
14. Internal heat generation rate: QGEN = 3.75 watts/gm Range C = open	14. Containment tube wall temperature, TW: TW = 740°F

Table 4-1 (Continued)

Parameters (Solid Susceptor)	Parameters (Heat Shielded Susceptor)
	15. Susceptor base temperature, TN1: TN1 = 752°F
	16. Heat shield base temperature, TS1: TS1 = 750°F
	17. Performance coefficient, PCTRQG: Range B = PCTRQG $\leq$ 1%
	18. Internal heat generation rate: QGEN = 3.75 watts/gm Range C = open

The maximum thickness appears to be best limited to values less than approximately 0.10" therefore: $0.01" \leq DR \leq 0.10$

As pointed out in Chapter 2, comparison of the two opposing configurations is best accomplished in terms of relative "working volumes".

The susceptor radius RN was identified as a parameter with some influence upon the operating temperature; however, the results of the scoping analysis indicate that it offers no large perturbation to the temperature profile and therefore may remain an open parameter. Available irradiation space within the core dictates that the outside radius of the calorimeter should necessarily be less than 0.375" and an outer radius of 0.25" or less for the calorimeter is "most" desirable. This implies that the radius of the "working volume" should not exceed 0.21", since the "working volume" radius, RWK, will be 0.25" minus the containment tube thickness, tw = 0.20" and minus the annular gap width, Gap 1 = 0.020". Subsequent analysis of calorimeter performance will be in terms of RN or RSN = RWK, that is, in a manner similar to Chapter 3, Figure 3-12.

According to the preceding, RN and RSN, the respective working volume radii, are to be the primary independent variables in terms of which calorimeter performance is to be evaluated. A quantitative measure of calorimeter performance is needed and it is felt that a ratio of the heat transfer rate by radiation to the total heat generation rate is the most representative measure for comparison. Consequently, the parameter defined for performance evaluation will be the heat transfer rate by radiation expressed as a percent of the

which operates within Range A and Range B is identified, it will be evaluated in terms of identifying the boundaries for Range C.

Operating Range C is a newly introduced parameter. It is defined in terms of the maximum and minimum value of the internal heat generation rate for which a given optimally designed calorimeter can be relied upon to yield accurate data. For example, consider the hypothetical case in which the maximum value of internal heat generation rate in a system is 4.5 watts/gm when the imbedded thermocouple measures a susceptor temperature of 1400°F. For any subsequent temperature measurement greater than 1400°F, the respective implied internal heat generation rate, say for example, 4.8 watts/gm, will be suspect. It will be suspect because of the thermocouple inaccuracy cited in Chapter 1. Specifically then, the calorimeter is considered to yield accurate measurements of implied heating rate values for that range of heating rates which stimulates the calorimeter thermocouple to measure temperatures within the primary operating range, Range A.

Other parameters listed in Table 4-1 and not previously identified include, containment tube wall temperature, susceptor base temperature, and the heat shield base temperature. These parameters are constants of the reactor system environment and in this case are representative of values existent in the EBR-II system.

The ensuing analysis will be a multi-phase study comprised in part of the sequence of steps listed and defined in the following table, Table 4-2. Table 4-2 will serve to identify the sequence in which the chosen study areas are examined and discussed.

Table 4-2

Sequence of Steps for Calorimeter Parametric Study

Step Identification	Description
Phase I	Determination of the calorimeter length necessary to promote operation at or near the mid-point of Range A.
Step 1	Solid susceptor geometry of Configuration A, Figure 2-3.
Step 2	Heat shielded susceptor geometry of Configuration B, Figure 2-4.
Phase II	Manipulation of the balance of variable parameters to achieve concurrent operation in Range B.
Step 1	Solid susceptor geometry of Configuration A, Figure 2-4
Step 2	Heat shielded susceptor geometry of Configuration B, Figure 2-5.

The parametric study follows the overall scheme depicted by the Parametric Study Tree of Figure 2-3, with amplification of minor branches as deemed necessary. For clarity an explanation accompanies the parametric tree branch for Phase I, Step 1, which proceeds according to scheme described by Figures 4-1 and 4-2. It should be noted that each "Surface Preparation Branch" has seven (7) possible "Length Branches", and each Length Branch has six possible "Susceptor Radius Branches".

A single permutation of the study implied by Figure 4-1 and 4-2 is described by the path of line segment a-f. Table 4-3 defines the components of the line segment path a-f. Table 4-4 contains the data collected from the Phase I, Step 1 analysis. Temperature T_{max} refers to the maximum temperature attained in the calorimeter susceptor body.

Linear interpolation of the temperature and length data is performed to obtain an estimate of the susceptor length necessary to insure that the calorimeter operates at or near the midpoint of Range A. The working radius in this case is the susceptor radius, RN.

Table 4-5 summarizes the conclusions of the solid susceptor length study, Phase I, Step 1, based upon the optimum working radius dimension, RN = 0.21".

The last column in Table 4-5 relates the sensitivity of the maximum temperature at the susceptor end, to perturbations caused by radius change. Note the unplated susceptors are an order of magnitude more susceptible to perturbation than are the gold plated susceptors. This is due to the fact that, for the gold plated susceptors, radiation

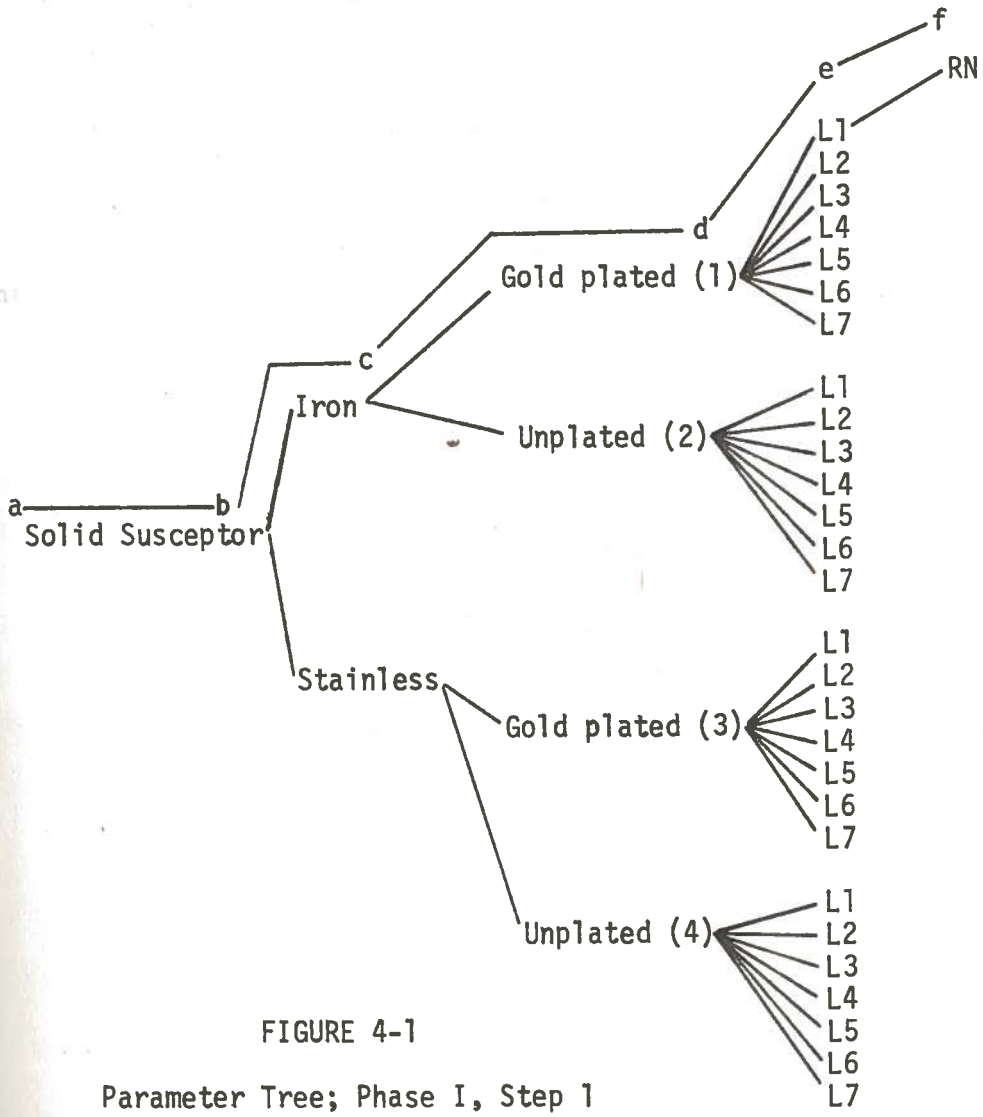

FIGURE 4-1

Parameter Tree; Phase I, Step 1

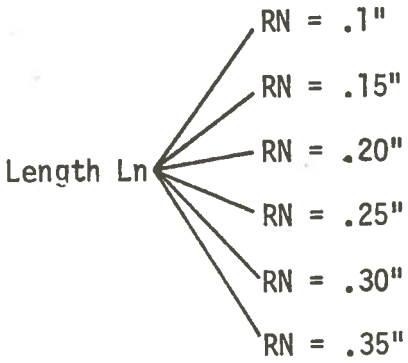

FIGURE 4-2

Radius Branches for Figure 4-1 Length Branches

Table 4-3

Example Study Path

Segment	
a-b	indicates the examination of the "configuration branch", solid susceptor
b-c	indicates the "material branch", iron
c-d	indicates the "surface preparation branch", gold plating
d-e	indicates the "length branch", $L_1 = 0.7"$
e-f	indicates the "radius branch", $R_1 = 0.1"$

Table 4-5

Conclusions of Phase I, Step 1

Configuration A

RWK = RN = 0.21"

Susceptor Material	Surface Preparation	Approximate value for T_{max} (°F)	Length required to operate in Range A	Temperature sensitivity to .01 inch radius variation
Stainless Steel	None	1362	0.95"	2.80°F
Stainless Steel	Gold Plating	1338	0.90"	0.44°F
Iron	None	1382	1.3"	5.32°F
Iron	Gold Plating	1359	1.2"	0.60°F

constitutes a much smaller net and relative contribution to the overall heat transfer. As a consequence as the radius increases the resulting reduction in radiation accounts for a smaller net and relative reduction in heat transfer (i.e., there is a reduction in an already small quantity) thus the temperature profile is less perturbed.

Phase I, Step 2, proceeds according to the scheme of the parametric trees in Figures 4-3 and 4-4.

Again the dominant parameter is the susceptor length with susceptor radius and heat shield thickness as variable parameters which also perturb operation in Range A. As a consequence, the examination is carried out much as for Phase I, Step 1, with additional computations for a change in heat shield thickness. Note that each length branch has 6 radius branches each of which have 2 shield thickness branches, Figure 4-4.

Tables 4-6 and 4-7 contain the data collected from Phase I, Step 2 analysis. Temperature T_{max} again refers to the maximum temperature attained by the calorimeter susceptor body.

Linear interpolation of the length and temperature data is performed to obtain an estimate of the susceptor length necessary to insure that the calorimeter operates at or near the midpoint of Range A.

Table 4-8 summarizes the conclusions of the heat shielded susceptor length study, Phase I, Step 2. Values are obtained for two separate heat shield thicknesses. The results are much the same as seen in the examination of Phase I, Step 1; the gold plated susceptors are an order of magnitude more susceptor to perturbation in maximum temperature as a function of susceptor radius.

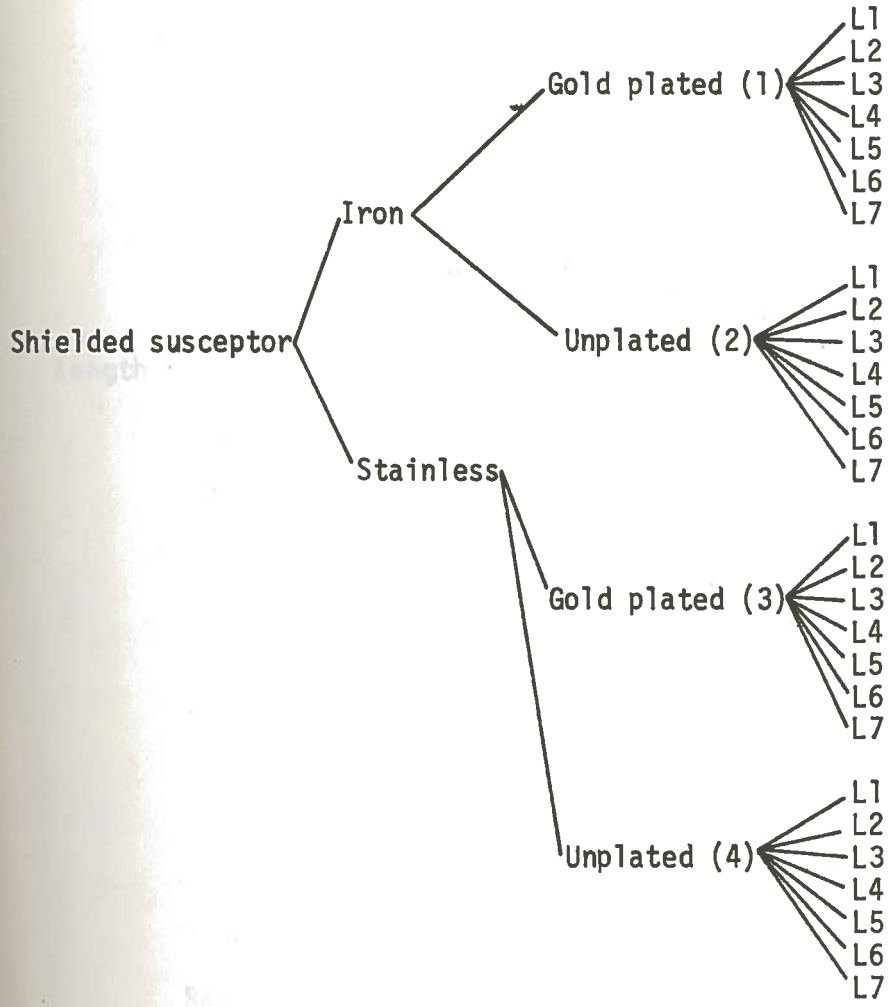

FIGURE 4-3

Parameter Tree for Phase I, Step 2

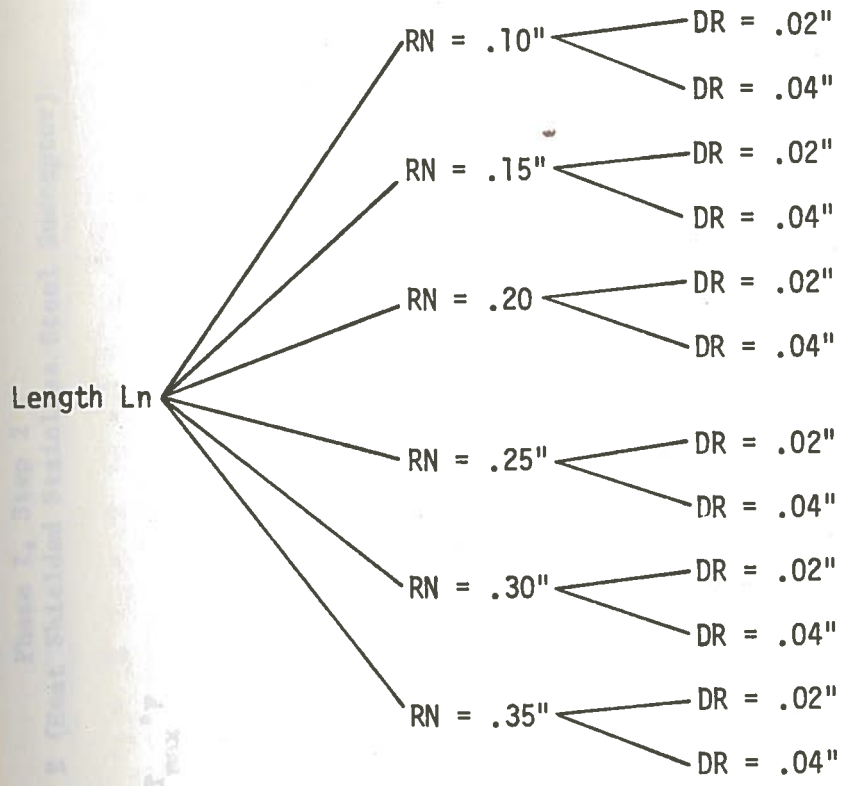

FIGURE 4-4

Radius and Heat Shield Branches for FIGURE 4-3

Table 4-6

Phase I, Step 2
Configuration B (Heat Shielded Stainless Steel Susceptor)

Temperatures T_{max} °F

L_i = susceptor length

Susceptor Radius	L_1 = .7	L_2 = .8	L_3 = .9	L_4 = 1.0	L_5 = 1.1	L_6 = 1.2	L = 1.3
Stainless Steel - Unplated - DR = .02							
.10	1127	1219	1324	1427	1526	*	*
.15	1126	1228	1336	1444	*	*	*
.20	1127	1230	1340	1453	*	*	*
.25	1127	1231	1342	1457	*	*	*
.30	1128	1232	1344	1460	*	*	*
.35	1128	1233	1345	1463	*	*	*
Stainless Steel - Unplated - DR = .04							
.10	1126	1226	1332	1438	*	*	*
.15	1127	1229	1338	1450	*	*	*
.20	1127	1231	1342	1456	*	*	*
.25	1128	1232	1343	1459	*	*	*
.30	1128	1232	1345	1462	*	*	*
.35	1128	1233	1346	1464	*	*	*

* $\geq$ 100°F out of Range A

Table 4-6 (Continued)

Susceptor Radius	L_1 = .7	L_2 = .8	L_3 = .9	L_4 = 1.0	L_5 = 1.1	L_6 = 1.2	L = 1.3
Stainless Steel - Au plated - DR = .02							
.10	*	1228	1343	1465	*	*	*
.15	*	1232	1348	*	*	*	*
.20	*	1232	1349	*	*	*	*
.25	*	1232	1350	*	*	*	*
.30	*	1232	1350	*	*	*	*
.35	1129	1233	1350	*	*	*	*
Stainless Steel - Au plated - DR = .04							
.10	*	1232	1347	1471	*	*	*
.15	*	1232	1349	*	*	*	*
.20	*	1232	1350	*	*	*	*
.25	*	1232	1350	*	*	*	*
.30	*	1233	1350	*	*	*	*
.35	1129	1233	1350	*	*	*	*

* $\geq$ 100°F out of Range A

Table 4-7

Phase I, Step 2

Configuration B (Heat Shielded Iron Susceptor Temperature)

Working Radius	L = .90	L = 1.0	L = 1.1	L = 1.2	L = 1.3	L = 1.4	L = 1.5
Iron - Unplated - DR = .02							
.10	1062	1126	1207	1292	1378	1468	*
.15	*	*	*	1315	1413	1514	*
.20	*	*	*	1330	1435	*	*
.25	*	*	*	1338	1450	*	*
.30	*	*	*	1344	1461	*	*
.35	*	*	1241	1348	1469	*	*
Iron - Unplated - DR = .04							
.10	1060	1134	1217	1306	1398	1488	*
.15	*	*	*	1324	1427	1533	*
.20	*	*	*	1335	1445	*	*
.25	*	*	*	1342	1457	*	*
.30	*	*	*	1347	1466	*	*
.35	*	*	*	1351	1473	*	*
Iron - Au plated - DR = .02							
.10	1071	1146	1246	1365	1506	*	*
.15	*	*	1250	1371	*	*	*
.20	*	*	1250	1372	*	*	*
.25	*	*	1251	1373	*	*	*
.30	*	*	1251	1373	*	*	*
.35	*	*	1251	1373	*	*	*

* $\geq$ 100°F out of Range A

Table 4-7 (Continued)

	Iron - Au plated - DR = .04						
Working Radius	L = .90	L = 1.0	L = 1.1	L = 1.2	L = 1.3	L = 1.4	L = 1.5
.10	1071	1149	1250	1370	*	*	*
.15	*	*	1250	1372	*	*	*
.20	*	*	1250	1373	*	*	*
.25	*	*	1251	1373	*	*	*
.30	*	*	1251	1373	*	*	*
.35	*	*	1252	1373	*	*	*

* $\geq$ 100°F out of Range A

Table 4-8

Conclusions of Phase I, Step 2

Configuration B

Susceptor Material	Surface Preparation	Approximate value for T_{max}(°F)	Heat shield Thickness DR	Length required to operate in Range A	Temperature sensitivity to .01 inch radius variation
Stainless Steel	polished	1340	0.02"	0.90"	.84°F
Stainless Steel	polished	1342	0.04"	0.90"	.56°F
Stainless Steel	Gold	1349	0.02"	0.90"	.28°F
Stainless Steel	Gold	1350	0.04"	0.90"	.12°F
Iron	polished	1365	0.02"	1.25"	2.94°F
Iron	polished	1368	0.04"	1.25"	2.40°F
Iron	Gold	1372	0.02"	1.2"	0.32°F
Iron	Gold	1373	0.04"	1.2"	0.12°F

With a determination of susceptor lengths necessary to promote operation of the chosen calorimeters within Range A ($1300°F \leq T \leq 1400°F$), Phase I of the study is complete.

The next phase involves a manipulation of the remaining parameters to achieve the concurrent operation in Range B. The evaluation involves a comparison of the relative merits of the two basic design configurations. The sequence according to Table 4-2, begins with Phase II, Step 1. Analysis follows the scheme depicted by the parametric tree of Figure 4-5.

The data obtained from the analysis is depicted graphically in Figures 4-6, 4-7, 4-8 and 4-9. The graphical data for individual calorimeters is presented in terms of the working volume radius RWK as the independent variable and the "coefficient of performance", PCTRQG as the dependent variable. Recall that, for the solid susceptor geometry of Configuration A, the working volume radius, RWK equals the susceptor radius, RN.

Figure 4-6 relates the graphical data for the solid susceptor, stainless steel, unplated calorimeter of length, L = 0.95 inches. At the minimum radius examined RN = 0.08", 12.8% of the total heat generated in the susceptor (i.e., PCTRQG = 12.8%) is transferred by radiation. At the maximum practical radius RN = 0.35", approximately 3.4% of the total heat generated is transferred by radiation. As qualitatively demonstrated in the Figure there is again the observed existence of an approximate 1/RN relationship. (A power curve fit, as performed in Chapter 3 for the scoping study, yields: $G = ax^b$ where for the curve fit a = 1.27 and b = -0.92. Qualitatively, the

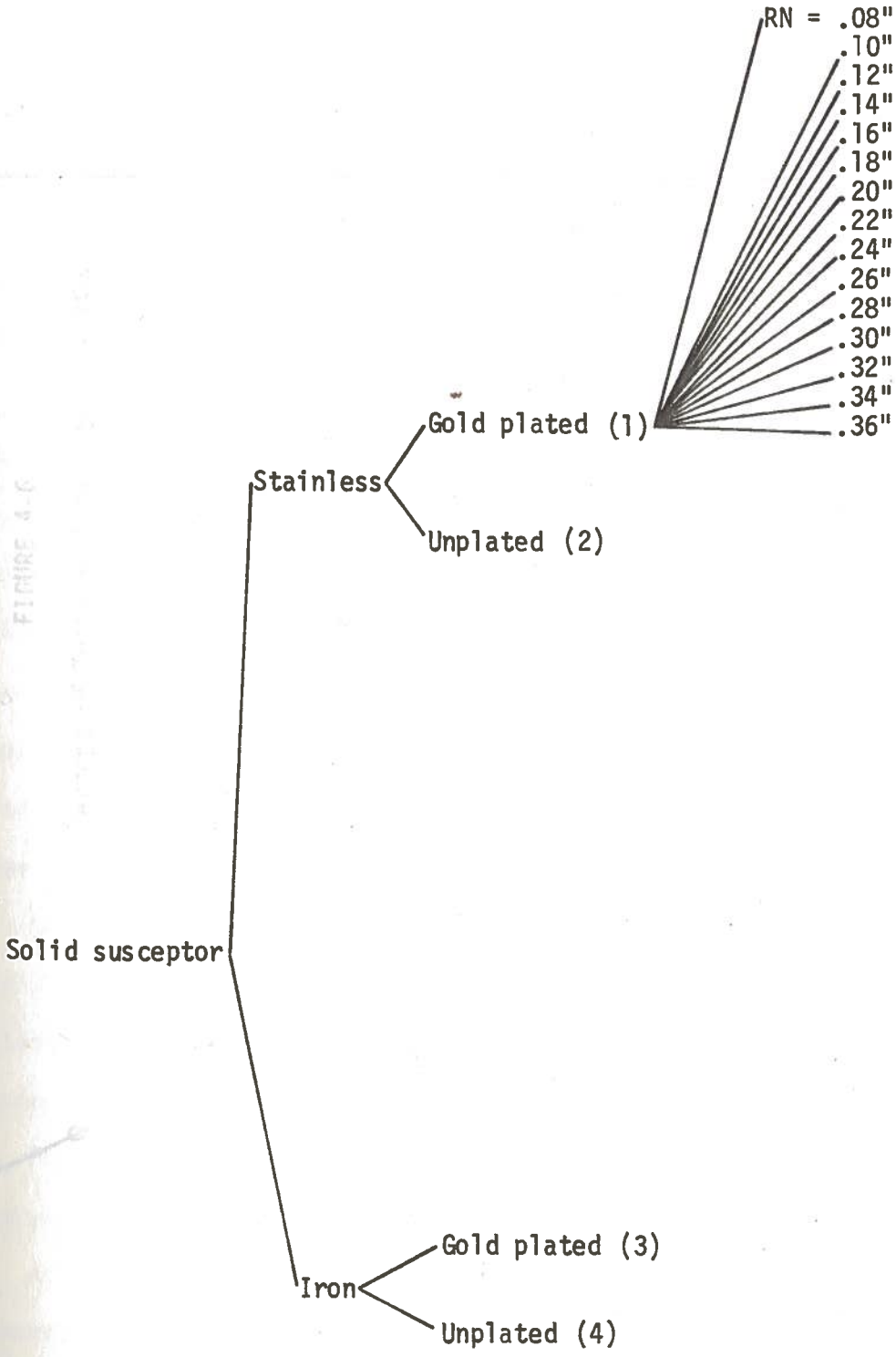

FIGURE 4-5

Parameter Tree for Phase II, Step 1

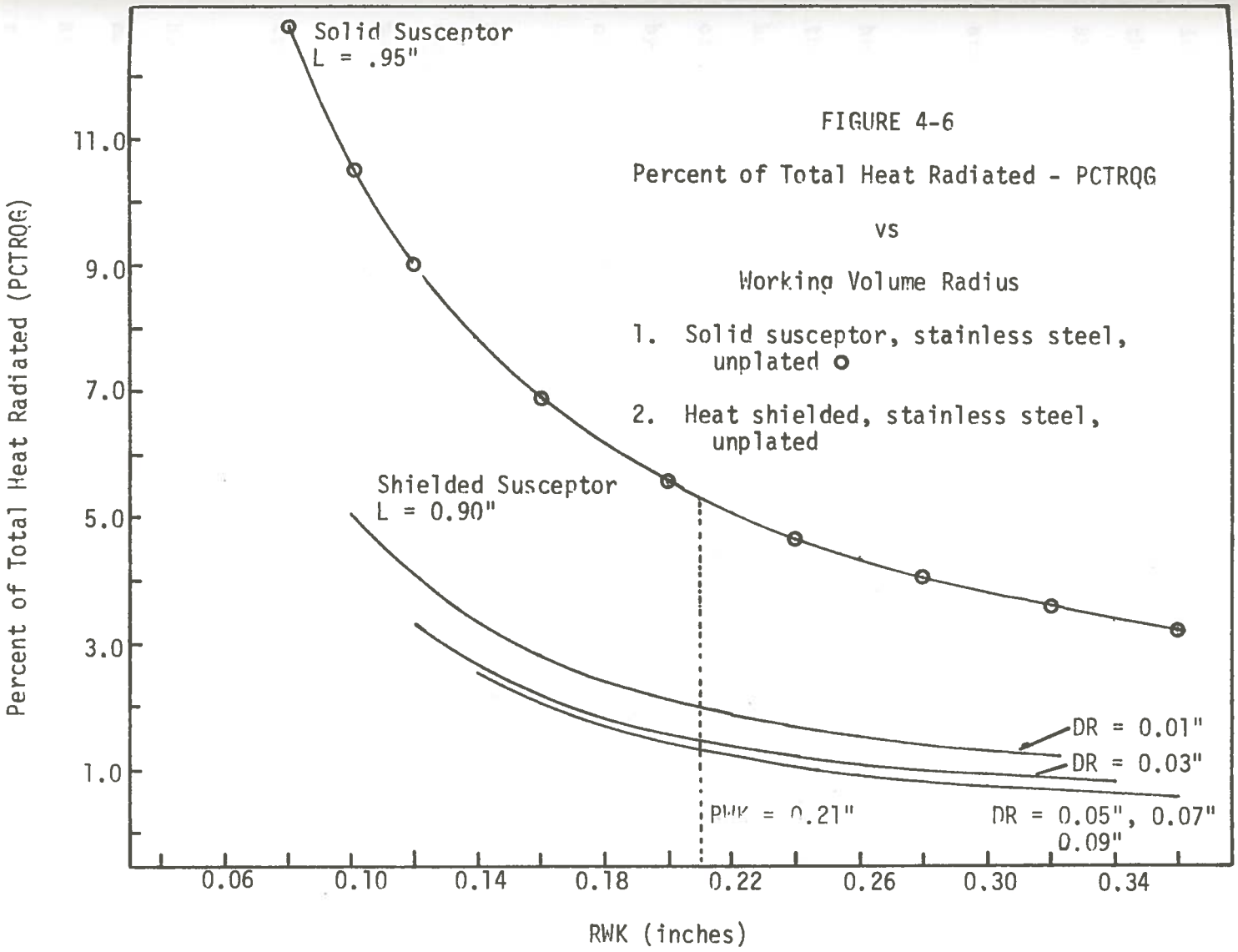

FIGURE 4-6

Percent of Total Heat Radiated - PCTRQG

vs

Working Volume Radius

1. Solid susceptor, stainless steel, unplated o
2. Heat shielded, stainless steel, unplated

act of increasing the susceptor radius does in fact reduce the relative amount of heat transferred by radiation; nonetheless, the efficiency with which this reduction is accomplished is insufficient in that the minimum percentage radiation is 3.4% and this is without the limits of Range B. In particular at the most desirable size of RN = 0.21", PCTRQG = 5.3%.

Figure 4-7 relates the graphical data for the solid susceptor, stainless steel, gold plated calorimeter of length, L = 0.9 inches.

At the minimum radius examined RN = 0.08", 2.7% of the total heat generated in the susceptor is transferred by radiation. At the maximum possible radius RN = .35", approximately .57% of the total heat generated is transferred by radiation. For the maximum radius of desirability RN = .21", .96% of the heat generated is transferred by radiation. This value is clearly, though barely, within the bounds of Range B, PCTRQG $\leq$ 1%.

The graphical data representative of gold plated calorimeter internals is plotted on semi-log coordinates in order to permit later comparison with the heat shielded cases; wherein there is an order of magnitude difference in PCTRQG.

Figure 4-8 relates the graphical data for the solid susceptor, iron, unplated, calorimeter of length, L = 1.3 inches.

At the minimum radius examined RN = 0.08", 22.5% of the total heat generated in the susceptor is transferred by radiation. At the maximum possible radius, in terms of available irradiation space, RN = 0.35", and 7.2% of the total heat generated is transferred by radiation. For the maximum radius of desirability, RN = 0.21:, 11.4%

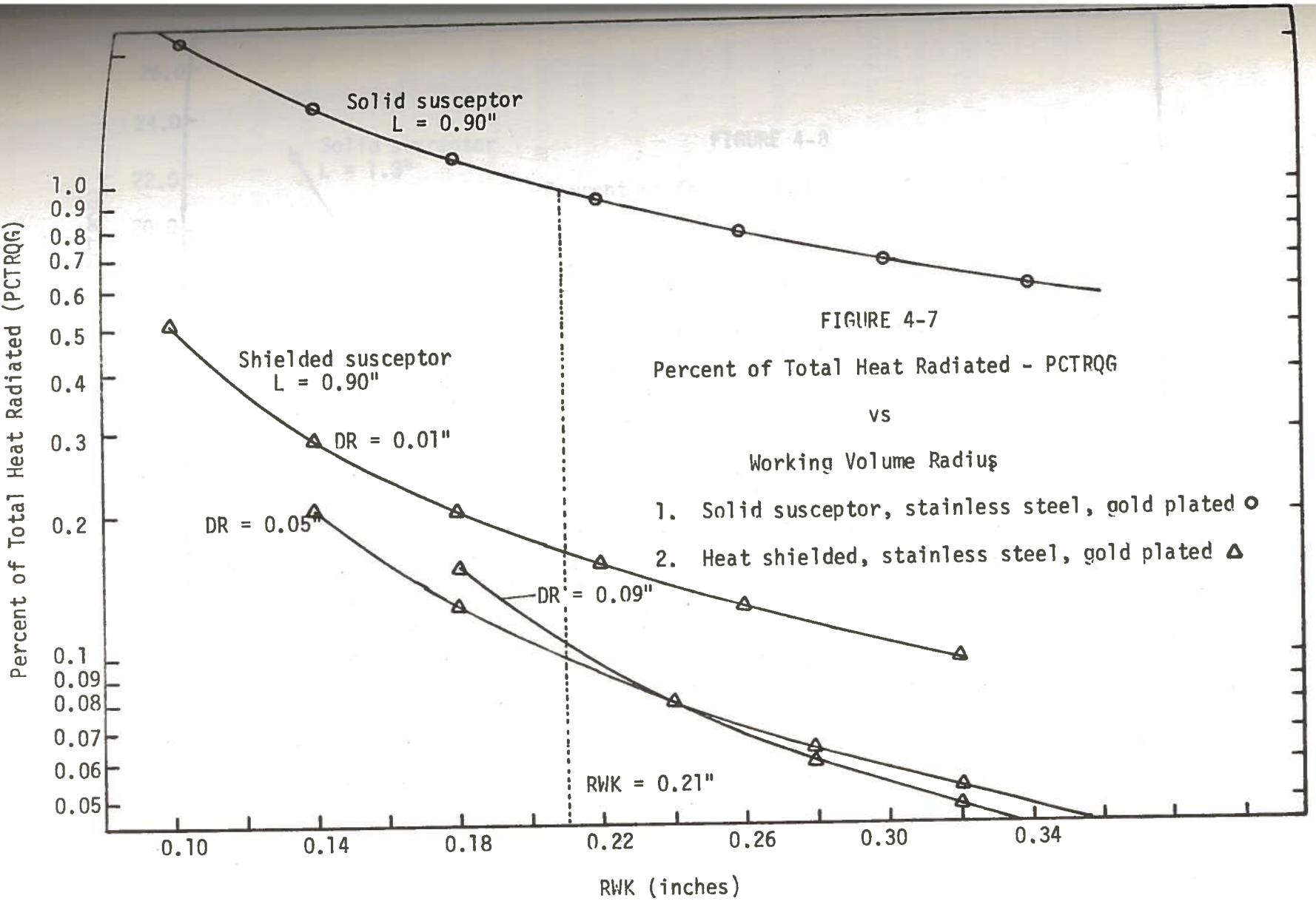

FIGURE 4-7

Percent of Total Heat Radiated - PCTRQG

vs

Working Volume Radius

1. Solid susceptor, stainless steel, gold plated ○
2. Heat shielded, stainless steel, gold plated △

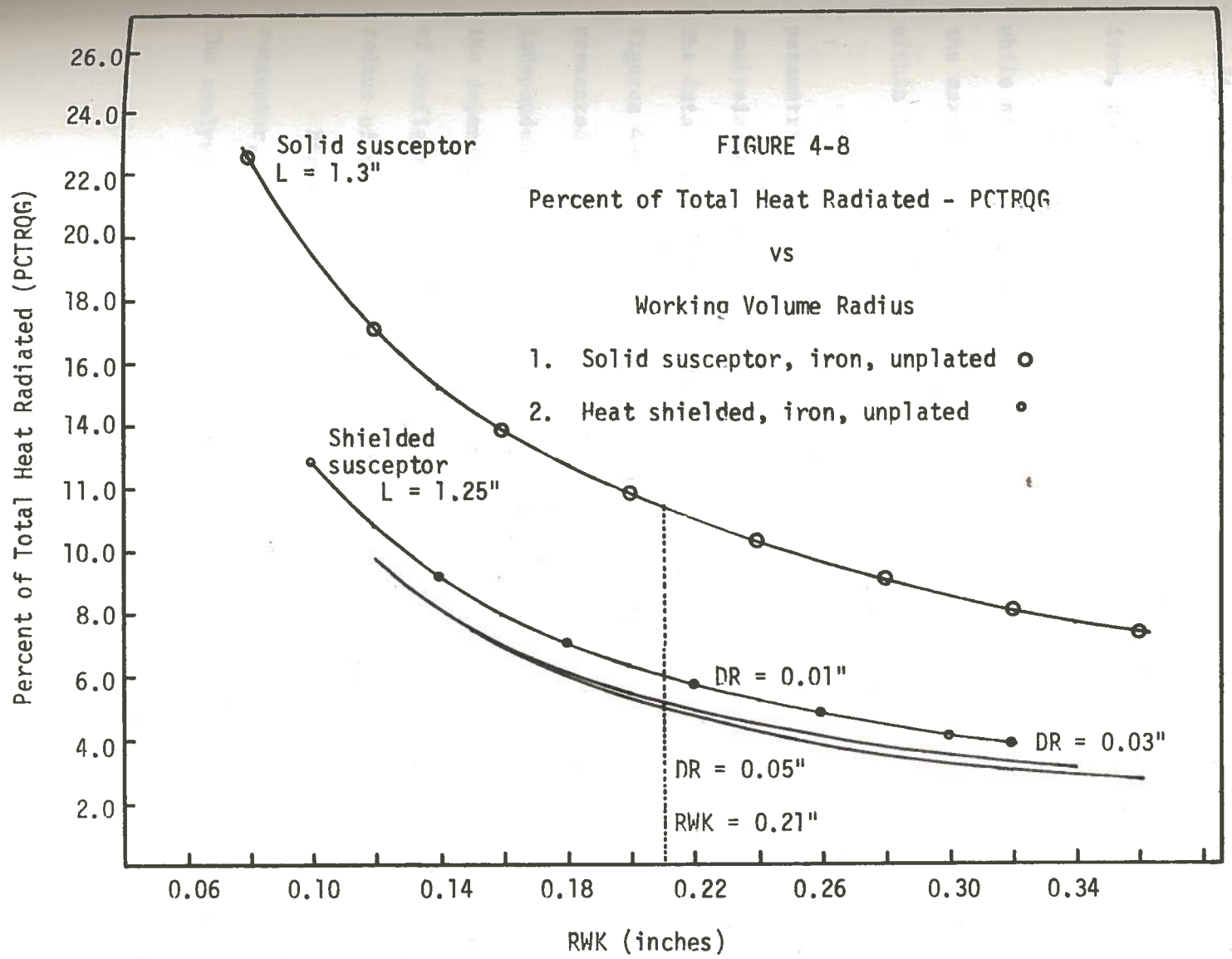

FIGURE 4-8

Percent of Total Heat Radiated - PCTRQG

vs

Working Volume Radius

1. Solid susceptor, iron, unplated
2. Heat shielded, iron, unplated

of the heat transferred is by radiation. Clearly the percent decrease in radiation is insufficient to the task for this material and configuration.

Figure 4-9 relates the graphical data for the solid susceptor, iron, gold plated calorimeter of length, L = 1.2 inches.

At the minimum radius examined, RN = .08", PCTRQG = 2.6%, while at the maximum possible radius RN = .35", PCTRQG = .56%, and at the maximum desirable radius RN = .21", PCTRQG = .94% which is within the bounds of Range B.

Analysis of Phase II, Step 2, proceeds according to the parametric study tree of Figures 4-10 and 4-11. This part of the analysis consists of an evaluation of the heat shielded susceptor. The data obtained from the analysis is depicted graphically in Figures 4-6, 4-7, 4-8, 4-9, and 4-12; where the data is again presented in terms of the working volume radius, RWK as the independent variable and the "coefficient of performance", PCTRQG as the dependent variable. Recall that for the heat shielded susceptor of Configuration A, the working volume radius RWK equals the outside radius of the heat shield.

Figure 4-6 relates the graphical data for the heat shielded susceptor, stainless steel, unplated calorimeter of length, L = 0.9". The analysis considers various heat shield thicknesses as is related.

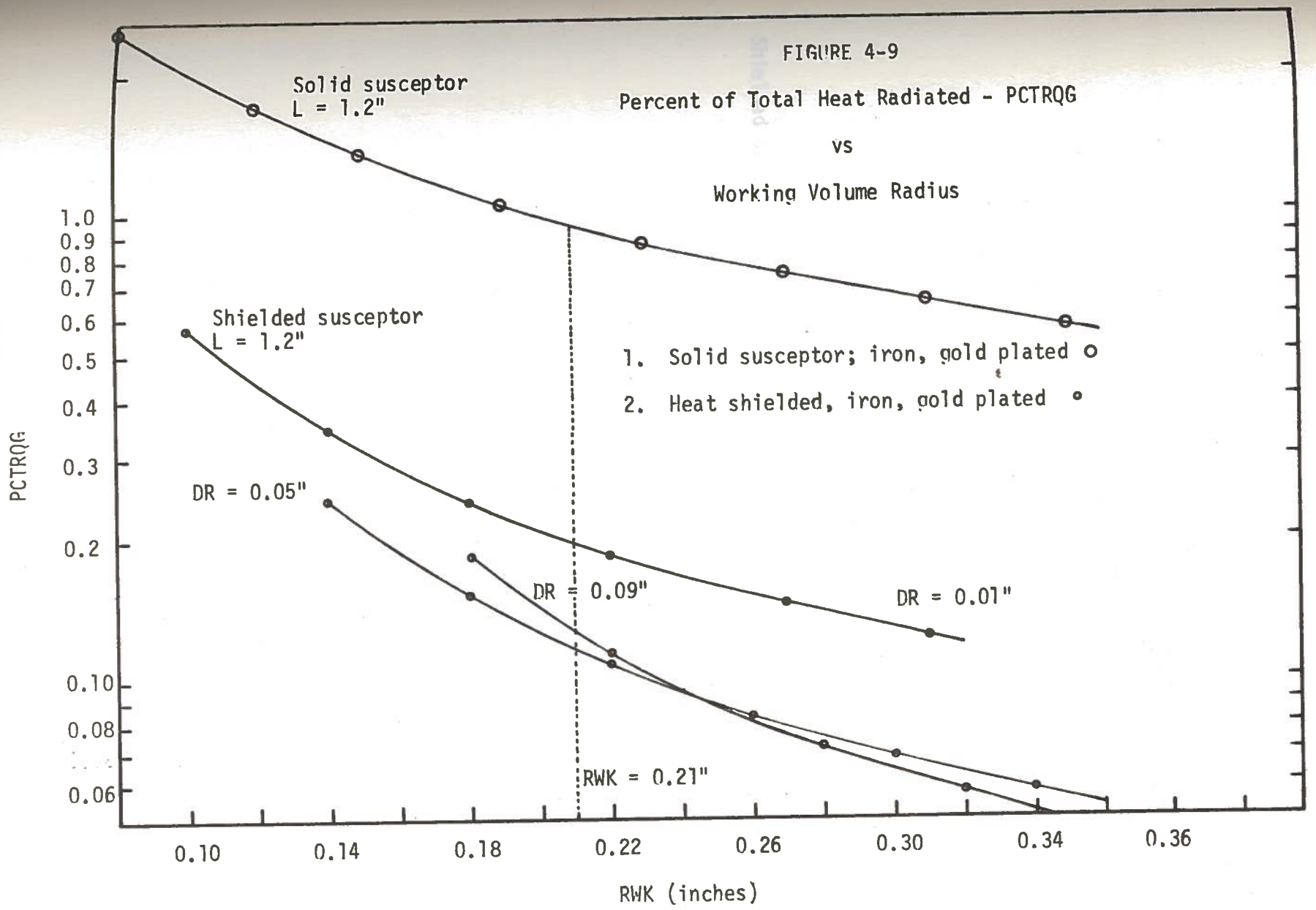
FIGURE 4-9
Percent of Total Heat Radiated - PCTRQG
vs
Working Volume Radius
Solid susceptor
L = 1.2"
Shielded susceptor
L = 1.2"
1. Solid susceptor; iron, gold plated
2. Heat shielded, iron, gold plated
DR = 0.05"
DR = 0.09"
DR = 0.01"
RWK = 0.21"
PCTRQG
1.0
0.9
0.8
0.7
0.6
0.5
0.4
0.3
0.2
0.10
0.08
0.06
0.10
0.14
0.18
0.22
0.26
0.30
0.34
0.36
RWK (inches)

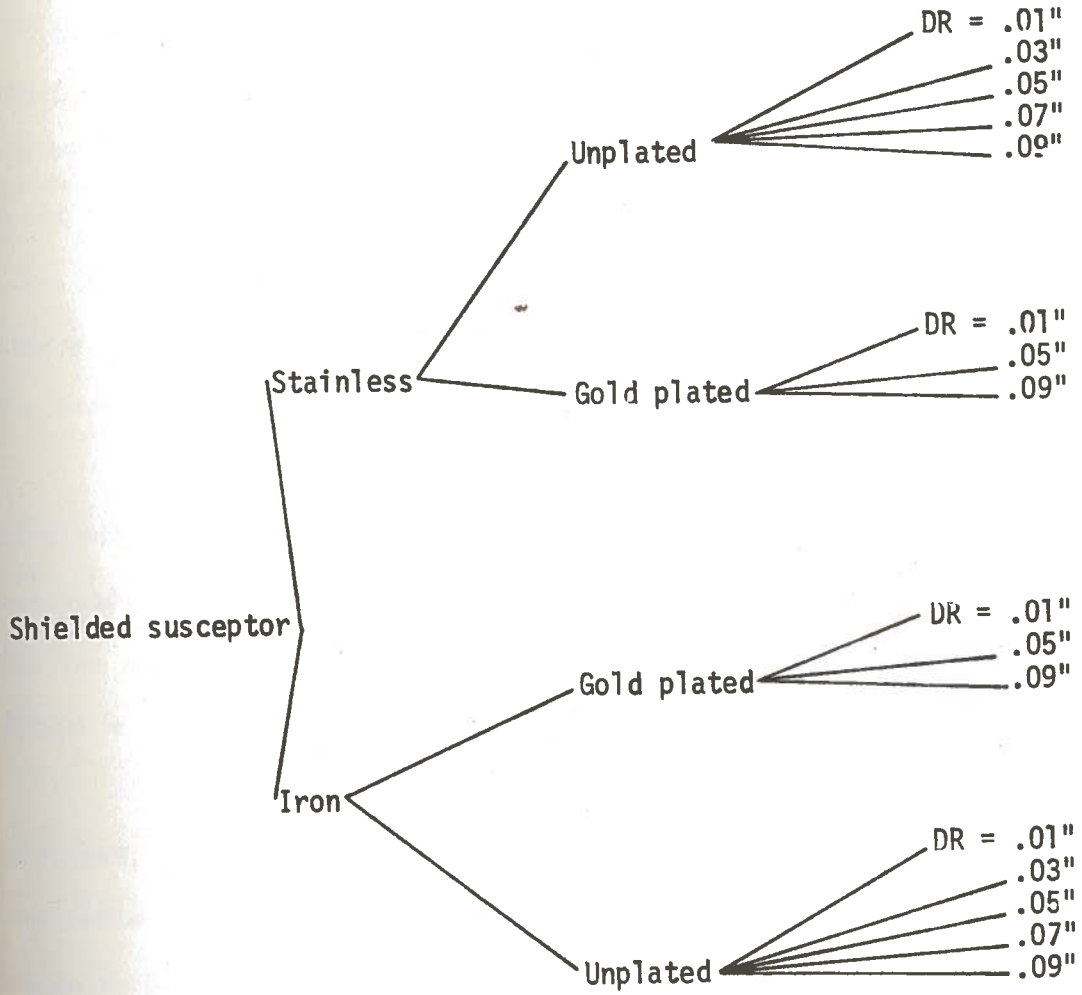

FIGURE 4-10

Parameter Tree for Phase II, Step 2

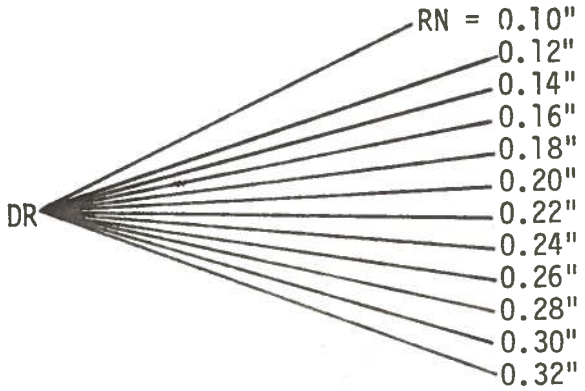

FIGURE 4-11

Radius Branches for FIGURE 4-10

For a .010" heat shield thickness and the minimum susceptor radius examined, RN = .07", this translates to a working radius of RSN = RN + Gap 1 + DR = .10", PCTRQG = 5.1%. For the maximum susceptor radius examined RN = .29", RSN = .32", PCTRQG = 1.24%. As for the solid susceptor the maximum desirable working volume radius is .21", i.e., to allow complete containment within a tube which has an outside radius of .25". RSN = .21", RN = .18", PCTRQG = 2% and this is outside the bounds of Range B, PCTRQG $\leq$ 1%.

For a .03" thick heat shield and the minimum susceptor radius examined, RN = .07:, RSN = .12", and PCTRQG = 3.31%. For the maximum susceptor radius examined, RN = .29", RSN = .34", and PCTRQG = .84%. For the maximum desirable working radius of RSN = .21", RN = .16", and PCTRQG = 1.49%. Again this value is without the bounds of Range B.

For a .05" thick heat shield and the minimum susceptor radius examined, RN = .07", RSN = .14", and PCTRQG = 2.58%. For the maximum desirable working radius, RSN = .21", RN = .14", and PCTRQG = 1.3%; which is beyond the bounds of Range B.

For heat shields of thicknesses of .05" and greater there is approximate congruency of effect.

Figure 4-8 relates the graphical data for the heat shielded susceptor, iron, and unplated calorimeter of length, L = 1.25". The analysis considers various heat shield thicknesses as is related.

For a .010" thick heat shield and the minimum susceptor radius examined, RN = 0.07", RSN = 0.10", and PCTRQG = 12.8% while for the maximum susceptor radius examined, RN = 0.29", RSN = .32", and PCTRQG = 3.91%. For the maximum desirable working radius, RSN =

.18", PCTRQG = 6%; this value is well beyond the limit established for Range B.

For a 0.030" thick heat shield and the minimum susceptor radius examined, RN = 0.07", RSN = .12", and PCTRQG = 9.73%. For the maximum susceptor radius examined, RN = .29", RSN = .34" and PCTRQG = 3.10%. For the maximum desirable working radius, RSN = .21", RN = .16", PCTRQG = 5.2% and again this value is considerably beyond the limits of Range B.

For a 0.050" thick heat shield and the minimum susceptor radius examined, RN = .07", RSN = .14", and PCTRQG = 8.22%. For the maximum susceptor radius examined, RN = .29", RSN = .36", and PCTRQG = 2.65%. For the maximum desirable working radius, RSN = .21", RN = .14", and PCTRQG = 5%. This value is without the limit of Range B.

For a 0.07" thick heat shield and the minimum susceptor radius examined, RN = .07", RSN = .16", and PCTRQG = 7.22%. For the maximum susceptor radius examined, RN = .29", RSN = .38", and PCTRQG = 2.34%. For the maximum desirable working radius, RSN = .21", RN = .12", and PCTRQG = 4.95%. As in all preceeding cases for this calorimeter, the value of PCTRQG is beyond the limits of Range B.

The data for the susceptor with a .090" thick heat shield was very near in value to that for the .070" heat shield and was therefore not added to the graphical representation.

Close examination of Figure 4-8 reveals the manifestation of an anomalous behavior pattern which is germaine to the ultimate evaluation of existent data and conditions. Figure 4-12 best illustrates the

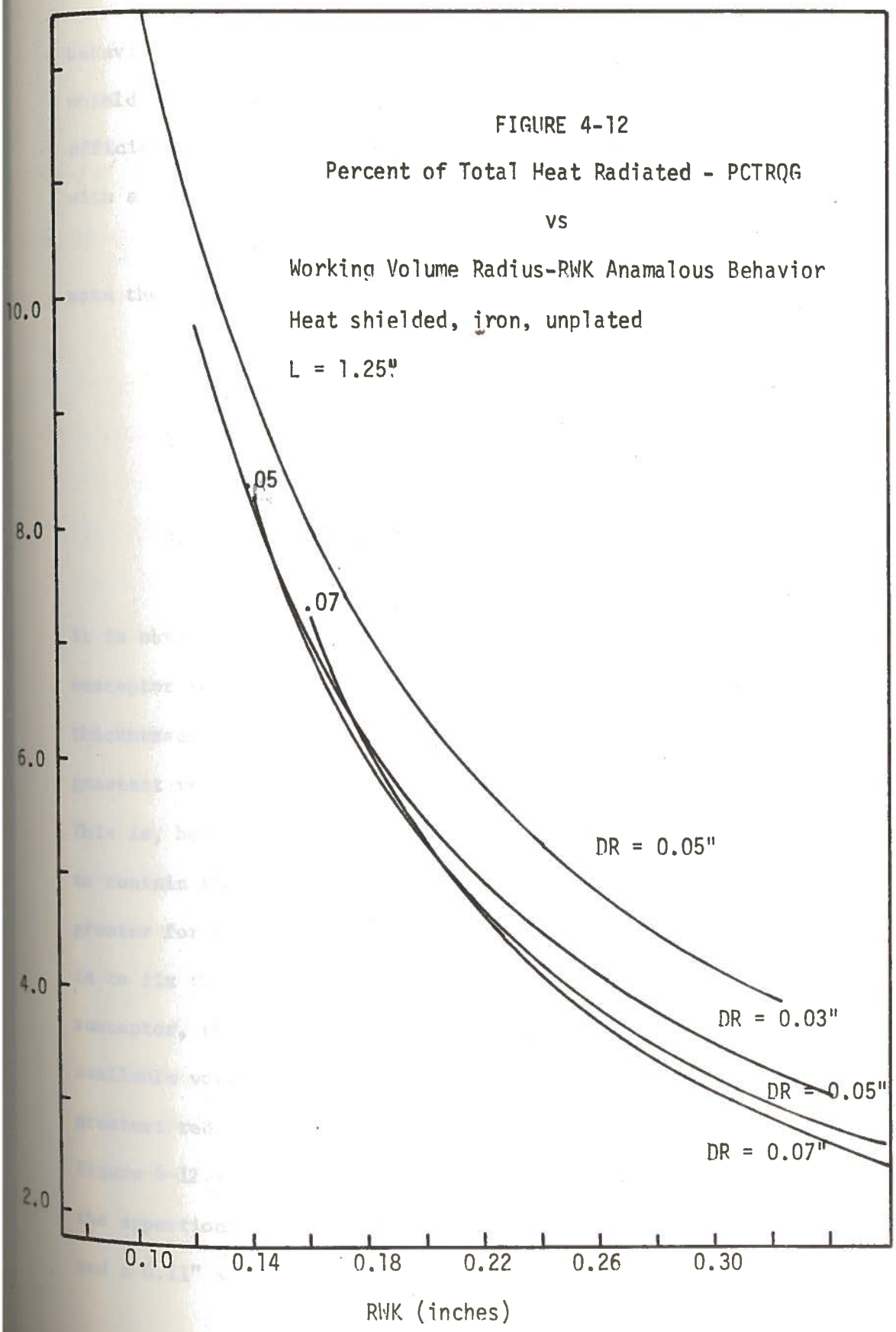

FIGURE 4-12

Percent of Total Heat Radiated - PCTRQG

vs

Working Volume Radius-RWK Anamalous Behavior

Heat shielded, iron, unplated

L = 1.25"

behavior. Notice in particular the PCTRQG vs. RSN curve for heat shield thickness of 0.070" and RSN = 0.16". This calorimeter is less efficient at percentage wise reduction of radiation than a calorimeter with a .03" thick heat shield and the same working radius.

For an explanation of the behavior, refer to Figure 4-12 and note the following points:

1. For the curve DR = .07" at RSN = .16" the susceptor radius is RN = .07", PCTRQG = 7.22%.
2. For the curve DR = .03" at RSN = .16" the susceptor radius is RN = .11", PCTRQG = 6.99%; and
3. For the curve DR = .07" RSN = .20" with susceptor radius RN = .11", PCTRQG = 5.48%.

It is obvious from an examination of the above that for a given susceptor radius that, when surrounded by heat shields of different thicknesses, the heat shield of greatest thickness also causes the greatest reduction in percentage of heat transferred by radiation. This is, however, accomplished at the expense of the volume necessary to contain the heat shield and susceptor, and which is necessarily greater for the thicker heat shield. On the other hand, if the aim is to fix the volume required to contain the heat shield and its susceptor, there is a most efficient way in which to apportion the available volume to each of the components in order to achieve the greatest reduction in percentage of total heat transferred by radiation. Figure 4-12 indicates that for a fixed working radius of RSN = 0.16", the apportioning of the volume in terms of a 0.03" thick heat shield and a 0.11" susceptor radius is more efficient than a 0.07" thick

heat shield and a 0.07" radius susceptor for reducing that percent of total heat generated which is transferred by radiation. Qualitatively, this is to be expected if one considers the following:

1. PCTRQG goes up as susceptor radius goes down, other parameters being equal;
2. PCTRQG goes down as heat shield thickness goes up, other parameters being equal, and;
3. For a fixed amount of cylindrical volume available for containing a heat shield and a susceptor, as the heat shield thickness goes up, the susceptor radius goes down.

Depending upon the functional relationship existing between 1. and 2., one or the other may exhibit dominance; that functional relationship is exhibited in Figure 4-12 with the respective ranges of dominance vividly depicted.

After making the discovery of this behavior for the unplated iron susceptor, a re-examination of the data for the unplated stainless steel calorimeter revealed the same behavior, but to a lesser extent. The anomally was not realized during the initial examination of the data.

Figure 4-7 relates the graphical data for the heat shielded susceptor, stainless steel, gold plated calorimeter of length, L = 0.9". The analysis considers various heat shield thicknesses as is related.

For a .010" thick heat shield and the minimum susceptor radius examined, RN = 0.07", RSN = 0.10", and PCTRQG = 0.507%. For the maximum susceptor radius examined, RN = 0.29", RSN = 0.32", PCTRQG = 0.1%. For the maximum desirable working radius, RSN = 0.21", RN = 0.18", and PCTRQG = 0.166%. The value is well below the limits of Range B.

For a 0.050" thick heat-shield and the minimum susceptor radius examined, RN = 0.07", RSN = 0.14", and PCTRQG = 0.2%. For the maximum susceptor radius examined, RN = 0.29", RSN = 0.36", PCTRQG = 0.04%. For the maximum desirable working radius, RSN = 0.21", RN = 0.14", PCTRQG = 0.099%, and again the limits required for Range B are more than satisfied.

For a 0.090" thick heat shield and the minimum susceptor radius examined, RN = 0.07", RSN = 0.18", and PCTRQG = 0.16%. For the maximum susceptor radius examined, RN = 0.29", RSN = 0.40", and PCTRQG = 0.03%. For the maximum desirable working radius, RSN = 0.21", RN = 0.10", and PCTRQG = 0.16%.

The anomalous behavior first noted in the immediately preceeding section is exhibited by this configuration as well. It is obvious that a susceptor with RN = 0.14" combined with a heat shield thickness of 0.050" is more efficient at reducing the percent radiation than is a susceptor with RN = 0.10" combined with a thicker heat shield of 0.090".

Figure 4-9 relates the graphical data for the heat shielded susceptor, iron, gold plated calorimeter of length, L = 1.2". The analysis considers various heat shield thicknesses as is related.

For a 0.010" thick heat shield and the minimum susceptor radius examined, RN = 0.07", RSN = 0.10", and PCTRQG = 0.58%. For the maximum susceptor radius examined, RN = 0.29", RSN = 0.32", PCTRQG = 0.12%. For the maximum desirable working radius, RSN = 0.21", RN = 0.18", PCTRQG = 0.2% which is substantially less than $\leq$ 1% requirement of Range B.

For a 0.05" thick heat shield and the minimum susceptor radius examined, RN = 0.07", RSN = 0.14", and PCTRQG = 0.25%. For the maximum susceptor radius examined, RN = 0.29", RSN = 0.36", and PCTRQG = 0.05%. For the maximum desirable working radius, RSN = 0.21", RN = 0.14", and PCTRQG = 0.116%.

For a 0.09" thick heat shield and the minimum susceptor radius examined, RN = 0.07", RSN = 0.18", and PCTRQG = 0.18%. For the maximum susceptor radius examined, RN = 0.29", RSN = 0.40", and PCTRQG = 0.04% and finally, for the maximum working radius RSN = 0.21", RN = 0.10", and PCTRQG = 0.126%. Again, the anomalous behavior is observed.

The most illustrative comparison of the relative abilities of the respective configurations to control and reduce the percentage of total heat radiated is by an examination of Figures 4-13 and 4-14. As for the preceding figures, the percent of total heat generated which is transferred by radiation is graphed as a function of the radius of the working volume, RWK.

In Table 4-10, derived from Table 4-9, the calorimeter configurations are ranked according to performance of the design criteria

Table 4-9

Phase II Study Summary Data

Calorimeter configuration; material: Surface preparation; length L = Heat shield thickness, DR =		PCTRQG for RWK = 0.21"
Phase II, Step 1		
Solid susceptor; stainless steel; unplated; L = 0.95"		5.3%
Solid susceptor; iron; unplated; L = 1.2"		11.4%
Solid susceptor; stainless steel; gold plated; L = 0.9"		0.96%
Solid susceptor; iron; gold plated; L = 1.2"		0.94%
Phase II, Step 2		
Heat shielded susceptor; stainless steel; unplated; L = 0.9"	DR = 0.01"	2.0%
	DR = 0.03"	1.49%
	DR = 0.05"	1.30%
Heat shielded susceptor; iron; unplated; L = 1.25"	DR = 0.01"	6.0%
	DR = 0.03"	5.2%
	DR = 0.05"	5.0%
	DR = 0.07"	4.95%
Heat shielded susceptor; stainless steel; gold plated; L = 0.9"	DR = 0.01"	0.17%
	DR = 0.05"	0.10%
	DR = 0.07"	0.16%
Heat shielded susceptor; iron; gold plated; L = 1.2"	DR = 0.01"	0.20%
	DR = 0.05"	0.12%
	DR = 0.09"	0.13%

requiring the suppression of radiation heat transfer relative to the total heat generated within the calorimeter susceptor.

Table 4-10
Phase II Comparison

1) Heat shielded, stainless steel, gold plated, L = 0.9", DR = 0.05", PCTRQG $\leq$ 0.1%

2) Heat shielded, iron, gold plated, L = 1.2", DR = 0.05", PCTRQG $\leq$ 0.12%

3) Solid susceptor iron, gold plated, L = 1.2", PCTRQG $\leq$ 0.94%

4) Solid susceptor stainless steel, gold plated, L = 0.9", PCTRQG $\leq$ 0.96%

5) Heat shielded, stainless steel, unplated, L = 0.9", DR = 0.05", PCTRQG $\leq$ 1.49%

6) Heat shielded susceptor, iron, unplated, L = 1.25", DR = 0.05", PCTRQG $\leq$ 5.0%

7) Solid susceptor, stainless steel, unplated, L = 0.95", PCTRQG $\leq$ 5.3%

8) Solid susceptor, iron, unplated, L = 1.2", PCTRQG $\leq$ 11.4%

Table 4-10 compares the performances at the most desirable working radius, RWK = 0.21". This working volume radius has been utilized throughout the analysis as a reference point due to the design criteria and parameter bounds; it has been hoped that the optimized calorimeter would have a working volume radius of $\leq$ 0.21". From Figures 4-13 and 4-14, it is ascertainable that, (1) the solid susceptor iron and stainless steel, unplated calorimeters are unable to approach the 1% limits of Range B, (2) the heat shielded iron calorimeter is also unable to achieve the desired reduction, (3) the

FIGURE 4-13

Percent of Total Heat Radiated - PCTRQG

vs

Working Volume Radius-RWK

Stainless steel calorimeters

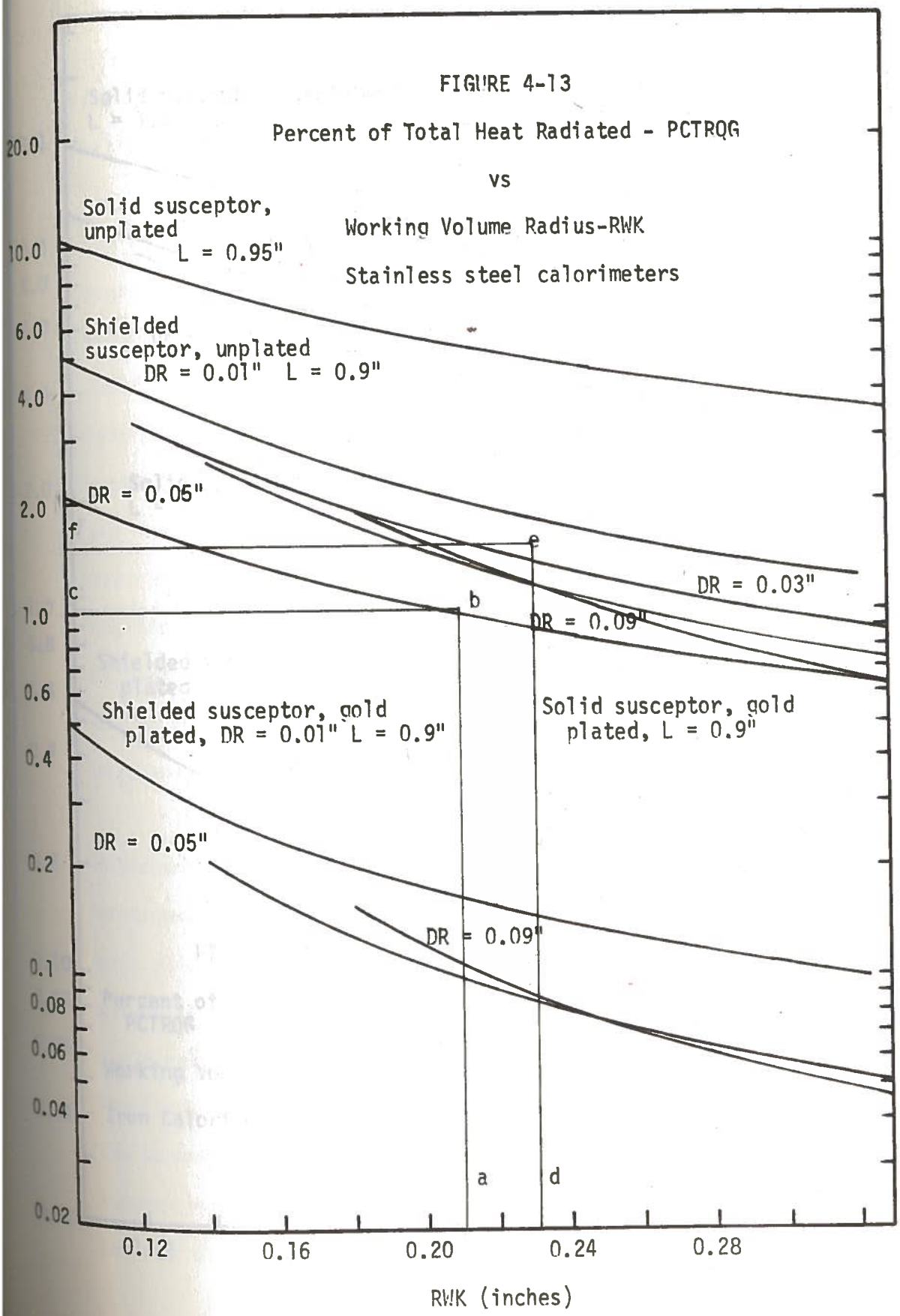

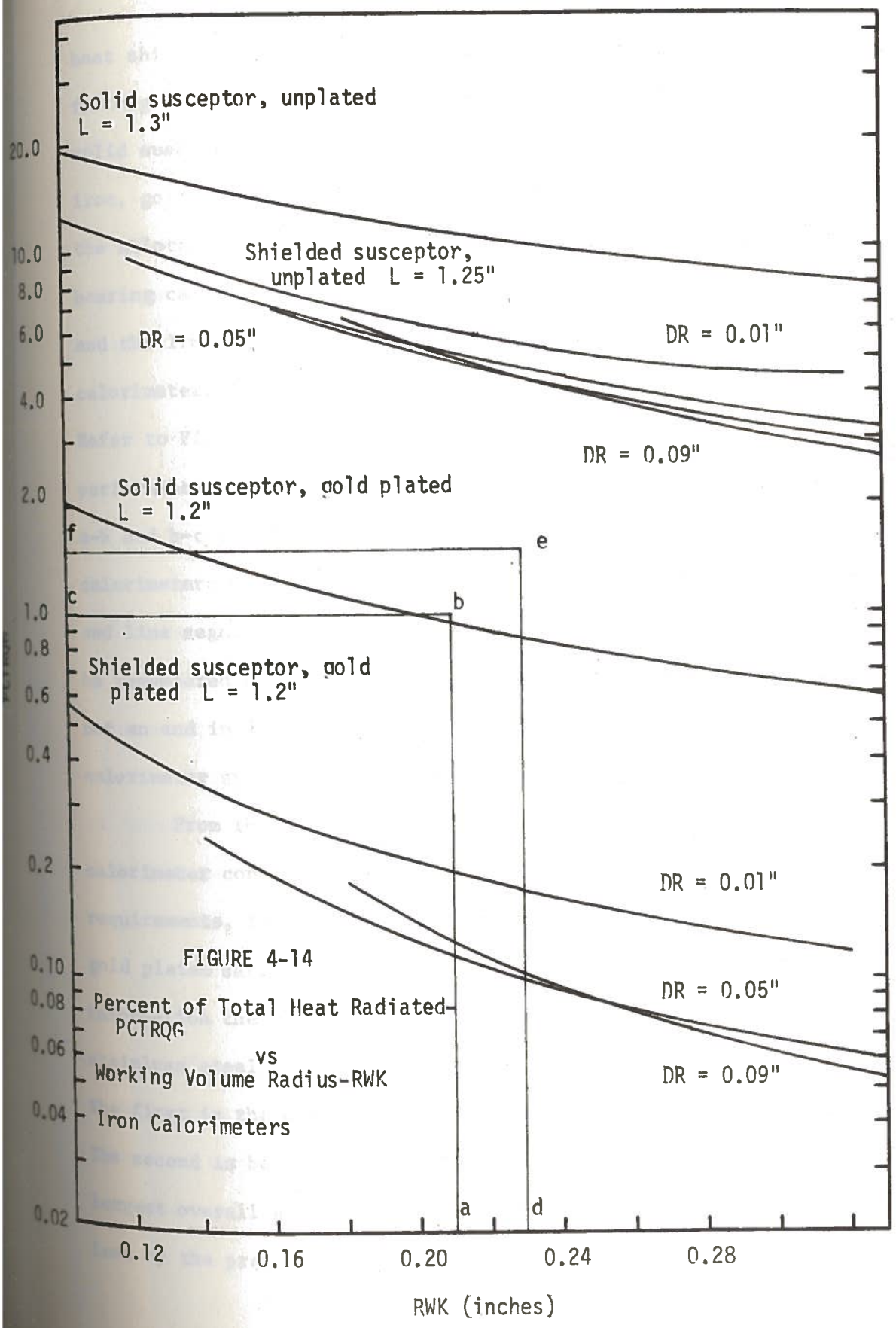

FIGURE 4-14

Percent of Total Heat Radiated-PCTRQG

vs

Working Volume Radius-RWK

Iron Calorimeters

heat shielded stainless steel, unplated susceptor, almost satisfies filling the 1% limits for a 0.21" radius of working volume, (4) the solid susceptor, stainless steel, gold plated and solid susceptor, iron, gold plated, do just satisfy the requirements of Range B within the allotted working volume, and (5) the two gold plated heat shield bearing calorimeters easily satisfy the requirements of both Range B and the limits on desirable working volume. It should be noted that calorimeters listed (3) and (4) are approximately equal in performance. Refer to Figures 4-13 and 4-14 and note that those calorimeters with performance values bounded by the coordinate axes and line segments a-b and b-c satisfy all requirements previously established. Those calorimeters with performance values bounded by the coordinate axes and line segments d-e and e-f satisfy a 1.5% PCTRQG limit. It must be remembered that reduction of the radiation heat transfer rate is not an end in and of itself; enhancing the overall accuracy of the calorimeter system is the primary concern of this study.

From the information related, it is obvious that two calorimeter configurations satisfy each of the "predefined" design requirements, that is, both configurations and both materials when gold plated satisfy the design requirements. With the present information the calorimeters of choice, would be the solid susceptor stainless steel and the solid susceptor iron. This is for two reasons. The first is the ease of fabrication for the solid susceptor design. The second is because the solid susceptor configuration has the largest overall susceptor mass and should therefore be perturbed less by the presence of the imbedded thermocouple.

Should any difficulties arise in terms of deleterious surface effects for the gold plated calorimeters as a result of radiation damage effects or differences in coefficients of thermal expansion, then there is a fallback line. The stainless steel, heat shielded, unplated calorimeter nearly satisfies the design requirements, and by a judicous choice of relaxing the requirements, may be made to perform adequately.

There is a limited range of heating rate values QGEN for which a particular optimized calorimeter will operate within Range A:

$$1300°F \leq T_{max} \leq 1400°F$$

This range, Range C is identified for the stainless steel calorimeters delineated in Table 4-9 in the accompanying Table 4-11.

It may be necessary to have a larger heat generation rate range of operation. If the thermocouple temperature measurements may be relied upon for temperatures up to 1450°F, then it is possible to establish a wider range for which accuracy may be expected. An auxillary range, Range C' is identified in Table 4-12. The new range is given by:

$$1250°F \leq \text{Range } A' \leq 1450°F$$

The validity of the lower limits 1300°F and 1250°F is questionable because an analysis was not performed to determine the effect of such low operating temperatures upon propogated error magnitude. See the propogation of error section of Chapter 5.

Table 4-11

Delineation of Operating Range C

Calorimeter Configuration	Lower limit of internal heat generation rates, $QGEN_{min}$	Upper limit of internal heat generation rates, $QGEN_{max}$
Solid susceptor; stainless steel; unplated; L = 0.95"; RWK = 0.21"	3.25 w/gm (1300°F)	3.98 w/gm (1400°F)
Solid susceptor; stainless steel; gold plated; L = 0.90"; RWK = 0.21"	3.46 w/gm (1300°F)	4.23 w/gm (1400°F)
Heat shielded susceptor; stainless steel; unplated; L = 0.90"; DR =	3.48 w/gm (1300°F)	4.27 w/gm (1400°F)
Solid susceptor; iron; gold plated, L = 1.2"; RWK = 0.21"	3.4 w/gm	4.0 w/gm

Table 4-12

Delineation of Operating Range C'

Calorimeter Configuration	Lower limit of internal heat generation rates, $QGEN_{min}$	Upper limit of internal heat generation rates, $QGEN_{max}$
Solid susceptor; stainless steel; unplated; L = 0.95", RWK = 0.21"	2.93 w/gm	4.38 w/gm
Solid susceptor; stainless steel; gold plated; L = 0.90"; RWK = 0.21"	3.12 w/gm	4.65 w/gm
Heat shielded susceptor; stainless steel; unplated; L = 0.90"; DR = 0.03"	3.13 w/gm	4.70 w/gm
Heat shielded susceptor; stainless steel; gold plated; L = 0.90"; DR = 0.01"	3.09 w/gm	4.58 w/gm
Solid susceptor; iron; gold plated; RWK = 0.21"	3.0 w/gm	4.3 w/gm

Chapter 5

Error Analysis

The final and perhaps most poignant calculational step remains to be performed. If the preceding steps in the analysis have been adequately carried out, calorimeters with the least inherent inaccuracies have been idenified. It remains as a final step in the design optimization, to determine the overall accuracy with which heating rate determinations can be expected to be made.

A system in many cases may be characterized by a set of variables x_i, y_j.... i = 1...n, j = 1...m. Existent therefrom may be a functional or dependent relationship amongst any subset of these variables such that for example:

$$y_k = f(x_1, x_2, ..., y_1, y_2, ...) \qquad (5\text{-}1)$$

where

$$i = 1, 2, ...a \qquad a \leq n$$

$$j = 1, 2, ...b \qquad b \leq m$$

and if j = k the expression (5-1) is transcendental. Knowing the values of the x's and y's, the value of y_k may be predicted. Often, physical scientists, for example, are familiar with natural laws which govern or relate the behavior of certain physical systems when stimulated. From these laws he may derive expressions (5-1) which describes or simulates the relationship (functional relationship) existing amongst the various

quantities which characterize the system. As a good example, recall the qualitative relationship, Equation (1-1), used to describe the temperature profile in the calorimeter susceptor.

$$T = f(\dot{Q}, k(T), \varepsilon(T), R, \ldots.) \qquad (1\text{-}1)$$

An equation such as (1-1) above is called a mathematical model. This model may be a closed form analytic expression, a transcendental expression, or a numerical algorithm in a digital computer code. A model of the preceeding form whether explicit or implicit is considered deterministic if, a) the independent variables are accurately quantified and b) the model "accurately" represents the interrelations existing in the system. If this is true, precise predictions can be made therefrom. a) and b) preceding are indicative of the sources of two types of error for which there is concern in this study. These potential errors are, 1) errors in the model used to describe the interrelationship of system parameters or statistics, and 2) random and/or systematic errors in the input variables which are propogated to the results of a calculated prediction. A random error[29] is the indefiniteness of results because of the finite precision of the experiment or measurement; a measure of the fluctuation in results after repeated experimentation. Systematic error[29] is the reproducible inaccuracy introduced into the measure of a quantity, by equipment limitations, calibration, or faulty technique. An error of the type related in 1) would obviate the ability to assess the effect of random and/or systematic error

propagation. Therefore, before making such an assessment, the validity of the model will be examined.

In the modeling of either of the Configurations A or B, several critical assumptions have been made and are repeated here for coherence. First, it is assumed that the susceptor body, body 1 (Figure 5-1) and the sink to which it radiates, body 2 are one-dimensional. Second, it is assumed that bodies 1 and 2 are made up of incremental lengths, Δz. Third, it is assumed that the radiation from a specific increment of body 1, for example, increment number 3, is dependent solely upon the properties of that increment and those of the increment directly across from it, 3'. The fourth and final assumption is that the two incremental bodies 3 and 3' exchange radiation "only" with each other. This last assumption was made and used because of its precedence in earlier analyses[1, 2, 5] and furthermore it permits simple modeling of this configuration.

The actual general case may be represented by Figure 5-2, a, b, c. For this case it is to be noted that body 1, point 3 exchanges radiation with an infinite number of points on body 2, four of which are represented by 1', 2', 3', and 4'. Recall that circumferentially the temperature is constant. The radiation exchange between 3 and each of the other points is a complex function of the temperatures and properties existing at the respective points. The temperature profiles for bodies one and two are represented by Figures 5-2a and 5-2c, respectively. Radiation is not one to one with the point directly opposite nor is it independent of the surrounding temperature environment.

Figure 5-1

Incremental Body Division for Modeling

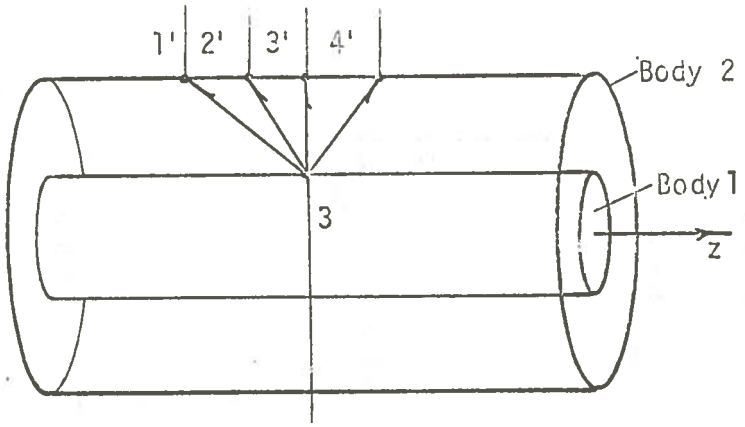

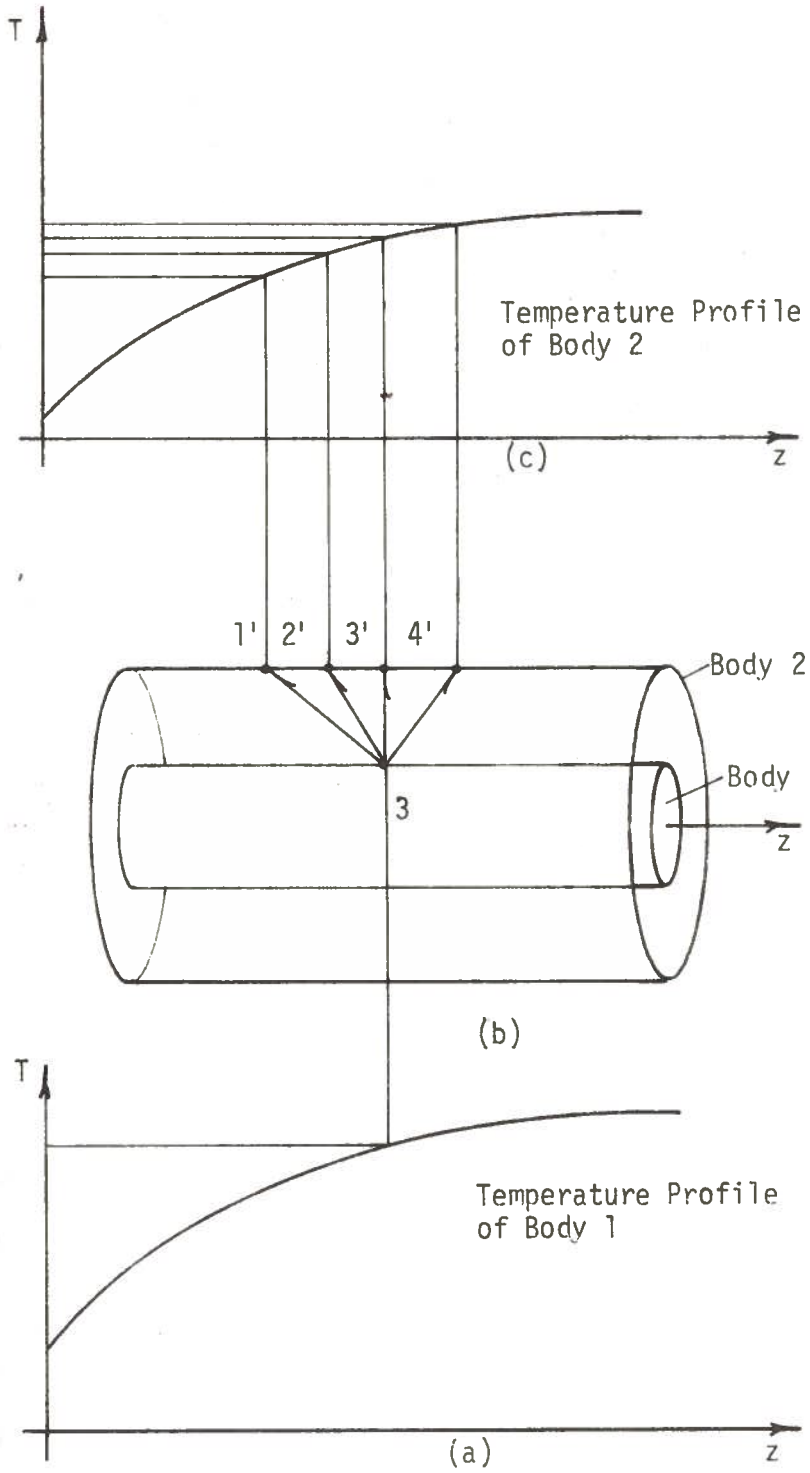

FIGURE 5-2

Radiation to a Sink with Spatially Varying Temperature

It seems that in the light of the preceding discussion, the least penalizing assumption to make for treatment of the complex radiation exchange, in terms of accuracy, is to treat the radiation phenomenon as an interacting exchange between incremental lengths of the bodies in question, with each increment possessing a representative set of properties much in the fashion described for the conduction phenomenon. As in the case of conduction, the finer the incremental division and hence the larger the number of points treated, the more accurate is the characterization expected to be.

Following is the development of a technique for more realistically treating the radiation phenomenon for the configurations at hand. From the technique a third generation computer program is developed. Generation III consists of a new subroutine, Subroutine HRAD, to replace Subroutine HIGH, in program PH-3. Subroutine HRAD provides a new and more realistic means for determining the convection-like radiation coefficient of Equation (3-34). This subroutine, Subroutine HRAD may be seen in Appendix F. It should be noted that the input format to the main program must be modified to accommodate the new subroutine, and this modification is described later in the present chapter. The new program of Generation III, PH-5, provides a means for evaluating the accuracy of the one to one assumption used throughout the preceding study.

As has been seen, it is often convenient and useful to describe "heat transfer" mathematically in a manner analogous to electrical networks. This approach was employed with great facility in Chapter 3. The following analysis is an extension of the concepts used in that chapter. It may be demonstrated[22,23,24] that network

analogies exist for treating radiation heat transfer from non-black bodies such that:

$$\dot{q}_{rad} = \frac{E_b - J_1}{(1 - \varepsilon_1)/\varepsilon_1 A_1} = \frac{E_b - J_1}{B} \tag{5-2}$$

$$B = 1 - \varepsilon_1/\varepsilon_1 A_1 \tag{5-3}$$

where

$\dot{q}_{rad}$ = total heat transferred from body 1.

E_b = the emissive power, σT_1^4, of body 1.

J_1 = the radiosity of body 1.

B = the "body emissive resistance".

ε_1 = total hemispherical emissivity of body 1.

A_1 = the surface area of body 1, from which radiation takes place.

In addition it may be demonstrated that

$$q_{1-2} = \frac{J_1 - J_2}{1/A_1 F_{1-2}} = \frac{J_1 - J_2}{S} \tag{5-4}$$

$$S = 1/A_1 F_{1-2} \tag{5-5}$$

where

q_{1-2} = the heat transferred from body 1 to body 2,

J_1 = radiosity of body 1,

J_2 = radiosity of body 2,

F_{1-2} = the radiation "shape or view factor" for heat transfer from body 1 to body 2, and

S = the "surface resistance" to radiation heat transfer.

Equation (3-30) results from a network analogy, treating radiation exchange between two gray bodies while utilizing Equations (5-2), (5-3), (5-4), and (5-5).

The two networks to be used for the model evaluation and comparison may be seen in Figures 5-3 and 5-4; Figure 5-3 depicts the heat transfer network utilized by Generation II program, PH-3, (similar to Figure 3-6). Figure 5-4 depicts the heat transfer network utilized by Generation III program, PH-5.

For a series of points, on gray bodies, exchanging energy by radiation, Kirchoff's Current Law analogies may be used;

where

E_i = the total emissive power of body 1, node i

E_j = the total emissive power of body 2, node j

J_i = the radiosity of body 1, nodal area i

B_i = the body resistance of body 1, node i

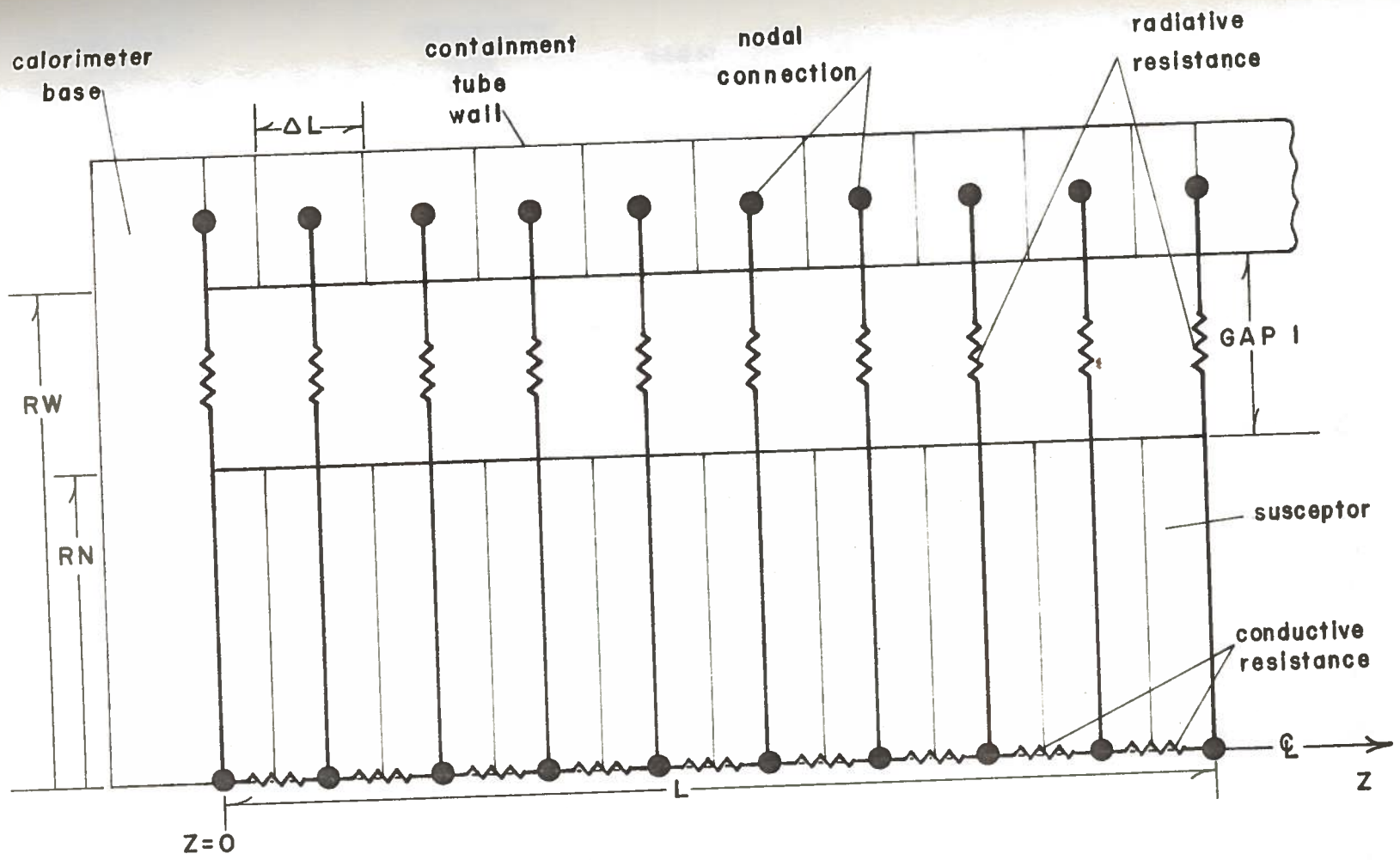

PH-3 10 axial node network for Configuration A subroutine HIGH

FIGURE 5-3

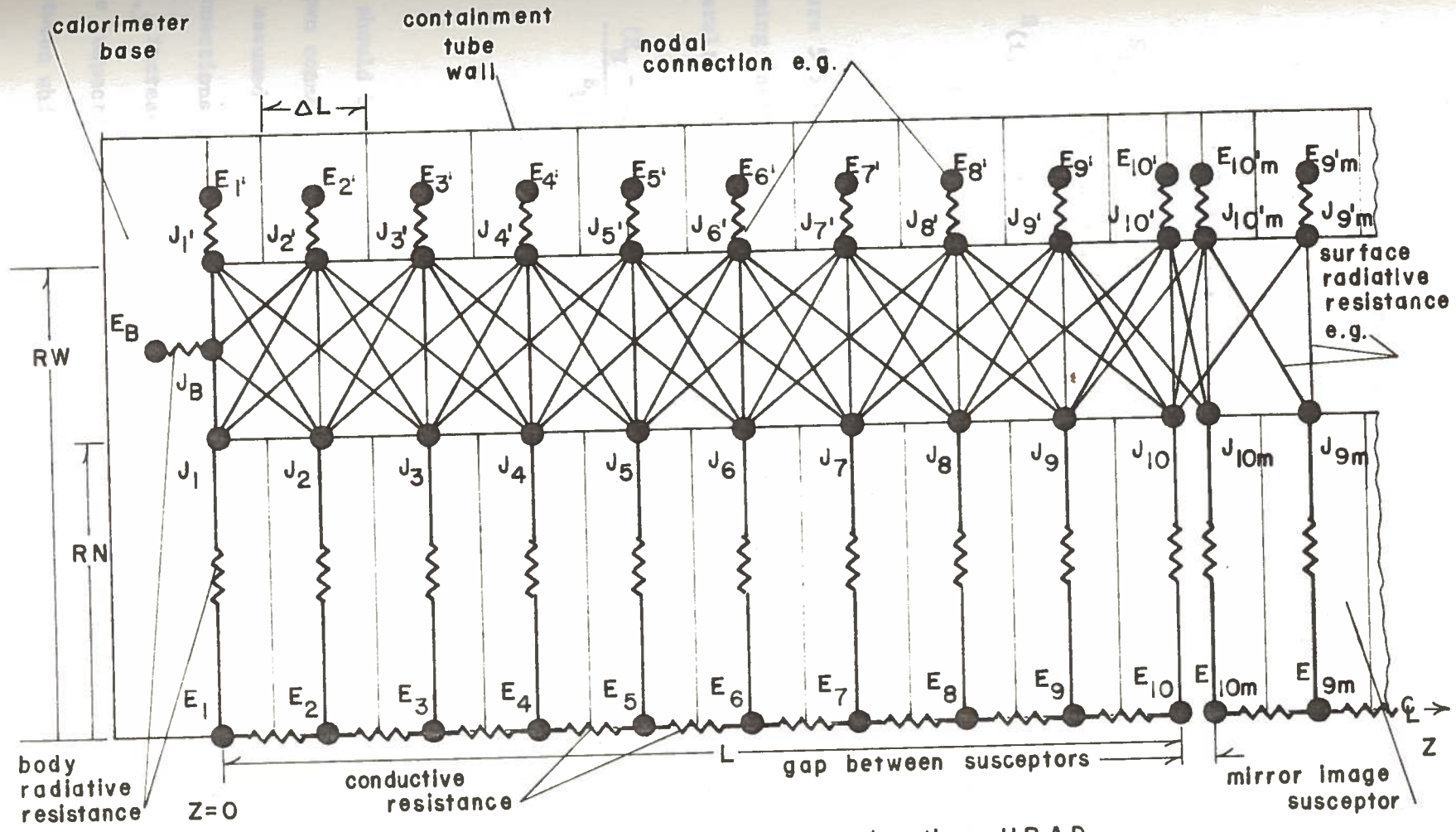

PH-5 10 axial node network for Configuration A subroutine HRAD

FIGURE 5-4

B_j = the body resistance of body 2, node j

$B_i = (1 - \varepsilon_i)/A_i\varepsilon_i$, and (5-3')

$B_j = (1 - \varepsilon_j)/A_j\varepsilon_j$ (5-3")

$S_{i,j}$ = the surface resistance between body 1, node i and body 2, node j

$S_{(i,j)} = 1/A_i F_{i-j}$. (5-5')

$i = 1, 2, 3, \ldots N, \ldots$ (5-5")

$j = 1, 2, 3, \ldots N, \ldots$

Figure 5-5 is representative of a general node exchange. Summing energy currents entering body 1, surface node N, yields in general:

$$\frac{(E_N - J_N)}{B_N} - \frac{(J_N - J_{N'-2})}{S_{(N,N'-2)}} - \frac{(J_N - J_{N'-1})}{S_{(N,N'-1)}} - \frac{(J_N - J_{N'})}{S_{(N,N')}}$$

$$- \frac{J_N - J_{N'+1}}{S_{(N,N'+1}} - \frac{J_N - J_{N'+2}}{S_{(N,N'+2)}} = 0 \qquad (5\text{-}6)$$

It should be noted that more than 5 surface connections (node N is shown connected to surface nodes N'-2, N'-1, N', N'+1, and N'+2) can be assumed to enhance accuracy, however, the value of additional connections becomes questionable as F_{i-j} decreases and concomitantly $S_{i,j}$ increases. As $S_{i,j}$ increases the "radiation current flow" in the respective branch decreases as does the effect upon the nodes between which it is connected. For the network seen in Figure 5-4

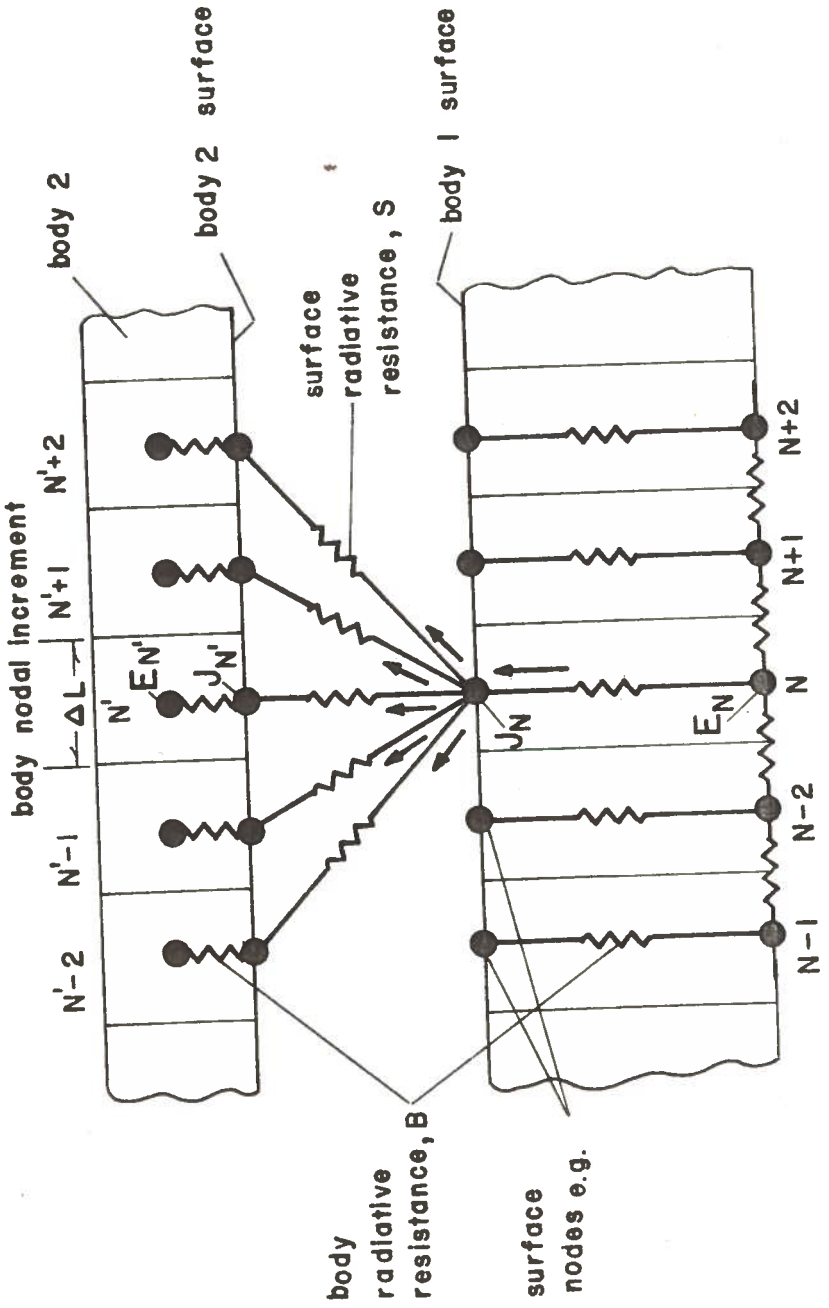

Representative node exchange

FIGURE 5-5

there are twenty one (21) nodes. An equation of the form (5-6) may be written for each node resulting in twenty-one equations and twenty-one unknown J's. Close examination of Figure 5-7 reveals that there are actually twenty-five unknowns, but a reduction in number results from the assumption of a mirror image susceptor (Figure 2-1a) so that:

$$J_{10} = J_{M}$$

$$J_{9} = J_{9_M}$$

$$J_{10'} = J_{10'_M}$$

$$J_{9'} = J_{9'_M}$$

The matrix equation for the network of Figure 5-4 is given by Equation (5-7):

$$
\begin{bmatrix}
C11 & \frac{1}{S_{B,1}} & \frac{1}{S_{B,2}} & 0 & 0 & 0 & 0 & 0 & 0 & 0 & 0 & \frac{1}{S_{B,1'}} & \frac{1}{S_{B,2'}} & 0 & 0 & 0 & 0 & 0 & 0 & 0 & 0 \\
\frac{1}{S_{1,B}} & C22 & 0 & 0 & 0 & 0 & 0 & 0 & 0 & 0 & 0 & \frac{1}{S_{1,1'}} & \frac{1}{S_{1,2'}} & \frac{1}{S_{1,3'}} & 0 & 0 & 0 & 0 & 0 & 0 & 0 \\
\frac{1}{S_{2,B}} & 0 & C33 & 0 & 0 & 0 & 0 & 0 & 0 & 0 & 0 & \frac{1}{S_{2,1'}} & \frac{1}{S_{2,2'}} & \frac{1}{S_{2,3'}} & \frac{1}{S_{2,4'}} & 0 & 0 & 0 & 0 & 0 & 0 \\
0 & 0 & 0 & C44 & 0 & 0 & 0 & 0 & 0 & 0 & 0 & \frac{1}{S_{3,1'}} & \frac{1}{S_{3,2'}} & \frac{1}{S_{3,3'}} & \frac{1}{S_{3,4'}} & \frac{1}{S_{3,5'}} & 0 & 0 & 0 & 0 & 0 \\
0 & 0 & 0 & 0 & C55 & 0 & 0 & 0 & 0 & 0 & 0 & 0 & \frac{1}{S_{4,2'}} & \frac{1}{S_{4,3'}} & \frac{1}{S_{4,4'}} & \frac{1}{S_{4,5'}} & \frac{1}{S_{4,6'}} & 0 & 0 & 0 & 0 \\
0 & 0 & 0 & 0 & 0 & C66 & 0 & 0 & 0 & 0 & 0 & 0 & 0 & \frac{1}{S_{5,3'}} & \frac{1}{S_{5,4'}} & \frac{1}{S_{5,5'}} & \frac{1}{S_{5,6'}} & \frac{1}{S_{5,7'}} & 0 & 0 & 0 \\
0 & 0 & 0 & 0 & 0 & 0 & C77 & 0 & 0 & 0 & 0 & 0 & 0 & 0 & \frac{1}{S_{6,4'}} & \frac{1}{S_{6,5'}} & \frac{1}{S_{6,6'}} & \frac{1}{S_{6,7'}} & \frac{1}{S_{6,8'}} & 0 & 0 \\
0 & 0 & 0 & 0 & 0 & 0 & 0 & C88 & 0 & 0 & 0 & 0 & 0 & 0 & 0 & \frac{1}{S_{7,5'}} & \frac{1}{S_{7,6'}} & \frac{1}{S_{7,7'}} & \frac{1}{S_{7,8'}} & \frac{1}{S_{7,9'}} & 0 \\
0 & 0 & 0 & 0 & 0 & 0 & 0 & 0 & C99 & 0 & 0 & 0 & 0 & 0 & 0 & 0 & \frac{1}{S_{8,6'}} & \frac{1}{S_{8,7'}} & \frac{1}{S_{8,8'}} & \frac{1}{S_{8,9'}} & \frac{1}{S_{8,10'}} \\
0 & 0 & 0 & 0 & 0 & 0 & 0 & 0 & 0 & C1010 & 0 & 0 & 0 & 0 & 0 & 0 & 0 & \frac{1}{S_{9,7'}} & \frac{1}{S_{9,8'}} & \frac{1}{S_{9,9'}} & k_1 \\
0 & 0 & 0 & 0 & 0 & 0 & 0 & 0 & 0 & 0 & C1111 & 0 & 0 & 0 & 0 & 0 & 0 & 0 & \frac{1}{S_{10,8'}} & k_2 & k_3 \\
\frac{1}{S_{B,1'}} & \frac{1}{S_{1,1'}} & \frac{1}{S_{2,1'}} & \frac{1}{S_{3,1'}} & 0 & 0 & 0 & 0 & 0 & 0 & 0 & C1212 & 0 & 0 & 0 & 0 & 0 & 0 & 0 & 0 & 0 \\
\frac{1}{S_{B,2'}} & \frac{1}{S_{1,2'}} & \frac{1}{S_{2,2'}} & \frac{1}{S_{3,2'}} & \frac{1}{S_{4,2'}} & 0 & 0 & 0 & 0 & 0 & 0 & 0 & C1313 & 0 & 0 & 0 & 0 & 0 & 0 & 0 & 0 \\
0 & \frac{1}{S_{1,3'}} & \frac{1}{S_{2,3'}} & \frac{1}{S_{3,3'}} & \frac{1}{S_{4,3'}} & \frac{1}{S_{5,3'}} & 0 & 0 & 0 & 0 & 0 & 0 & 0 & C1414 & 0 & 0 & 0 & 0 & 0 & 0 & 0 \\
0 & 0 & \frac{1}{S_{2,4'}} & \frac{1}{S_{3,4'}} & \frac{1}{S_{4,4'}} & \frac{1}{S_{5,4'}} & \frac{1}{S_{6,4'}} & 0 & 0 & 0 & 0 & 0 & 0 & 0 & C1515 & 0 & 0 & 0 & 0 & 0 & 0 \\
0 & 0 & 0 & \frac{1}{S_{3,5'}} & \frac{1}{S_{4,5'}} & \frac{1}{S_{5,5'}} & \frac{1}{S_{6,5'}S_{7,5'}} & 0 & 0 & 0 & 0 & 0 & 0 & 0 & 0 & C1616 & 0 & 0 & 0 & 0 & 0 \\
0 & 0 & 0 & 0 & \frac{1}{S_{4,6'}} & \frac{1}{S_{5,6'}} & \frac{1}{S_{6,6'}S_{7,6'}} & \frac{1}{S_{8,6'}} & 0 & 0 & 0 & 0 & 0 & 0 & 0 & 0 & C1717 & 0 & 0 & 0 & 0 \\
0 & 0 & 0 & 0 & 0 & \frac{1}{S_{5,7'}} & \frac{1}{S_{6,7'}S_{7,7'}} & \frac{1}{S_{8,7'}} & \frac{1}{S_{9,7'}} & 0 & 0 & 0 & 0 & 0 & 0 & 0 & 0 & C1818 & 0 & 0 & 0 \\
0 & 0 & 0 & 0 & 0 & 0 & \frac{1}{S_{6,8'}S_{7,8'}} & \frac{1}{S_{8,8'}} & \frac{1}{S_{9,8'}} & \frac{1}{S_{10,8'}} & 0 & 0 & 0 & 0 & 0 & 0 & 0 & 0 & C1919 & 0 & 0 \\
0 & 0 & 0 & 0 & 0 & 0 & 0 & \frac{1}{S_{7,9'}} & \frac{1}{S_{8,9'}} & \frac{1}{S_{9,9'}} & k_{1'} & 0 & 0 & 0 & 0 & 0 & 0 & 0 & 0 & C2020 & 0 \\
0 & 0 & 0 & 0 & 0 & 0 & 0 & 0 & \frac{1}{S_{8,10'}} & k_{2'} & k_{3'} & 0 & 0 & 0 & 0 & 0 & 0 & 0 & 0 & 0 & C2121
\end{bmatrix}
\times
\begin{bmatrix} J_B \\ J_1 \\ J_2 \\ J_3 \\ J_4 \\ J_5 \\ J_6 \\ J_7 \\ J_8 \\ J_9 \\ J_{10} \\ J_{1'} \\ J_{2'} \\ J_{3'} \\ J_{4'} \\ J_{5'} \\ J_{6'} \\ J_{7'} \\ J_{8'} \\ J_{9'} \\ J_{10'} \end{bmatrix}
=
\begin{bmatrix} \frac{-E_B}{B_B} \\ \frac{-E_1}{B_1} \\ \frac{-E_2}{B_2} \\ \frac{-E_3}{B_3} \\ \frac{-E_4}{B_4} \\ \frac{-E_5}{B_5} \\ \frac{-E_6}{B_6} \\ \frac{-E_7}{B_7} \\ \frac{-E_8}{B_8} \\ \frac{-E_9}{B_9} \\ \frac{-E_{10}}{B_{10}} \\ \frac{-E_{1'}}{B_{1'}} \\ \frac{-E_{2'}}{B_{2'}} \\ \frac{-E_{3'}}{B_{3'}} \\ \frac{-E_{4'}}{B_{4'}} \\ \frac{-E_{5'}}{B_{5'}} \\ \frac{-E_{6'}}{B_{6'}} \\ \frac{-E_{7'}}{B_{7'}} \\ \frac{-E_{8'}}{B_{8'}} \\ \frac{-E_{9'}}{B_{9'}} \\ \frac{-E_{10'}}{B_{10'}} \end{bmatrix}
\qquad (5\text{-}7)
$$

where

$$k_1 = \frac{1}{S_{9,10'}} + \frac{1}{S_{9,10'M}} \qquad (5\text{-}7.1)$$

$$k_2 = \frac{1}{S_{10,9'}} + \frac{1}{S_{10,9'M}} \qquad (5\text{-}7.2)$$

$$k_3 = \frac{1}{S_{10,10'}} + \frac{1}{S_{10,10'M}} \qquad (5\text{-}7.3)$$

$$k_{1'} = \frac{1}{S_{10,9'}} + \frac{1}{S_{10M,9'}} \qquad (5\text{-}7.4)$$

$$k_{2'} = \frac{1}{S_{9,10'}} + \frac{1}{S_{9M,10'}} \qquad (5\text{-}7.5)$$

$$k_{3'} = \frac{1}{S_{10,10'}} + \frac{1}{S_{10M,10'}} \qquad (5\text{-}7.6)$$

$$C_{11} = -\left[\frac{1}{B_B} + \frac{1}{S_{B,1'}} + \frac{1}{S_{B,2'}} + \frac{1}{S_{B,1}} + \frac{1}{S_{B,2}}\right] \qquad (5\text{-}7.7)$$

$$C_{22} = -\left[\frac{1}{B_1} + \frac{1}{S_{1,B}} + \frac{1}{S_{1,1'}} + \frac{1}{S_{1,2'}} + \frac{1}{S_{1,3'}}\right] \qquad (5\text{-}7.8)$$

$$C_{33} = -\left[\frac{1}{B_2} + \frac{1}{S_{2,B}} + \frac{1}{S_{2,1'}} + \frac{1}{S_{2,2'}} + \frac{1}{S_{2,3'}} + \frac{1}{S_{2,4'}}\right] \qquad (5\text{-}7.9)$$

$$C_{44} = -\left[\frac{1}{B_3} + \frac{1}{S_{3,1'}} + \frac{1}{S_{3,2'}} + \frac{1}{S_{3,3'}} + \frac{1}{S_{3,4'}} + \frac{1}{S_{3,5'}}\right] \qquad (5\text{-}7.10)$$

$$C_{ii} = -[\frac{1}{B_{i-1}} + \frac{1}{S_{(i-1),(i-3)'}} + \frac{1}{S_{(i-1),(i-2)'}}$$

$$+ \frac{1}{S_{(i-1),(i-1)'}} + \frac{1}{S_{(i-1),(i)}} + \frac{1}{S_{(i-1),(i+1)}}] \qquad (5\text{-}7.11)$$

$i = 5, 6, \ldots\ldots, 9$

$$C_{1010} = -[\frac{1}{B_9} + \frac{1}{S_{9,7'}} + \frac{1}{S_{9,8'}} + \frac{1}{S_{9,9'}} + \frac{1}{S_{9,10'}} + \frac{1}{S_{9,10'M}}] \qquad (5\text{-}7.16)$$

$$C_{1111} = -[\frac{1}{B_{10}} + \frac{1}{S_{10,8'}} + \frac{1}{S_{10,9'}} + \frac{1}{S_{10,10'}} + \frac{1}{S_{10,10'M}}$$

$$+ \frac{1}{S_{10,9'M}}] \qquad (5\text{-}7.17)$$

$$C_{1212} = -[\frac{1}{B_{1'}} + \frac{1}{S_{B,1'}} + \frac{1}{S_{1,1'}} + \frac{1}{S_{2,1'}} + \frac{1}{S_{3,1'}}] \qquad (5\text{-}7.18)$$

$$C_{1313} = -[\frac{1}{B_{2'}} + \frac{1}{S_{B,2'}} + \frac{1}{S_{1,2'}} + \frac{1}{S_{2,2'}} + \frac{1}{S_{3,2'}} + \frac{1}{S_{4,2'}}] \qquad (5\text{-}7.19)$$

$$C_{jj} = -[\frac{1}{B_{(j-11)'}} + \frac{1}{S_{(j-13),(j-11)'}}$$

$$+ \frac{1}{S_{(j-12),(j-11)'}} + \frac{1}{S_{(j-11),(j-11)'}}$$

$$+\frac{1}{S_{(j-10),(j-11)'}}+\frac{1}{S_{(j-9),(j-11)'}}] \qquad (5\text{-}7.20)$$

$j = 14,....19$

$$C_{2020} = -[\frac{1}{B_{9'}}+\frac{1}{S_{7,9'}}+\frac{1}{S_{8,9'}}+\frac{1}{S_{9,9'}}+\frac{1}{S_{10,9'}}+\frac{1}{S_{10M,9'}}] \qquad (5\text{-}7.26)$$

$$C_{2121} = -[\frac{1}{B_{10'}}+\frac{1}{S_{8,10'}}+\frac{1}{S_{9,10'}}+\frac{1}{S_{10,10'}}+\frac{1}{S_{10M,10'}}$$

$$+\frac{1}{S_{9M,10'}}] \qquad (5\text{-}7.27)$$

A solution of the system of equations for the unknowns J's requires a calculation of "shape factors" for each body increment (Appendix F). Subroutine HRAD (Appendix E) uses the shape factors and associated incremental areas to calculate the surface resistances of each node according to Equation (5-5'). This information is input data for the main program; it is input as a 21 x 21 matrix in the variable C(I,J). C(I,J) constitutes the elements of the coefficient matrix in Equation (5-7), except for the main diagonal elements. The main diagonal terms are given by the C_{ii} and C_{jj} terms previously defined; one term of each element contains the body resistance term, B_i or B_j, which is a function of the body's temperature dependent emissivity ε_i or ε_j,

Equations (5-3') or (5-3"). The subroutine therefore calculates the temperature dependent body resistance for each temperature iteration set. In addition it calculates the body emissive powers E_i and E_j for each iteration.

Solution of the system is accomplished with a Gauss-Siedel-Hoteling[30] scheme and results in a column vector containing the 21 J values. For each node of body 1, the respective value of E_i and J_i are used in Equation (5-2) to calculate $\dot{q}_{rad}$. A new radiation coefficient is then calculated according to the following definition:

$$H_i = \frac{q_{rad}}{A_i(T_i - T_j)} \tag{5-8}$$

where

H_i = the new convection-like radiation coefficient for node N,

A_i = the radiation heat transfer area (surface area) for node N,

T_i = the temperature of the body 1, node i, and

T_j = the temperature of the body 2, node j = i.

The new coefficient of Equation (5-8) is used in the general algorithm Equation (3-34) instead of the old coefficient defined by Equation (3-29). Six to eight iterations are required for a single solution of the 21 x 21 system; this solution is required for each temperature iteration and as a consequence the time required for convergence of the temperature profile is substantially increased. In general, if

the average number of iterations to solve the matrix is n, the number of iterations required for convergence of the temperature profile is n-fold. Good initial guesses are of marked benefit for efficient utilization of program PH-5.

Computer runs are to be made utilizing the new program PH-5. The data generated is to be compared to analogous runs performed by program PH-3. The comparison will be in terms of the converged temperature profile and respective values of heat transfer rates. In this way, it will be possible to compare the modeling techniques and ascertain the validity of the one to one model which has been relied on so heavily for this study, as well as similar studies performed using program THTB.

The modeling data for the configurations to be examined and compared is related in accompanying Tables G-4 and G-5, Appendix G. Additional information is supplied for PH-5, that is, the complex geometry modeled requires shape factor and nodal area data. This data is supplied in Table G-6. The shape factor data is generated with relations given in Appendix F.

Table 5-1 summarizes the conclusions of the comparison runs. For the two situations examined the temperature profiles generated by PH-3 and PH-5 respectively, are approximately congruent. PH-5 predicts slightly higher values for the heat radiated, 3.81% for the unplated susceptor and 2.38% for the gold plated susceptor, hence a higher value for the relative percentage radiated. While the algorithm in subroutine HRAD more realistically treats the complex radiation phenomenon, the more simple algorithm of subroutine HIGH

Table 5-1

Summary of Modeling Comparison
Temperature °F

Node	Solid Susceptor (unplated)		Solid Susceptor (gold plated)	
	HIGH	HRAD	HIGH	HRAD
1	752.0	752.0	752.0	752.0
2	882.1	882.3	887.1	887.1
3	991.5	991.5	1001.0	1001.0
4	1082.5	1082.6	1096.1	1096.0
5	1156.9	1157.10	1174.0	1173.9
6	1216.1	1216.2	1236.2	1236.2
7	1261.1	1261.1	1283.6	1283.5
8	1292.7	1292.6	1317.0	1317.0
9	1311.5	1311.2	1336.9	1336.8
10	1317.7	1317.6	1343.5	1343.5
PCTRQG	4.65¢	4.83%	.99%	1.02%
QR	9.6 BTU/hr	9.98 BTU/hr	2.05 BTU/hr	2.1 BTU/hr

appears not to suffer a great loss in accuracy because of that simplicity. The compatibility of the results may be because of the constant sink temperature, that is, any given transmitting node on the susceptor body "sees" and hence radiates to the same constant temperature sink in either case. The dispersal of the energy is judged to be irrelevant. There was insufficient time to evaluate the case of a heat shielded configuration, however, the results would probably prove somewhat different. In such a case, a given radiating or transmitting node would "see" and hence radiate to more than one sink, each with its own "different" temperature.

It should be a simple matter to use the convection-like radiation heat transfer coefficients of Equation (5-8) in Program THTB if, instead of the shape factor information required as input data[20], a pseudo shape factor could be used such as:

$$F''_{i-m} = \frac{H_i}{F'_{i-m}} \qquad (5\text{-}9)$$

where,

F''_{i-m} = the pseudo shape factor for radiation exchange between node i and node m;

H_i = the radiation coefficient generated by HRAD in PH-5 for node i; and

F'_{i-m} = the corrected shape factor[31] presently required for THTB.

In general, it is not possible to know the value of measured quantities with infinite precision, that is, the error existent between

the true and the measured values is not readily ascertainable; what is likely, is that the average or mean value of the measured quantities may be known as well as the variance of the measurements about the respective means. This being the case, it is often useful to determine the net effect upon a deterministic prediction, afforded by a model of the form previously seen in Equation (1-1):

$$T = f(\dot{Q}, \rho, k(T), \varepsilon(T), \vec{R}, \ldots,),$$

as a consequence of independent variables with various uncertainties or variances in their value being used to accomplish a prediction. That is, due to uncertainties in the independent variables, it is desirable to know the resulting uncertainty in the prediction or dependent variable. In order to accomplish the preceeding task the following information is required. Suppose the following accurate deterministic model exists

$$w = f(x, y, z, \ldots,)$$

for which the variables are random and independent. If this is the case then, each of the independent variables possesses a mean value μ_x, μ_y, μ_z,.... and a variance σ_x^2, σ_y^2, σ_z^2,.... respectively. The specific information required is the mean value of w, that is, μ_w and its variance σ_w^2.

A Taylor series expansion of w about the means of the respective variables will ultimately yield an expression of the form[32]:

$$\sigma_w^2 \simeq \left(\frac{\partial f}{\partial x}\right)^2 \sigma_x^2 + \left(\frac{\partial f}{\partial y}\right)^2 \sigma_y^2 + \left(\frac{\partial f}{\partial z}\right)^2 \sigma_z^2 + \ldots. \qquad (5\text{-}9)$$

or in more general terms

$$\sigma_w^2 \simeq \sum_{i=1}^{n} V_{x_i}^2 \qquad (5\text{-}10)$$

where

$$V_{x_i}^2 = \left(\frac{\partial f}{\partial x_i}\right)^2 \sigma_{x_i}^2 \qquad (5\text{-}11)$$

and x_i necessarily corresponds to the x_ith independent variable of the function $w = f(x_1, x_2, \ldots, x_i)$. The expansion used to generate Equation (5-9) requires that w be a linear function of its variables[32,34] Necessarily then the mean value for w, namely μ_w is given by,

$$\mu_w = f(\mu_x, \mu_y, \mu_z, \ldots)$$

Equation (5-9) or (5-10) is exact for linear functions and approximate for non-linear functions.

An ideal first application for the expression (5-9) is an examination of the simplified model of Equation (1-2'). This explicit expression is purely analytic and therefore lends itself readily to analysis by Equation (5-9). It additionally affords the advantage of being the limiting case to the propogation of error analysis to be performed on the optimized calorimeter configurations. For the simplied model, the heat transport mechanism is pure conduction, that is, the expression (1-2) was derived from the general heat transfer Equation (3-4) by considering zero radiation from the sides and end of the susceptor. Equation (1-2') is a direct result of Equation (1-2).

Equation (1-2') is repeated for convenience:

$$\dot{Q} = \frac{k[T(z) - T_o]}{\rho(Lz - z^2/2)} \qquad (1\text{-}2')$$

for which it is easy to generate the required partial derivative factors of Equation (5-9):

$$\frac{\partial \dot{Q}}{\partial T_o} = -\frac{k}{\rho(Lz - z^2/2)}$$

$$\frac{\partial \dot{Q}}{\partial T(z)} = -\frac{k}{\rho(Lz - z^2/2)}$$

$$\frac{\partial \dot{Q}}{\partial k} = \frac{T(z) - T_o}{\rho(Lz - z^2/2)}$$

$$\frac{\partial \dot{Q}}{\partial L} = -\frac{k(T(z) - T_o)z}{\rho(Lz - z^2/2)}$$

The standard deviation terms which make up the balance of factors required for applying the analysis of Equation (5-9) to the model of Equation (1-2'), are given for each of the parameters of interest in Table (5-2). In addition, Table 5-2 includes the various parameter mean values. Expression (5-9) is expanded in terms of the parameters of interest to obtain:

$$\sigma_Q^2 \simeq \left(\frac{\partial \dot{Q}}{\partial T_o}\right)^2 (\sigma_{T_o})^2 + \left(\frac{\partial \dot{Q}}{\partial T(L)}\right) (\sigma_{T(L)})^2 + \left(\frac{\partial \dot{Q}}{\partial k}\right)^2 \sigma_k^2$$

$$+ \left(\frac{\partial \dot{Q}}{\partial L}\right)^2 \sigma_L^2$$

Table 5-2

Parameter Mean and Standard Deviation for 1-D Error Study

Parameter	Parameter mean value, μ	Parameter Standard Deviation σ
QGEN	3.75 watts/gm	μ = 3.75
T_o	750°F	$\pm$3/16% of μ = 1.41°F
T(z) = T(.9)	1350°F	$\pm$3/16% of μ = 2.53°F
$\bar{k}$	13.44 BTU/hr ft°F	$\pm$2.5% of μ = .3375 BTU/hr ft°F
L	.9"	$\pm$.1% of μ = .001"

Table 5-3

Weighted Variance Contribution of Parameters

Variance term	Value
V^2_{To}	7.85×10^{-5}
$V^2_{T(L)}$	2.53×10^{-4}
V^2_k	8.79×10^{-3}
V^2_L	6.94×10^{-5}

The individual weighted variance terms are given Table 5-3.

It is often useful and demonstrative to relate a given standard deviation, normalized to the mean of the parameter to which it is associated. This is the form in which statistical information is often related in the literature[27]. (The data presented in Table 5-2 is related in this way). For this same reason the standard deviation $\sigma_{\dot{Q}}$ for the internal heat generation rate term just calculated is normalized to the assumed average value of 3.75 watts/gm so that

$$\sigma_{\dot{Q}}\% = 2.56\%.$$

At this time it should be noted that the limiting case propogated variance, 2.56% is only slightly larger than the variance in the thermal conductivity term (Table 5-2). An examination of the relative magnitudes of the weighted variance terms in Table 5-3 reveals that the dominant term is the weighted variance in thermal conductivity. It is interesting to note that for the normalized propogated variance contribution by thermal conductivity given by:

$$V_k^2 = \left(\frac{\partial \dot{Q}}{\partial k}\right)^2 \left(\frac{\sigma_k}{\dot{Q}}\right)^2 ;$$

that

$$\frac{\partial \dot{Q}}{\partial k} = \frac{T(z) - T_o}{\rho(Lz - z^2/2)}$$

and therefore,

$$\frac{\partial \dot{Q}}{\partial k} = \frac{\dot{Q}}{k}$$

$$= .279$$

so that

$$V_k^2 = \left(\frac{\dot{Q}}{k}\right)^2 \frac{\sigma_k^2}{\dot{Q}^2}$$

$$= \left(\frac{.025\ k}{k}\right)^2$$

$$V_k = 2.5\%$$

The limiting case value of $\sigma_{\dot{Q}} = 2.56\%$ is expected to be the lower limit of attainable accuracy for the optimized calorimeters when fabricated from stainless steel. These calorimeters reduce but do not remove the contribution by radiation heat transfer.

In light of the fact that the thermal conductivity uncertainty, $\sigma = \pm 2.5\%$, dominated the preceeding analysis it was decided to perform a similar limiting case analysis for the iron susceptor, item number 3, in Table 4-9. For this material, iron, the uncertainty in thermal conductivity is $\sigma_k = \pm\ 1\%$. Subsequent calculations yield a normalized value for $\sigma_{\dot{Q}}$ to be

$$\sigma_{\dot{Q}} \simeq 1.02\%$$

Before leaving the analysis of the error propogation in the simplified model, an explanation promised in Chapter 2 will be supplied. Recall that it was said to be desirable "for reasons of accuracy" to have the calorimeter operate at the maximum possible temperature, that is, within the limits of constraints imposed by other considerations.

Consider the weighted variance term for the contribution by the general temperature term T(z), that is

$$V^2_{T(z)} = \left(\frac{\partial \dot{Q}}{\partial T(z)}\right)^2 \sigma^2_{T(z)}$$

$$= \left(\frac{k}{\rho(Lz - z^2/2)}\right) \sigma^2_{T(z)} .$$

When this term is normalized to $\dot{Q}$ it becomes

$$\bar{V}^2_{T(z)} = \frac{\left(\frac{k}{\rho(Lz - z^2/2)}\right) (\sigma_{T(z)})^2}{\dot{Q}}$$

$$= \left(\frac{k}{\dot{Q}\rho(Lz - z^2/2)}\right)^2 \sigma^2_{T(z)}$$

$$= \left(\frac{1}{T(z) - T_o}\right)^2 \sigma^2_{T(z)}$$

from which it is intuitively clear that as ΔT or T(z), the maximum temperature measured, increases the weighting factor and hence the overall term decreases.

The next step of the analysis will be a determination of the item number 10, in Error Parameter, Table 2-2. This determination will satisfy the final goal of the study.

To begin, recall Expression (5-9) or (5-10) and note that the unique factors in each term are the partial derivatives of the function defining the variable of interest. For the simple model of Figure 1-2, Equation (1-2) was derived and from which, it was not difficult to obtain Equation (1-2'). Generation of the desired partial derivatives was straight-forward. The error analysis or standard deviation determination required to satisfy the final requirement of the study will be more circuitous. By analogy with Equation (1-2), the relationship defining the temperature profile in the calorimeter exists as a numerical algorithm in a computer code; the relationship analogous to Equation (1-2') is in contrast only an "implicit" function of that numerical algorithm. It is not possible then to perform a straightforward partial differiation to define the desired partial derivatives. It will be necessary to numerically generate approximations to those partial derivatives.

In tabular form or graphically, it is necessary to generate relations (recall Equation (3-38)) of the form:

$$\dot{Q}(k) = f_{2_1}(T = T_{avg},\ k,\ \varepsilon_1 = \varepsilon_{avg}, \ldots\ldots)$$

$$\dot{Q}(T) = f_{2_2}(T,\ k = k_{avg},\ \varepsilon_1 = \varepsilon_{avg}, \ldots\ldots)$$

$$\dot{Q}(\varepsilon_1) = f_{2_3}(T = T_{avg},\ k = k_{avg},\ \varepsilon_1, \ldots\ldots)$$

$$\vdots$$

where, f_{2_1} is a function of k only; f_{2_2} is a function of T only, f_{2_3} is a function of ε_1 only, and etcetera for the remaining variables. In addition:

T_{avg} = the average or mean value of T;

k_{avg} = the average or mean value of k;

$\varepsilon_{1_{avg}}$ = the average or mean value of ε_1;

.

.

.

.

.

From the graph or tabular values so generated for each function, it will be possible, for example, to approximate the value of:

$$\frac{\partial Q}{\partial k}\Bigg|_{\text{other variables constant}}$$

by

$$\frac{\Delta Q}{\Delta k}\Bigg|_{\text{other variables constant.}}$$

Actually it is advisable to make at least two approximations such as:

$$\frac{\dot{\Delta Q}}{\Delta k} = \frac{\dot{Q}(k + \Delta k) - \dot{Q}(k)}{\Delta k}, \qquad (5\text{-}10)$$

and

$$\frac{\dot{\Delta Q}}{\Delta k} = \frac{\dot{Q}(k - \Delta k) - \dot{Q}(k)}{-\Delta k}, \qquad (5\text{-}11)$$

and finally, to approximate $\partial\dot{Q}/\partial k$ by the average of the two. In order for the overall approximation to be valid, recall that the assumption was made that $\dot{Q}$ had to be approximately linear in its variables,

therefore, if the approximations just given for the partial derivative of $\dot{Q}$ are very different, the implication is that the function $\dot{Q}$ is grossly non-linear with respect to that variable, and the approximation is invalid to begin with. For small enough variation in the chosen independent variable, that is, over the range envisioned, the function $\dot{Q}$ should be slowly varying and hence approximately linear. In actual fact it is not even possible to obtain the numerical quantities given by Equations (5-10) and (5-11) directly; this is of course due to the implicit nature of the function which has been described as $\dot{Q}$ (recall Figures 3-4 and 3-5). The circuitious approach used, is to numerically generate the function,

$$T = f(\dot{Q},\ k = k_{avg},\ \varepsilon_1 = \varepsilon_{1_{avg}},\ldots.)$$

from the numerical algorithm. Note that the only independent variable, as written, is $\dot{Q}$ and consequently:

$$T = f(\dot{Q}).$$

For illustration the data obtained is represented graphically; in point of fact calculations are performed on tabular data. Suppose that Figure 5-10 represents that data in the form of the curve $f(\dot{Q})$. Further, suppose that it is desirable to approximate $\partial\dot{Q}/\partial\varepsilon_1$, therefore, ε_1 is perturbed by a small amount of $\Delta\varepsilon_1$. A new function and new data are generated by

$$T_{+\Delta\varepsilon_1} = f(\dot{Q},\ k = k_{avg},\ \varepsilon_1 = \varepsilon_{1_{avg}} + \Delta\varepsilon_1,\ldots.)$$

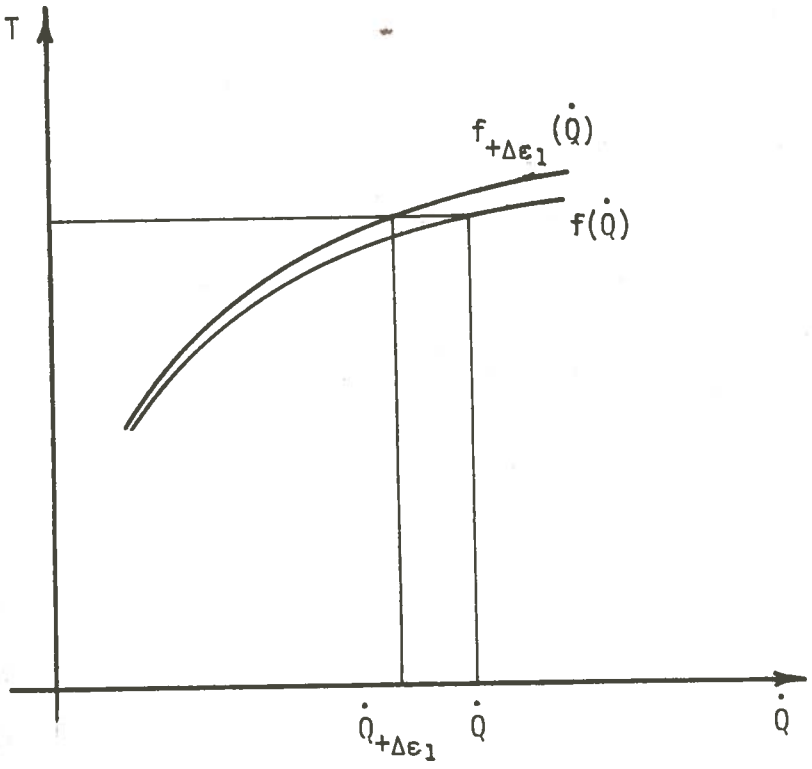

FIGURE 5-6

Numerical Approximation of Partial Derivatives from an Implicit Function

The new data is represented in Figure 5-10 by $f_{+\Delta\varepsilon_1}(\dot{Q})$. Interpolation is performed between data points on $f_{+\Delta\varepsilon_1}(\dot{Q})$ to obtain a value of $\dot{Q}$ designated $\dot{Q}_{+\Delta\varepsilon_1}$ such that $f(\dot{Q}) = f_{+\Delta\varepsilon_1}(\dot{Q}_{+\Delta\varepsilon_1})$. The partial derivative is then approximated as

$$\left.\frac{\partial Q}{\partial \varepsilon_1}\right|_{\substack{T = \text{constant;} \\ \text{other variables} \\ \text{constant}}} \simeq \left.\frac{\dot{Q} - \dot{Q}_{+\Delta\varepsilon_1}}{\Delta\varepsilon_1}\right|_{\substack{T = \text{constant;} \\ \text{other variables} \\ \text{constant}}}$$

In a similar manner another approximation is obtained by perturbing ε_1 by $-\Delta\varepsilon_1$. The preceding operation is carried out for all of the relevant variables needed to satisfy a calculation with Equation (5-9) or (5-10).

The error analysis is to be performed for four different calorimeters; they are identified in Tables 5-4 and 5-5, which relate relevant geometrical and operational parameter values. As seen in Tables 5-4 and 5-5, the material parameter, chosen for the calormeters in the error study, is stainless steel. A case was made in Chapter 2 for utilizing iron in place of stainless steel from which to fabricate the calorimeter. The reasoning was based upon the fact that stainless steel and iron present the same average electron density to interacting gamma radiation. In addition it has been noted in this chapter that for the limiting case, an iron calorimeter will permit measurements with a substantially lower inherent propogated error. The reason for ignoring this information is threefold: 1) iron and stainless steel do not present "exactly" identical gamma interaction medium, 2) stainless steel is the exact material for which heating rates are required

Table 5-4

Relevant Parameter Data for Configuration A

Parameter	Solid susceptor, stainless steel, unplated Average or mean value, μ	Solid susceptor, stainless steel, gold plated Average or mean value, μ
RW	0.23"	0.23"
RN	0.21"	0.21"
Gap 1	0.020"	0.020"
L	0.95"	0.9"
Base Temperature, TN1	752°F	752°F
Containment Tube Wall Temperature	740°F	740°F
QGEN	3.75 w/gm	3.75 w/gm

Table 5-5

Relevant Parameter Data for Configuration B

Parameter	Heat shielded, stainless steel, unplated Average or mean value, μ	Heat shielded, stainless steel, gold plated Average or mean value, μ
RW	0.23"	0.23"
Gap 1	0.020"	0.020"
DR	0.03"	0.01"
RS	0.18"	0.20"
Gap 2	0.020"	0.020"
RN	0.16"	0.18"
Base Temperature	752°F	752°F
Heat shield base temperature	750°F	750°F
Containment tube wall temperature	740°F	740°F
QGEN	3.75 w/gm	3.75 w/gm

in the EBR-II environment, 3) a realistic accuracy measurement for stainless steel should be established based upon 2) preceeding. The values given in the tables are assumed to be average or mean values.

The parameters identified as contributors to the propogated variance in $\dot{Q}$ are listed in Table 5-6 with their respective standard deviations. The uncertainties are assumed to be the $\pm$ 1 σ (68.23% confidence interval) percentage of the variable mean unless otherwise stated.

Table 5-7 contains the partial derivative approximations. Table 5-8 contains the standard deviation associated with each parameter. Table 5-9 contains, for each calorimeter, the weighted variance contributions made by each parameter as well as the propogated variance, standard deviation and normalized standard deviation.

A comparison of $\sigma_{\dot{Q}}\%$ in Table 5-12 indicates that each of the stainless steel calorimeters examined approaches the limiting case value of 2.56%. The two calorimeters with gold plated susceptors have essentially removed the error contribution due to uncertainties in radiation quantification; this is best described by the relative magnitudes of the weighted variance terms $V^2_{\varepsilon+}$ and $V^2_{\varepsilon-}$. The values of these terms for the two calorimeters cited offer the minimum contribution to the total variance term. Clearly the dominant parameter is the weighted variance term for the thermal conductivity of stainless steel, as it was for the limiting case. (Equation 5-9) appears to be linear in σ_k for the systems examined.

Table 5-6

Parameters Significant to Error Propogation Study
with Respective Standard Deviation

Parameter	Solid Susceptor Variables	Heat Shielded Susceptor Variables
L	0.001"	0.001"
Gap 1	0.002"	0.002"
Gap 2	--	0.002"
RN	0.001"	0.001"
k (stainless steel)	±2.5%	±2.5%
ε (stainless steel)	±12.5%	±12.5%
ε (gold)	±2.5%	±2.5%
Containment tube wall temperature	±3/16%	±3/16%
Base temperature	±3/16%	±3/16%
Heat shield base temperature	--	±3/16%
Maximum temperature	±3/16%	±3/16%

Table 5-7

Approximations to Partial Derivates

Partial Deriv. Approx.	Solid Susceptor $\varepsilon = \varepsilon_{ss}$	Solid Susceptor $\varepsilon = \varepsilon_{Au}$	Shielded Susceptor $\varepsilon = \varepsilon_{ss}$	Shielded Susceptor $\varepsilon = \varepsilon_{Au}$
$\Delta Q/\Delta RN$+watt/inch	6.25	7.143	7.143	0
$\Delta Q/\Delta RN$-watt/inch	6.25	7.143	7.143	0
$\Delta Q/\Delta L$+watt/inch	7.143	14.286	7.143	7.143
$\Delta Q/\Delta L$-watt/inch	7.143	7.143	14.29	7.143
$\Delta Q/\Delta k_{ss}$+watt-hr-ft°F/BTU	.236	.238	.253	.258
$\Delta Q/\Delta k_{ss}$-watt-hr-ft°F/BTU	.238	.250	.244	.256
$\Delta Q/\Delta \varepsilon$+watt	.815	4.60	.51	0
$\Delta Q/\Delta \varepsilon$-watt	.955	4.64	.466	0
$\Delta Q/\Delta T_w$+watt/°F	0	0	0	0
$\Delta Q/\Delta T_w$-watt/°F	0	0	0	0
$\Delta Q/\Delta TN1$+watt/°F	5.066×10^{-3}	.010	5.066×10^{-3}	5.066×10^{-3}
$\Delta Q/\Delta TN1$-watt/°F	5.066×10^{3}	5.066×10^{-3}	5.066×10^{-3}	5.066×10^{-3}
$\Delta Q/\Delta T$+watt/°F	8.33×10^{-3}	6.25×10^{-3}	8.33×10^{-3}	7.14×10^{-3}
$\Delta Q/\Delta T$-watt/°F	6.25×10^{-3}	8.33×10^{-3}	7.14×10^{-3}	7.14×10^{-3}
$\Delta Q/\Delta TS1$+watt/°F			5.066×10^{-3}	0
$\Delta Q/\Delta TS2$-watt/°F			5.066×10^{-3}	0
$\Delta Q/\Delta DR$+watt/inch			$7.1r \times 10^{-3}$	0

Table 5-7 (Continued)

Partial Deriv. Approx.	Solid Susceptor $\varepsilon = \varepsilon_{ss}$	Solid Susceptor $\varepsilon = \varepsilon_{Au}$	Shielded Susceptor $\varepsilon = \varepsilon_{ss}$	Shielded Susceptor $\varepsilon = \varepsilon_{Au}$
Q/ DR-watt/°F	0	0	7.14×10^{-8}	0
Q/ Gap+watt/inch	0	0	3.572	0
Q/ Gap-watt/inch	0	0	3.572	0

Table 5-8

Standard Deviation Associated with Particular Parameters

Variance	Solid Susceptor $\varepsilon = \varepsilon_{ss}$	Solid Susceptor $\varepsilon = \varepsilon_{Au}$	Shielded Susceptor $\varepsilon = \varepsilon_{ss}$	Shielded Susceptor $\varepsilon = \varepsilon_{Au}$
σRN	.001"	.001"	.001"	.001"
σL	.001"	.001"	.001"	.001"
σk_{ss}	.374 BTU/hr ft°F	.3707 BTU/hr ft°F	.3702 BTU/hr ft°F	.3715 BTU/hr ft°F
$\sigma \varepsilon$	.0437	1.519×10^{-3}	.04206	1.0×10^{-3}
σT_w	1.38°F	1.38°F	1.38°F	1.38°F
σTN	1.41°F	1.41°F	1.41°F	1.41°F
σTS			1.41°F	1.41°F
σDR			.002"	.002"
σT_{max}	2.56°F	2.51°F	2.50°F	2.51°F
σDR			.001"	.001"
σGap			.002"	.002"

Table 5-9

Weighted Variance Contribution of Parameters

$$\Sigma\ (\sigma_{x_i})^2\ (\frac{\partial f}{\partial x_i})^2 = \Sigma\ V_{xi}^2$$

	Solid Susceptor $\epsilon = \epsilon_{ss}$ L = .95 RN = .21 T_{max} =	Solid Susceptor $\epsilon = \epsilon_{Au}$ L = .9" RN = .21 T_{max} =	Shielded Susceptor $\epsilon = \epsilon_{ss}$ L = .9" RN = .16 DR = .03" RSN = .21 T_{max} =	Shielded Susceptor $\epsilon = \epsilon_{Au}$ L = .9 RN = .18 DR = .01" RSN = .21 T_{max} =
V^2RN+	3.91×10^{-5}	5.102×10^{-5}	5.102×10^{-5}	0
V^2RN-	3.91×10^{-5}	5.102×10^{-5}	5.102×10^{-5}	0
V^2L+	5.102×10^{-5}	2.041×10^{-4}	5.102×10^{-5}	5.102×10^{-5}
V^2L-	5.102×10^{-5}	5.102×10^{-5}	2.041×10^{-4}	5.102×10^{-5}
V^2kss+	7.82×10^{-3}	7.70×10^{-3}	8.72×10^{-3}	9.179×10^{-3}
V^2ksa-	7.93×10^{-3}	8.59×10^{-3}	8.18×10^{-3}	9.074×10^{-3}
V^2_{ϵ}+	1.27×10^{-3}	4.96×10^{-5}	5.76×10^{-4}	0
V^2_{ϵ}-	1.74×10^{-3}	4.96×10^{-5}	3.83×10^{-4}	0
V^2Tw+	0	0	0	0
V^2Tw-	0	0	0	0
V^2TN+	5.102×10^{-5}	2.041×10^{-4}	5.10×10^{-5}	5.10×10^{-5}
V^2TN-	5.102×10^{-5}	5.10×10^{-5}	5.10×10^{-5}	5.10×10^{-5}
V^2Tmax	3.34×10^{-4}	3.20×10^{-4}	3.75×10^{-4}	3.23×10^{-4}
V^2TS1+			5.10×10^{-5}	0
V^2TS1-			5.10×10^{-5}	0
V^2DR+			5.10×10^{-5}	0
V^2DR-			5.10×10^{-5}	0
V^2Gap 1			5.10×10^{-5}	0
V^2Gap 2			5.10×10^{-5}	0
σQ^2	1.015×10^{-2}	9.42×10^{-3}	1.014×10^{-2}	9.50×10^{-3}
σQ	1.007×10^{-1}	9.71×10^{-2}	1.014×10^{-2}	9.50×10^{-2}
σQ%	2.69%	2.58%	2.68%	2.6%

The two gold plated calorimeters afford essentially the same standard deviation approximately 2.6% and similarly for the two unplated calorimeters which have a standard deviation value of approximately 2.7%. It is clear that the standard deviation for the system, $\sigma_{\dot{Q}}$, should be significantly reduced by fabricating the calorimeter susceptor from iron for which $\sigma_k = 1\%$, instead of stainless steel for which $\sigma_k = 2.5\%$. If it is assumed that the solid susceptor, iron, gold plated calorimeter will respond to the parameter perturbations in approximately the same way as its counter part, then a propogation of error study should predict the standard deviation for $\sigma_{\dot{Q}}$ to be less than or equal to approximately 1.1%. Recall that the limiting case calculation gave a lower limit value of 1.02%. Unfortunately, there was not sufficient time to verify this assumption.

Finally then it is to be noted that the perturbation to the system by the axially imbedded chromel alumel thermocouple has been neglected. The Koenig experiment[2] demonstrated that this contribution to the configuration of interest would be insignificant.

Chapter 6

Summary and Conclusions

The analysis of Chapter 4 quantified the capability of each calorimeter to accomplish one of the primary goals of the parametric study, that is the reduction of the relative radiation energy transfer rate. Table 4-8 and 4-9 relate the comparison data. The preliminary choice for an optimized design consequently was calorimeter (4), Table 4-9. Chapter 5 analysis dispelled any concern about modeling error as would be introduced by the "one to one" nodal exchange of radiant energy for the preliminary choice calorimeter. The propogation of error study of Chapter 5 revealed that each calorimeter evaluated for error magnitude, satisfied the "basic design critera" (6) requiring the identification of a calorimeter which for the immediate future can make heating rate measurements with uncertainties less than 5%. Furthermore the analysis determined that each of these calorimeters is capable of meeting the long range goal of measurements with uncertainties less than 3%. A correlation of the data in Tables 4-8 and 5-12 indicates that accurate measurements do not necessitate the complete suppression of radiation heat transfer. As an example, the solid susceptor, stainless steel, unplated calorimeter of Table 4-9, item number (6) has a 5.3% relative radiation rate and a predicted error limit of σ equals 2.69%. Immediate and long range goals as delineated may be satisfied with this calorimeter.

The error study stopped short of a determination of the upper limit of an acceptable relative radiation rate, in terms of its effect upon error propogation.

The following recommendations and conclusions are drawn from the composite study:

1. An upper limit to acceptable relative radiation rates should be determined in part by performing a propogation of error study on the iron calorimeters identified in Table 4-9. This study may obviate the immediate necessity for gold plating and/or building heat shielded calorimeters.
2. Calorimeter measurements for the configurations examined have errors dominated by uncertainties in the thermal conductivity of the calorimeter material. The question to be answered is, do iron calorimeters respond in the same way as the stainless steel calorimeters? If so, they will also be dominated by the thermal conductivity error, and additionally this would mean that the iron calorimeters may be capable of maximum attainable accuracy.
3. Based upon an affirmative answer to the question asked in 2. it will be necessary to experimentally determine if comparable iron and stainless steel calorimeters respond identically to the same

gamma radiation environment. This may be determined by using iron calorimeters conjunctively with stainless steel calorimeters in a properly designed experiment.

4. From the present point of view, the solid susceptor is the configuration of choice, because it is accurate while affording the simplest construction. Furthermore, it appears unnecessary to suppress radiation to the low levels accomplishable with the heat shielded calorimeters.

5. If gold plating may be accomplished with ease from the physical or mechanical standpoint then the solid susceptor iron and solid susceptor stainless steel calorimeters when gold plated will more than satisfy accuracy requirements for the 3 to 5% range.

6. The heat shielded calorimeters are apparently unnecessary.

7. If gold plating is unsuccessful then a relatively accurate full back line has already been identified. Both of the unplated stainless steel calorimeters of Table 5-9 have error bounds of approximately 2.7%.

As implied in 1. preceding, the error study for the iron calorimeters may prove them capable of the maximum accuracy even without gold plating.

REFERENCES

1. R. A. Laskiewicz, J. F. Koenig, Comparisons of Measured with Calculated Gamma Heating in Subassembly XX05, ANL-RNP-39, pp. 1.23-25, April 1975.

2. J. F. Koenig, R. G. Matlock, C. C. Ford, Design of Axial-heat flow Gamma Calorimeter, ANL-RDP-2, February 1972.

3. C. C. Price, Gamma Heat Measurements in EBR-II Using Passive Calorimeters, Argonne Natl. Laboratory, Idaho Falls, Idaho, 1976.

4. S. Glasstone and A. Sesonske, Nuclear Reactor Engineering, Van Nostrand Reinhold, New York, NY, 1967.

5. C. C. Price, private communications (1975).

6. C. H. Hogg, "Gamma Heating Measurements in the MTR," IDO-16093 (1953).

7. W. F. Witzig, "WAPD-1 Experiments in the MTR," WAPD-79 (1953).

8. C. H. Hogg, "Gamma-Ray Dosage Measurement," IDO-16205 (1954).

9. L. D. Weber and C. H. Hogg, "MTR Gamma Heat Generation Measurements," IDO-16652 (1961).

10. H. Greenspan, C. N. Kelber, D. Okrent (Eds.), Computing Methods in Reactor Physics, Gordon and Breach Publishers, New York, NY. (1968).

11. W. N. McElroy, "Fast Reactor Flux - Spectral Characterization," Proc. Am. Nuc. Soc. Topical Meeting on Irradiation Experimentation in Fast Reactors, Jackson, Wyoming (1973).

12. B. R. Sehgal and D. Meneghetti, "Analysis of Dosimetry Measurements in EBR-II and EBR-II ZPR-3 Critical," Proc. Am. Nuc. Soc. Topical Meeting on Irradiation Experimentation in Fast Reactors, Jackson, Wyoming (1973).

13. D. Meneghetti, private communication (1976).

14. B. J. Toppel, A. L. Rago and D. M. O'Shea, "MC^2, A Code to Calculate Multigroup Cross Sections," ANL-7318 (1967).

15. R. W. Hardie and W. W. Little, Jr., "1DX, A One-Dimensional Diffusion Code for Generating Effective Nuclear Cross Sections," BNWL-954 (1969).

16. W. E. Ford, III and D. H. Wallace, "POPOP4, A Code for Converting Gamma-Ray Spectra to Secondary Gamma-Ray Production Cross Sections," CTC-12, ORNL (1969).

17. L. B. Miller, G. H. Golden, R. E. Jarka, and K. E. Phillips, "Characterization of the Power in an Experimental Irradiation Subassembly of Mixed-Oxide Fuel in EBR-II," ANL/EBR-047 (1971).

18. L. B. Miller and R. E. Jarka, "Local Modification of Irradiation Conditions," ANL/EBR-035 (1971).

19. G. L. Hofman, "An In-Reactor Temperature Monitor," Nucl. Technol. 19, 204 (1973).

20. G. L. Stephens, D. J. Campbell, Program THTB for Analysis of General Transient Heat Transfer Systems, G.E.-TIS No. R60FPD647, 1961.

21. Memo, J. F. Koenig and C. C. Ford to R. G. Matlock, Temperature Distribution in New HEDL Gamma Heat Monitor, April 3, 1973.

22. J. P. Holman, Heat Transfer, McGraw Hill, New York, NY, 1963.

23. A. J. Chapman, Heat Transfer, third edition, MacMillan, New York, NY, 1971.

24. R. Siegel and J. R. Howel, Thermal Radiation Heat Transfer, McGraw Hill, New York, NY, 1972.

25. M. M. El-Wakil, Nuclear Heat Transport, International Textbook Co., Scranton, Pa., 1971.

26. H. A. Larson, private communication (1976).

27. Y. S. Touloukian, R. W. Powel, C. Y. Ho, P. G. Klemens, Thermophysical Properties of Matter, Vol. 1, Ifi/Plenum, New York, NY, 1970.

28. Y. S. Touloukian, D. P. Dewitt, Thermophysical Properties of Matter, Vol. 7, Ifi/Plenum, New York, NY, 1970.

29. Yonathan Bard, Nonlinear Parameter Estimation, Academic Press, New York, NY, 1974.

30. A. Russo and D. S. Clark, private communications (1976).

31. D. Meneghetti, Reactor Environment, ANL-RDP-37, 1974.

32. J. C. R. Li, Statistical Inference, Edwards Bros., Inc., Ann Arbor, Michigan.

33. Memo, L. B. Miller to C. C. Price, Gamma Heating in XX05 and YY02, September 5, 1973.

34. J. R. Blum and J. I. Rosenblatt, Probability and Statistics, W. B. Saunders Co., Philadelphia, Pa., 1972.

APPENDIX A[1,2]

Koenig Calorimeter Experiment (Design, fabrication, and experimental details)

Space and material limitations in the XX05 instrumented subassembly required that the calorimeter be of smaller diameter than the preliminary design. The final design is shown in Fig. 1-1 with the calorimeter diameter being 0.144-in. O.D. rather than the 0.230-in. diameter of the preliminary calculations. The error due to radial heat transfer would increase as the mass to surface area is decreased with decreasing radius.

For the new design, the error in the uncertainty due to the emissivity of stainless steel was increased to $\pm$ 30° out of a 500°F temperature rise[21] for the calculated rise for a heat deposition of 5 W/g. The ungrounded sheathed chromel-alumel thermocouple of 1/16-in. O.D. contained 0.010-in. diameter thermocouple wire insulated by magnesium oxide. The sheath was brazed into the calorimeter body with nicrobraze 50 (13% Cr, 10% P, balance Ni) in order to thermally bond the thermocouple to the body. The thermocouple junction, determined by radiography, was 0.020-in. from the end of the well, or 0.741-in. from the cold end of the calorimeter. The calorimeter body was 0.144-in. O.D. and 0.886-in. long and contained a 0.0635-in. diameter hole for the thermocouple sheath. The body was 316 stainless steel (ASTM-A-276) machined to a 63 RMS finish. The calorimeter body was welded to the containment tube under a vacuum of 0.1 Torr which was two decades lower than that required to minimize radial conduction.

Two active calorimeters were incorporated into the XX05 instrumented subassembly. The "top" calorimeter was positioned radially 7.72 in. from the core's axial centerline and 1.38 in. above the midplane; while the "bottom" calorimeter was located radially 8.03-in. from the axial centerline and 1.22 in. below the midplane. Both calorimeters operated satisfactorily throughout the 26,104 MWD life of XX05 for a total neutron fluence of 8.6×10^{22} (7.8×10^{22}) nvt.

R. A. Laskiewicz made first principal calculations using the DOT transport code, while J. F. Koenig analyzed the data obtained from the XX05 calorimeters utilizing the program THTB.

The internal heat generation was obtained from a model of the calorimeter, and use of the generalized heat transfer code, THTB. The calorimeter was assumed to be a solid stainless steel rather than the composite 316 stainless steel, nicrobraze 50, magnesium oxide, chromel and alumel. This was done to minimize computer running time since previous calculations showed that the maximum error in the thermocouple reading caused by the heterogeneity was small, 1.5°F for the case of 5 W/gm. Calculations were made at a number of heat generation rates using the high and low emissivity values. Radiation was allowed between calorimeter surface node and the corresponding inner surface node on the calorimeter tube. A vacuum of 1μ Hg was assumed in the gas space. The surface of the cold end was assumed to be at a temperature of 1000°F as was the outside surface of the 0.230-in. O.D. tube. Although the actual sink temperature will vary from this, the

temperature rise will be essentially the same. The thermal conductivity was obtained from Thermal Physical Properties of Materials[27,28]. The density of the 316 stainless steel was obtained from Thermal Physical Properties of Materials.[27,28]

A calorimeter of this type will measure the gamma ray deposition in the calorimeter from gammas originating from the surrounding fuel, and structure as well as gammas originating from the calorimeter itself. The majority of the heat will be deposited from gamma origination from the immediate surrounding fueled subassemblies, since the source in the structural XX05 subassembly will only be due to the neutron absorption in the stainless steel. The neutron absorption in the stainless steel medium of the calorimeter susceptor will, however, produce activation products which will decay with beta and gamma emissions. A portion of the gamma decay will be absorbed in the calorimeter and contribute to the total gamma flux and measured heat deposition. This is not of concern since the gamma heating rather than the gamma source is the purpose of the measurement. It is important, however, that the measurements were made in a structural subassembly since the gamma heating is less than in a fueled subassembly. These effects will be compensated in calculation techniques.[33] The beta decay of the activation products will add to the temperature rise of the calorimeter, since the beta particle will be absorbed in the stainless steel. Scoping calculations were done to determine if self beta heating could produce a sizable error in the heating measurement. Using the maximum isotope compositions in stainless steel, an absorption cross section of 1 barn, a flux of 3×10^{15}

n/cm^2-sec and assuming that all the decay energy was associated with the beta particle, it was found that the maximum beta heating contribution was less than 4% of the total, if Mn^{56} was ignored. More detailed calculations were done using the (n, γ) cross section for Mn^{55} but still assuming that all decay energy was associated with the beta particle. In this case, the contribution decreased from 12% of the total to about 0.2%. If more detailed calculations were made for the other isotopes to include the (n, γ) cross section and the actual energy associated with beta decay, the contributions would decrease by a similar magnitude. It would be expected that absorption of betas formed in the calorimeter would be less than 1% of the total heat deposition. Therefore, beta heating by self-absorption may be neglected.

APPENDIX B

Generation I Computer Codes

Listing of PH 1

```
C       1-D HEAT TRANSFER IN A PIN FIN WITH RADIATION CHAR.  AS CONVECTION
        DIMENSION TN(6,2),AW(6),AN(6),EF(6),C3(6,1),C4(6,1),QC(2),HN(6,1)
        REAL L,K
        READ(5,1)  RN,RW,L
      1 FORMAT (3(E10.3,1X))
        READ(5,500)MK
    500 FORMAT (I5)
        READ (5,2) SIGMA,E1,E2,Z1,Z2,K
      2 FORMAT (6(E10.3,1X))
        READ (5,1) TF,T1,QGEN
    300 READ(5,3) (TN(I,1),I=2,6),QC(1)
      3 FORMAT (5(E10.3,1X),E10.3)
        J=2
        M=1
        TN(1,1)=0
        PI=3.1415
        WRITE(6,4)
      4 FORMAT (16X,'DATA',9X,'CONVERGENCE CRITERIA',6X,'GEOMETRY',//)
        WRITE (6,5) E1.Z1,RN
      5 FORMAT (12X,'E1=',E10.3,7X,'Z1=',E10.3,8X, 'RN=', E10.3)
        WRITE (6,6) E2,Z2,RW
      6 FORMAT (12X,'E2=',E10.3,7X,'Z2=',E10.3,8X, 'RW=',E10.3)
        WRITE (6,7) K,L,QGEN
      7 FORMAT (13X, 'K=',E10.3,28X,'L=',E10.3,/,9X,'QGEN=',E10.3,///)
        WRITE (6,8) T1
      8 FORMAT (28X,'N',1X,'INITIAL TEMP(N)',//28X,'1',3X,E10.3)
        DO 10 I=2,6
        WRITE(6,9)I,TN(I,1)
      9 FORMAT (28X,I1,3X,E10.3)
     10 CONTINUE
        WRITE (6,11)  TF
     11 FORMAT (27X,'TF',3X,E10.3,///)
        C1=L/(5.0*PI*K*(RN)**2)
        C2=1.0/C1
        CALL AREA(PI,RW,RN,L,AW,AN)
        CALL EXFCTR(AW,AN,E1,E2,EF)
     23 CALL HIGH (1,EF,SIGMA,TN,TF,HN)
        DO 12 I=2,5
        C3(I,J-1)=2,5/(HN(I,J-1)*PI*RN*L)
        C4(I,J-1)=1.0/C3(I,J-1)
     12 CONTINUE
        C3(1,J-1)= 5.0/(HN(1,J-1)*PI*RN*L)
        C3(6,J-1)= 5.0/(HN(6,J-1)*PI*RN*L)
        C4(6,J-1)= 1.0/C3(6,J-1)
```

```
   QC(J)=-((TN(2,J-1)-T1)/C1+(TF-T1)/C3(1,J-1)+(QGEN)*(PI*RN**2)*(L/1
  10.))
   DO 13 I=3,5
   TN(I,J)=(TN(I-1,J-1)/C1+TN(I+1,J-1)/C1+TF/C3(I,J-1)+((QGEN)*(PI*
  1RN**2)*(L/5.)))/(2*C2+C4(I,J-1))
13 CONTINUE
   TN(2,J)=(T1/C1)+TN(3,J-1)/C1+TF/C3(2,J-1)+QGEN*PI*RN**2*(L/5.)
  1)/(2*C2+C4(I,J-1)
   TN(6,J)=(TN(5,J-1)/C1+TF/C3(6,J-1)+QGEN*PI*RN**2*(L/10.))/(C2+C4(6
  1,J-1))
   IF(ABS(QC(J)-QC(J-1))·GT·Z1) GB TB 22
   DO 14 I=2,6
   IF(ABS(TN(I,J)-TN(I,J-1))·GT·Z2) GB TB 22
14 CONTINUE
   QR=0
   SUM= HN(1,J-1)*AN(1)*(T1-TF)
   DO 15 I-2,6
   QR=QR + HN(I,J-1)* AN(I)*(TN(I,J-1)-TF)
15 CONTINUE
   QR=QR+SUM
   RATIO= QR/QC(J)
   WRITE(6,16)
16 FORMAT(33X,'CONCLUSIONS',/,23X,'N',4X,'H(N)',14X,'TEMP(N)',//)
   WRITE(6,17) HN(1,J-1),T1
17 FORMAT(23X,'1',1X,E10.3,9X,E10.3)
   DO 19 I=2,6
   WRITE(6,18) I, HN(I,J-1), TN(I,J)
18 FORMAT(23X,11,1X,E10.3,9X,E10.3)
19 CONTINUE
   WRITE(6,20) QC(J),QR
20 FORMAT(1X,//,22X,'QC=',E10.3,6X,'QR=',E10.3)
   WRITE(6,21) RN,RATIO
21 FORMAT(22X,'RN=',E10.3,3X,'QR/QC=',E10.3)
   GO TO 24
22 IF(M·GT·MK)GO TO 25
   M=M+1
   QC(1)=QC(2)
   DO 100 I=2,6
100 TN(I,1)=TN(I,2)
   GO TO 23
24 IF(RN·EQ·0.335) GO TO 25
   RN=RN+.01
   GO TO 300
25 STOP
   END
   SUBROUTINE AREA(PI,RW,RN,L,AW,AN)
   DIMENSION AW(1),AN(1)
   REAL L
   AN(1)=(PI*RN*L)/5.0
   AN(6)=AN(1)
   AW(1)=(PI*L*RW)5.0
   AW(6)=AW(1)
   DO 1 I=2,5
   AN(I) = (2*PI*RN*L)/5.0
   AW(I) = (2*PI*RW*L)/5.0
```

```
1 CONTINUE
  RETURN
  END
  SUBROUTINE EXFCTR(AW,AN,E1,E2,EF)
  DIMENSION AW(1),AN(1),EF(1)
  DO 1 I=1,6
  EF(I)=AW(I)*E1*E2)/(AW(I)*E2+AN(I)*(1.0-E2))
1 CONTINUE
  RETURN
  END
  SUBROUTINE HIGH(J,EF,SIGMA,TN,TF,HN)
  DIMENSION EF(1),TN(6,1),HN(6,1)
  HN(1,J)= EF(1)*SIGMA*((T1+460.)**4-(TF+460.)**4)/(T1-TF)
  DO 1 I=2,6
  HN(I,J)=(EF(I)*SIGMA*((TN(I,J)+460.0)**4-(TF+460.)**4))/(TN(I,J)-T
 1F)
1 CONTINUE
  RETURN
  END
```

Listing of PH 2

```
C       1-D HT. TRANS. PIN FIN RAD. CHAR. AS CONV.  HT. SHIELD
        DIMENSION TN(6,50),TS(6,50),AN(6),AW(6),AS(6),EFNS(6),EFSN(6),
       1EFSW(6),CN3(6,50),CN4(6,50),CSW3(6,50),CSW4(6,50),CSN3(6,50),
       2CSN4(6,50),HNS(6,50),HSW(6,50),HSN(6,50),QCN(60),QCS(50)
        REAL L,K
        READ(5,1) RN,RS,RW,L
      1 FORMAT (4F10.3)
        READ(5,2) SIGMA,E1,E2,E3,Z1,Z2,Z3,K
      2 FORMAT (E10.4, 7F10.3)
        READ(5,1) TW,TN1,TS1,QGEN
        READ(5,3) (TN(I,1),I=2,6),QCN(1)
      3 FORMAT (6F10.3)
        READ(5,3) (TS(I,1),I=2,6),QCS(1)
        DO 80 J=1,50
        TN(1,J)=TN1
        TS(1,J)=TS1
     80 CONTINUE
        READ(5,101) DR
    101 FORMAT (F10.3)
        PI = 3.1415
        WRITE(6,4)
      4 FORMAT(20X,'DATA',9X,'CONVERGENCE CRITERIA',6X,'GEOMETRY',//)
        WRITE(6,5) E1,Z1,RS
      5 FORMAT(16X,'E1=',E10.3,7X,'Z1=',E10.3,8X,'RS=',E10.3)
        WRITE(6,6) E2,Z2,RN
      6 FORMAT(16X,'E2=',E10.3,7X,'Z2=',E10.3,8X,'RN=',E10.3)
        WRITE(6,7) E3,Z3,RW
      7 FORMAT(16X,'E3=',E10.3,7X,'Z3=',E10.3,8X,'RW=',E10.3)
        WRITE(6,8) K,L,QGEN
      8 FORMAT(17X,'K=',E10.3,28X,'L=',E10.3,/,1X,13X,'QGEN=',E10.3,//)
        WRITE(6,9)
      9 FORMAT(20X,'N',1X,'INITIAL TEMP(N)',5X,'NS',1X,'INITIAL TEMPS(NS)'
       1,//)
        DO 11 I=1,6
        WRITE(6,10) I,TN(I,1),I,TS(I,1)
     10 FORMAT(20X,I1,3X,E11.4,9X,I1,E11.4)
     11 CONTINUE
        WRITE(6,92) TW
     92 FORMAT(19X,'TW',3X,E10.3,//)
        CN1 = L/(5.0*PI*(K/12.0)*RN**2)
        CN2 = 1.0/CN1
        CALL AREA(PI,RN,RS,RW,L,AN,AS,AW)
        CALL EXFCTR(AN,AS,AW,E1,E2,E3,EFNS,EFSN,EFSW)
        J=1
        CALL HIGHN(J,EFNS,SIGMA,TN,TS,HNS,TS1,TN1)
        DO 23 J=2,50
        DO 12 I=2,5
        CN3(I,J-1) = 5.0/(HNS(I,J-1)*PI*RN*L*2.0)
        CN4(I,J-1) = 1.0/CN3(I,J-1)
```

```
 12 CONTINUE
    CN3(1,J-1) = 5.0/(HNS(1,J-1)*PI*RN*L)
    CN3(6,J-1) = 5.0/(HNS(6,J-1)*PI*RN*L)
    CN4(6,J-1) = 1.0/CN3(6,J-1)
    QCN(J) = -((TN(2,J-1)TN1)/CN1 + (TS1-TN1)/CN3(1,J-1) + QGEN*PI*(R
   1N**2)*L/10.0)
    DO 13 I=3,5
    TN(I,J) = (TN(I-1,J-1)/CN1 + TN(I+1,J-1)/CN1 + TS(I,J-1)/CN3(I,J-1
   1) + (QGEN*(PI*RN**2)*L/5.0))/(2.*CN2+CN4(I,J-1))
 13 CONTINUE
    TN(2,J) = (TN1/CN1 + TN(3,J-1)/CN1 + TS(2,J-1)/CN3(2,J-1) + QGEN*(
   1PI*RN**2)*L/5.0)/(2.*CN2 + CN4(I,J-1)
    TN(6,J) = (TN(5,J-1)/CN1 + TS(6,J-1)/CN3(6,J-1)+QGEN*(PI*RN**2)*L/
   110.0).(CN2+CN4(6,J-1))
    CALL HIGHSW(J,EFSW,SIGMA,TS,TW,HSW,TS1)
    CALL HIGHSN(J,EFSN,SIGMA,TS,TN,HSN,TS1,TN1)
    DO 55 I=2,5
    CSW3(I,J-1) = 5.0/(HSW(I,J-1)*PI*RS*L*2.0)
    CSW4(I,J-1) = 1.0/CSW3(I,J-1)
 55 CONTINUE
    CS1 = L/(5.0*(K/12.)*PI*((RS+DR)**2-RS**2))
    CS2 = 1.0/CS1
    CSW3(1,J-1) = 5.0/(HSW(1,J-1)*PI*RS*L)
    CSW3(6,J-1) = 5.0/(HSW(6,J-1)*PI*RS*L)
    CSW4(6,J-1) = 1.0/CSW3(6,J-1)
    DO 56 I=2,5
    CSN3(I,J-1) = 5.0/(HSN(I,J-1)*PI*RS*L*2.0)
    CSN4(I,J-1) = 1.0/CSN3(I,J-1)
 56 CONTINUE
    CSN3(1,J-1) = 5.0/(HSN(1,J-1)*PI*RS*L)
    CSN3(6,J-1) = 5.0/(HSN(6,J-1)*PI*RS*L)
    CSN4(6,J-1) = 1.0/CSN3(6,J-1)
    QCS(J) = -((TS(2,J-1)-TS1)/CS1+(TW-TS1)/CSW3(1,J-1)+(TN1-TS1)/CSN3
   1(1,J-1)+QGEN*(PI*((RS+DR)**2-RS**2)*L/10.0))
    DO 57 I=3,5
    TS(I,J) = (TS(I-1,J-1)/CS1+TS(I+1,J-1)/CS1+TW/CSW3(I,J-1)+TN(I,J-1
   1)/CSN3(I,J-1)+QGEN*PI*((RS+DR)**2-RS**2)*L/5.0)/(2.*CS2+CSW4(I,J-
   21)+CSN4(I,J-1))
 57 CONTINUE
    TS(2,J) = (TS1/CS1+TS(3,J-1)/CS1+TW/CSW3(2,J-1)+TN(2,J-1)/CSN3(2,J
   1-1)+QGEN*PI*((RS+DR)**2-RS**2)*L/5.0)/(2.*CS2+CSW4(2,J-1)+CSN4(2,J
   2-1))
    TS(6,J) = (TS(5,J-1)/CS1+TW/CSW3(6,J-1)+TN(6,J-1)/CSN3(6,J-1)+QGEN
   1*PI*((RS+DR)**2 RS**2)*L/10.)/(CS2+CSW4(6,J 1)+CSN4(6,J-1))
    WRITE(6,100) (TN(I,J) ,I=1,6)
    WRITE(6,100) (TS(I,J) ,I=1,6)
100 FORMAT(10X,6(E11.4,1X))
    IF(ABS(TN(I,J)-TN(I,J-1)) .GT. Z2) GO TO 22
 14 CONTINUE
    DO 15 I=2,6
    IF(ABS(TS(I,J)-TS(I,J-1)) .GT. Z3) GO TO 22
 15 CONTINUE
    QR=0
    SUM = HNS(1,J-1)*AN(1)*(TN1-TS1)
    DO 16 I=2,6
```

```
   QR= QR+HNS(I,J-1)*AN(I)*(TN(I,J-1)=TS(I,J-1))
16 CONTINUE
   QR = QR + SUM
   RATIO = QR/QCN(J)
   WRITE(6,17)
17 FORMAT(53X,'CONCLUSIONS',/,20X,'N',7X,'HNS',10X,'TEMP(N)',11X,'NS'
  1,6X,'HSN',9X,'H SW',10X,'TEMPS(NS)',//)
   DO 19 I=1,6
   WRITE(6,18) I,HNS(I,J-1),TN(I,J),I,HSN(I,J-1),HSW(I,J-1),TS(I,J)
18 FORMAT(20X,I1,2X,E10.3,5X,E11.4,11X,I1,2X,E10.3,2X,E10.3,5X,E11.4)
19 CONTINUE
   WRITE(6,20) QCN(J),QR
20 FORMAT(1X,//,20X,'QCN=',E10.3,9X,'QR=',E10.3)
   WRITE(6,21)RN,RATIO
21 FORMAT(21X,'RN=',E10.3,5X,'QR/QCN=',E10.3,////)
   GO TO 24
22 CALL HIGHN(J,EFNS,SIGMA,TN,TS,HNS,TS1,TN1)
23 CONTINUE
24 STOP
   END
   SUBROUTINE AREA(PI,RN,RS,RW,L,AN,AS,AW)
   DIMENSION AN(1),AS(1),AW(1)
   REAL L
   AN(1) = (PI*RN*L)/5.0
   AN(6) = AN(1)
   AS(1) = (PI*RS*L)/5.0
   AS(6) = AS(1)
   AW(1) = (PI*RW*L)/5.0
   AW(6) = AW(1)
   DO 1 I=2,5
   AN(I) = (2*PI*RN*L)/5.0
   AS(I) = (2*PI*RS*L)/5.0
   AW(I) = (2*PI*RW*L)/5.0
 1 CONTINUE
   RETURN
   END
   SUBROUTINE EXFCTR(AN,AS,AW,E1,E2,E3,EFNS,EFSN,EFSW)
   DIMENSION AN(1),AS(1),AW(1),EFNS(1),EFSN(1),EFSW(1)
   DO 1 I=1,6
   EFNS(I) = (AS(I)*E1*E3)/(AS(I)*E3+AN(I)*E1*(1.0 E3))
   EFSN(I) = AN(I)*EFNS(I)/AS(I)
   EFSW(I) = (AW(I)*E3*E2)/(AW(I)*E2+AS(I)*E3(1.0-E2))
 1 CONTINUE
   RETURN
   END
   SUBROUTINE HIGHN(J,EFNS,SIGMA,TN,TS,HNS,TS1,TN1)
   DIMENSION EFNS(1),TN(6,1),TS(6,1),TNS(6,1)
   HNS(1,J) = EFNS(1)*(SIGMA/144.0)*((TN1+460.)**4-(TS1+460.)**4)/(TN
  11-TS1)
   DO 1 I=2,6
   HNS(I,J) = EFNS(I)*(SIGMA/144.)*((TN(I,J)+460.)**4-(TS(I,J)+460.)*
  1*4)/(TN(I,J)-TS(I,J))
 1 CONTINUE
```

```
      RETURN
      END
      SUBROUTINE HIGHSN(J,EFSN,SIGMA,TS,TN,HSN,TS1,TN1)
      DIMENSION EFSN(1),TS(6,1),HSN(6,1)
      HSN(1,J-1) = EFSN(1)*(SIGMA/144.)*((TS1+460.)**4-(TN1+460.)**4)/(T
     1S1-TN1)
      DO 1 I=2,6
      HSN(I,J-1) = EFSN(I)*(SIGMA/144.)*((TS(I,J-1)+460.)**4-(TN(I,J-1)+
     1460.)**4)/(TS(I,J-1)=TN(I,J-1))
    1 CONTINUE
      RETURN
      END
      SUBROUTINE HIGHSW(J,EFSW,SIGMA,TS,TW,HSW,TS1)
      DIMENSION EFSW(1),TS(6,1),HSW(6,1)
      HSW(1,J-1) = EFSW(1)*(SIGMA/144.)*((TS1+460.)**4-(TW+460.)**4/(TS
     11-TW)
      DO 1 I=2,6
      HSW(I,J-1) = EFSW(I)*(SIGMA/144.)*((TS(I,J-1)+460.)**4-(TW+460.)**
     14)/(TS(I,J-1)-TW)
    1 CONTINUE
      RETURN
      END
```

APPENDIX C

Material Properties[27,28]

Tables C-1, C-2, and C-3 list the material properties used in the preceeding analysis.

Table C-1

Properties of 304 Stainless Steel

Temperature °F	Thermal Conductivity BTU/hr-ft-°F	Total Hemispherical Emissivity	Density lbm/ft^3
68	—	--	492.7
700	11.85	.1948	--
900	12.74	.2135	--
1100	13.64	.2527	--
1300	14.64	.3193	--
1500	15.66	.4201	--
1600	16.19	.4854	--

Least squares curve for thermal conductivity, K:

$$K_{SS}(T) = 5.530 \times 10^{-7}T^2 + 3.545 \times 10^{-3}T + 9.09 \qquad \text{(C-1)}$$

Least squares curve for total hemispherical emissivity, ε:

$$\varepsilon_{SS}(T) = 3.421 \times 10^{-7}T^2 - 4.75 \times 10^{-4}T + .3607 \qquad \text{(C-2)}$$

Table C-2

Properties of Armco Iron

Temperature °F	Thermal Conductivity BTU/hr-ft-°F	Total Hemispherical Emissivity	Density g/cm^3
68	--	--	7.87
260.3	38	--	--
383	--	.320	--
440.3	34.3	--	--
620.3	30.7	--	--
743	--	.405	--
800.3	27.3	--	--
980.3	24.4	--	--
1112.0	--	.535	--
1160.0	21.5	--	--
1340.0	18.7	--	--
1446.0	16.9	.570	--
1508.0	--	--	--

Least squares curve for the thermal conductivity of Armco-Iron:

$$K_{Fe}(T) = -1.07 \times 10^{-7}T^2 + 4.370 \times 10^{-4}T + .1609 \qquad \text{(C-3)}$$

Least squares curve for the total hemispherical emissivity of Armco-Iron:

$$\varepsilon_{Fe}(T) = 3.421 \times 10^{-7}T^2 - 4.745 \times 10^{-4}T + .3607 \qquad \text{(C-4)}$$

Table C-3

Properties of Elemental Gold

Temperature °F	Total Hemispherical Emissivity ε	Density g/cm^3
68	--	19.32
383	.040	--
743	.048	--
1112	.050	--
1508	.068	--

Least squares curve for the total hemispherical emissivity of elemental gold:

$$\varepsilon_{Au}(T) = 2.31 \times 10^{-5} T + 2.985 \times 10^{-2} \qquad \text{(C-5)}$$

Program THTB utilizes the tabular values preceeding to determine temperature dependent thermal properties. Programs PH-3, PH-4, and PH-5 use the least squares functions C-1, C-2, C-3, C-4, and C-5 to determine the value of temperature dependent thermal properties; the least squares coefficients constitute data cards for these programs.

APPENDIX D

Program THTB[20]

The initial format of this parametric study envisioned utilization of program THTB as the primary tool for analyses, i.e., (see Chapter 3). The effect of varying the chosen parameter was to be assessed by virtue of the implicit functionality $T = T(Q, K, E_1, E_2, RN, RS, \ldots)$.

Program THTB (Transient Heat Transfer Big) is a program for analysis of general three dimensional heat transfer systems. Its primary mission was for analysis of heat transfer problems pertaining to large jet engines, aircraft nuclear propulsion components, and missiles and associated space vehicles. In general, THTB utilizes a finite difference analysis of three dimensional transient heat flow. The modes of heat exchange which this program handles are:

1) Conduction
2) Convection
3) Gray body diffuse radiation
4) Surface flux
5) Internal generation
6) Non-Sink mass flow
7) Latent heat effects

Geometrical Considerations

The object to be analyzed is subdivided into a series of small volumes called nodes (similar to the simple 1-D development); said

nodes may have either regular (right parallelopipeds) geometry or irregular (cylindrical, truncated prism etc.). Each node may have at most 6 sides; energy balance expressions are written for each node in a manner similar to that described in the simple 1-D development, Chapter 3 with heat transport resistances defined in a respectively analogous manner.

Running Time[3]

The running time is quite variable and depends on the type of geometry and the number of nodes. A good upper bound would be to allow 1 second per node per time step.

Machine Requirements for the THTB[20]

THTB is a 3600 Fortran language program for use on the CDC-3600 machine with 64k core memory. The 3600 scope overlay feature is employed. THTB has been modified to run on the ANL IBM 360/190.

APPENDIX E

Generation II Programs

Listing of PH-3

```
C         I-D HT. XFR IN A PIN FIN RADIATION CHARACTERIZED AS CONVECTION
C         TEMP DEPENDENT K AND EMISSIVITIES
          REAL L,K,MAXRN
          DIMENSION TN(100,2),AWR(100),ANR(100),EF(100),K(100),QC(2),EN(100)
         1,EW(100),C1(100),C2(100),C3(100),C4(100),HN(100),TAVG(100),AMAT1(2
         2),AMAT2(2),AMAT3(2)
          READ(5,1) RNI,L,NODEN,MAXRN,RO
        1 FORMAT(2E10.3,I10,2E10.3)
          READ(5,914) QGENM,DELQG
      914 FORMAT(2E10.3)
          READ(5,500) MAXIT
      500 FORMAT(I5)
          READ(5,2) SIGMA,Z1,Z2
        2 FORMAT (3(E11.4))
          READ(5,40) AKO,AK1,AK2,AK3,AMAT1
       40 FORMAT(4E11.4,2A4)
          READ(5,40) AENO,AEN1,AEN2,AEN3,AMAT2
          READ(5,40) AEWO,AEW1,AEW2,AEW3,AMAT3
          READ(5,2 ) TF, T1, QGEN
      300 READ(5,3) (TN(I,1),I=2,NODEN)
        3 FORMAT(7E11.4)
          READ(5,41)QC(1)
       41 FORMAT(E11.4)
          RN=RNI
      905 CONTINUE
          RW=RN+.020
          M=1
          TN(1,1)=T1
          TN(1,2)=T1
          PI=3.1415
          WRITE(6,4)
        4 FORMAT(16X,'DATA',9X,'CONVERGENCE CRITERIA',6X,'GEOMETRY',//)
          WRITE(6,913) RNI
      913 FORMAT(53X,'RNI=',E11.4)
          WRITE(6,5) Z1,RN
        5 FORMAT(33X,'Z1=',E11.4,7X,'RN=',E11.4)
          WRITE(6,6) Z2, RW
        6 FORMAT(33X,'Z2=',E11.4,7X,'RW=',E11.4)
          WRITE(6,7) L,QGEN
        7 FORMAT(13X,'L='E11.4,28X,'QGEN=',E11.4,///)
          WRITE(6,912) QGENM,DELQG
      912 FORMAT(53X,'QGENM=',E11.4,2X,'DELQG=',E11.4)
          WRITE(6,8) T1
```

```
    8 FORMAT(28X,'N',1X,'INITIAL TEMP(N)',//28X,'1',3X,E10.3)
      DO 10 I=2,NODEN
      WRITE(6,9)I,TN(I,1)
    9 FORMAT(27X,I2,3X,E11.4)
   10 CONTINUE
      WRITE(6,11) TF
   11 FORMAT(27X,'TF',3X,E11.4,///)
      WRITE(6,603) AKO,AK1,AK2,AK3,AMAT1
  603 FORMAT(6X,'THERMAL CONDUCTIVITY DATA',//,6X,4E11.4,2X,2A4)
      WRITE(6,604) AENO,AEN1,AEN2,AEN3,AMAT2
  604 FORMAT(6X,'SUCCEPTOR EMISSIVITY DATA',//,6X,4E11.4,2X,2A4)
      WRITE(6,605) AEWO,AEW1,AEW2,AEW3,AMAT3
  605 FORMAT(6X,'WALL EMISSIVITY DATA',//,6X,4E11.4,2A4)
      JNODEN=NODEN-1
      RNODEN=NODEN
  600 CALL THERMK(AKO,AK1,AK2,AK3,T1,TN,K,NODEN,TAVG)
      CALL SEMIS(AENO,AEN1,AEN2,T1,TN,EN,NODEN)
      CALL WEMIS(AEWO,AEW1,AEW2,TF,EW,NODEN)
      CALL AREARD(PI,RW,RN,L,AWR,ANR,NODEN)
      CALL EXFCTR(AWR,ANR,EN,EW,EF,NODEN)
      CALL HIGH(EF,SIGMA,TN,TF,HN,NODEN,T1)
      DO 601 I=1,JNODEN
      C1(I)=L/((RNODEN-1.)*(K(I)/12.0)*PI*RN**2)
      C2(I)=1.0/C1(I)
  601 CONTINUE
C     RADIATIVE RESISTANCE
      DO 12 I=2,JNODEN
      C3(I)=(RNODEN-1.0)/(HN(I)*2.0*PI*RN*L)
      C4(I)=1.0/C3(I)
   12 CONTINUE
      C3(1)=(RNODEN-1.0)/(HN(1)*PI*RN*L)
      C3(NODEN)=(RNODEN-1.0)/(HN(NODEN)*PI*RN*L)
      C4(NODEN)-1.0/C3(NODEN)
      QC(2)=-((TN(2,1) - T1)/C1(1)+(TF-T1)/C3(1)+QGEN*55.95*RO*PI*RN
     1**2)*L/(2*(RNODEN-1.0)))
      DO 13 I=3,JNODEN
      TN(I,2)=(TN(I-1,1)/C1(L-1)+TN(I+1,1)/C1(I)+TF/C3(I)+QGEN*55.95*R
     10*PI*RN**2*L/(RNODEN-1.0))/(C2(I-1)+C2(I)+C4(I))
   13 CONTINUE
      TN(2,2)=(T1/C1(1)+TN(3,1)/C1(2)+TF/C3(2)+QGEN*55.95*RO*PI*RN**
     12*L/(RNODEN-1.0))/(C2(1)+C2(2)+C4(2))
      TN(NODEN,2)=(TN(JNODEN,1)/C1(JNODEN)+TF/C3(NODEN)+QGEN*55.95*RO*
     1PI*RN**2*L/(2.0*(RNODEN 1.0)))/(C2(JNODEN)+C4(NODEN))
      IF(ABS(QC(2)-QC(1)).GT.Z1)GO TO 27
      DO 14 I=2,NODEN
      IF(ABS(TN(I,2)-TN(I,1)).GT.Z2) GO TO 27
   14 CONTINUE
      QR=0.0
      SUM=HN(1)*ANR(1)*(T1-TF)
      DO 15 I=2,NODEN
      QR=QR+HN(I)*ANR(I)*(TN(I,1)-TF)
   15 CONTINUE
      QR=QR + SUM
      QTOT=ABS(QR)+ABS(QC(1))
```

```
      PCTRC=(QR/QC(1)*100.
      VOL=PI*RN**2*L
      QGENT=QGEN*55.95*RO*VOL
      PCTRQG=(QR/QGENT)*100.
      PCTRQT=(QR/QTOT)*100.
      DEVQS=QTOT-(QGEN*VOL*55.95*RO)
      ITERAT=M
      WRITE(6,16)
   16 FORMAT(33X,'CONCLUSIONS',/,23X,'N',4X,'HN(N)',14X,'TEMP(N)',//)
      WRITE(6,17) HN(1),T1
   17 FORMAT(23X,'1',1X,E10.3,8X,E11.4)
      DO 19 I=2,NODEN
      WRITE(6,18) I,HN(I),TN(I,1)
   18 FORMAT(22X,I2,1X,E10.3,8X,E11.4)
   19 CONTINUE
      WRITE(6,20) QC(1),QR
   20 FORMAT(1X,//,22X,'QC=',E10.3,6X,'QR=',E10.3)
      WRITE(6,21) QTOT,DEVQS
   21 FORMAT(20X,'QTOT='E10.3,3X,'DEVQS='E10.3)
      WRITE(6,22) RN,PCTRC,PCTRQG
   22 FORMAT(22X,'RN=',E10.3,3X,'PCTRC='E10.3,3X,'PCTRQG='E10.3)
      WRITE(6,610)PCTRQT
  610 FORMAT(38X,'PCTRQT=',E10.3)
      WRITE(6,800)QGENT
  800 FORMAT(38X,'QGENT=',E10.3)
      WRITE(6,26)M
   26 FORMAT(2X,'ITERATIONS='I4)
      WRITE(6,900)MAXRN
  900 FORMAT(10X,'MAXRN=',E11.4)
      GO TO 24
   27 CONTINUE
      IF(M.GT.MAXIT) GO TO 25
      M=M+1
      QC(1)=QC(2)
      DO 100 I=2,NODEN
      TN(I,1)=TN(I,2)
  100 CONTINUE
      GO TO 600
   24 CONTINUE
      IF(RN.GT.MAXRN) GO TO 25
      RN=RN+.020
      DO 906 I=2,NODEN
      TN(I,1)=TN(I,2)
  906 CONTINUE
      GO TO 905
   25 CONTINUE
      DO 910 I=2,NODEN
      TN(I,1)=TN(I,2)
  910 CONTINUE
      RN=RNI
      QGEN=QGEN+DELQG
      IF(QGEN.LT.QGENM) GO TO 905
```

```
911 STOP
    END
    SUBROUTINE THERMK(AKO,AK1,AK2,AK3,T1,TN,K,NODEN,TAVG)
    DIMENSION TN(NODEN,1),K(NODEN),TAVG(NODEN)
    REAL K
    JNODEN=NODEN 1
    TAVG(1)=(TN(2,1)+T1)/2.0
    DO 1 I=2,JNODEN
    TAVG(I)=(TN(I+1,1)+TN(I,1))/2.0
  1 CONTINUE
    K(1)=AKO+TAVG(1)*(AK1+TAVG(1)*(AK2+AK3*TAVG(1)))    -
    DO 2 I=2,JNODEN
    K(I)=AKO+TAVG(I)*(AK1+TAVG(I)*AK2+AK3*TAVG(I)))
  2 CONTINUE
    RETURN
    END
    SUBROUNTINE SEMIS(AENO,AEN1,AEN2,T1,TN,EN,NODEN)
    DIMENSION TN(NODEN,1),EN(NODEN)
    EN(1)=AENO + T1*(AEN1 + T1*AEN2)
    DO 1 I=2,NODEN
    EN(I)=AENO + TN(I,1)*(AEN1 + TN(I,1)*AEN2)
  1 CONTINUE
    RETURN
    END
    SUBROUTINE WEMIS(AEWO,AEW1,AEW2,TF,EW,NODEN)
    DIMENSION EW(NODEN)
    EW(1)= AEWO + TF*(AEW1 + TF*AEW2)
    DO 1 I=2,NODEN
    EW(I)=EW(1)
  1 CONTINUE
    RETURN
    END
    SUBROUTINE AREARD(PI,RW,RN,L,AWR,ANR,NODEN)
    DIMENSION AWR(NODEN),ANR(NODEN)
    REAL L
    RNODEN = NODEN
    ANR(1)=2.0*PI*RN*L/(2.*(RNODEN-1.0))
    ANR(NODEN)=ANR(1)
    AWR(1)=2.0*PI RWL/(2.*(RNODEN-1.0))
    AWR(NODEN)=AWR(1)
    JNODEN=NODEN-1
    DO 1 I=2,JNODEN
    ANR(I)=2.0*PI*RN*L/(RNODEN-1.)
    AWR(I)=2.0*PI*RW*L/(RNODEN-1.0)
  1 CONTINUE
    RETURN
    END
    SUBROUTINE EXFCTR(AWR,ANR,EN,EW,EF,NODEN)
    DIMENSION EN(NODEN),EW(NODEN),EF(NODEN),AWR(NODEN),ANR(NODEN)
    DO 1 I=1,NODEN
    EF(I)=AWR(I)*EW(I)*EN(I)/(AWR(I)*EW(I)+ANR(I)*EN(I)*(1.0-EW(I))
   1)
  1 CONTINUE
    RETURN
    END
```

```
      SUBROUTINE HIGH(EF,SIGMA,TN,TF,HN,NODEN,T1)
      DIMENSION EF(NODEN),TN(NODEN,1),HN(NODEN)
      HN(1)=EF(1)*(SIGMA/144.)*((T1+460.)**4-(TF+460.)**4)/(T1-TF)
      DO 1 I=2,NODEN
      HN(I)=EF(I)*(SIGMA/144.)*((TN(I,1)+460.)**4-(TF+460.)**4)/(TN
     1(I,1)-TF)
    1 CONTINUE
      RETURN
      END
```

PH-3 Users Guide

Refer to Figure 2-3

A. Input Data

Input Card 1 FORMAT(2E10.3,I10,2E10.3)

1. RNI - minimum or initial susceptor radius to be evaluated (inches).
2. L - susceptor length (inches).
3. NODEN - maximum number of susceptor nodes.
4. MAXRN - maximum susceptor radius to be evaluated (inches).
5. RO - density of susceptor material (gm/cc)

Input Card 2 FORMAT(2E10.3)

1. QGENM - when the incrementing the internal heat generation rate, this is the maximum value for which calculations are made (watts/gm).
2. DELQG - the increment by which QGEN, the internal heat generation rate is changed during each step (watts/gm).

Input Card 3 FORMAT(I5)

1. MAXIT - the maximum number of iterations which PH-3 will cycle through in attempting to converge to a given temperature profile.

Input Card 4 FORMAT(3(11.4))

1. SIGMA - Boltzman's constant equals .1714 x 10^{-8} BTU/hr-ft^2-°R^4
2. Z1 - convergence criteria for the heat transfer value at node one.
3. Z2 - convergence criteria for the temperature at each node (see Chapter 3, Equation (3-36)).

Input Card 5 FORMAT(4E11.4,2A4)

$K(T) = AK0 + AK1(T) + AK2(T)^2 + AK3(T)^3$

K(T) = thermal conductivity of a given material as a function of temperature T (K(T) is generally a least squares fit to experimental data).

1. AK0 - zeroth order coefficient
2. AK1 - 1st order coefficient
3. AK2 - 2nd order coefficient
4. AK3 - 3rd order coefficient
5. AMAT1 - signature of material for which K(T) is defined, e.g. k_{ss} implies thermal conductivity for stainless steel.

Input Card 6 FORMAT(4E11.4,2A4)

$EN(T) = AEN0 + AEN1[T] + AEN2[T]^2 + AEN3[T]^3$

EN(T) = the temperature dependent emissivity of the susceptor body (EN(T) is generally a least squares fit to experimentally generated data).

1. AEN0 - zeroth order coefficient
2. AEN1 - 1st order coefficient
3. AEN2 - 2nd order coefficient
4. AEN3 - 3rd order coefficient
5. AMAT2 - signature of the material for which EN(T) is defined, e.g. E_{ss} implies thermal emissivity for stainless steel.

Input Card 7 FORMAT(4E11.4,2A4)

$EW(T) = AEW0 + AEW1[T] + AEW2[T]^2 + AEW3[T]^3$

EW(T) = the temperature dependent emissivity of the containment tube wall.

1. AEW0 - zeroth coefficient
2. AEW1 - 1st order coefficient
3. AEW2 - 2nd order coefficient
4. AEW3 - 3rd order coefficient
5. AMAT3 - signature of the material for which EW(T) is defined.

Input Card 8 FORMAT(3E11.4)

1. TF - constant containment tube wall temperature (°F).
2. T1 - temperature of the susceptor base, node 1 (°F).
3. QGEN - the internal heat generation rate (watts/gm).

Input Card 9 FORMAT(7E11.4)

1. TN(I,1) - the initial temperature guess for each susceptor node, NODEN-1 in number, skips the first node (°F).

Input Card 10 FORMAT(E11.4)

1. QC(1) - the initial guess for the heat conducted from node 1, the susceptor base (BTU/hr).

B. Output Characters

Output data is labeled for ease of interpretation. Output characters or symbols are identified in the following list:

1. RW - inside radius of the containment tube (inches).
2. HN(1) - the convection-like radiation heat transfer coefficient for the first susceptor node, see Equation (3-29).
3. HN(I) - the convection-like radiation heat transfer coefficient for each of the (NODEN-1) nodes after the first node, see Equation (3-29).
4. QR - the total heat radiated from the susceptor body (the summation over all susceptor body nodes) (BTU/hr).
5. QTOT - the sum of the absolute values of QR and QC(1).

6. DEVQS - the difference between QTOT and the total heat generated within the susceptor volume, QGEN times the susceptor volume times the material density times the conversion constant 55.95 (BTU/hr).
7. PCTRC - the ratio of QR to QC(1) times 100, the percent of total heat radiated from the susceptor body relative to the total heat conducted from the susceptor base.
8. PCTRQG - the ratio of QR to QGENT times 100, i.e., the percent of total heat radiated from the susceptor body relative to the total heat generated within the susceptor body.
9. PCTRQT - the ratio of QR to QTOT times 100.
10. QGENT - the total heat generated within the susceptor body, (BTU/hr).

Listing of PH-4

```
C         1-D HT. TRANS. PIN FIN RAD. CHAR. AS CONV. H+ SHIELD
C         TEMP DEP K & EMISSIVITIES
          REAL L,K
          REAL LI
          REAL KN,KS
          REAL LMAX
          DIMENSION CN1(100),CN2(100),CS1(100),CS2(100),CN3(100),CN4(100),CS
         1W3(100),CSW4(100),CSN3(100),CSN4(100),QCN(2),QCS(2),AMAT1(2),AMAT2
         2(2),AMAT3(2),AMAT4(2),AMAT5(2)
          COMMON TN(100,2),KN(100),TNAVG(100),TS(100,2),KS(100),TSAVG(100),E
         1N(100),ES(100),EW(100),ANS(100),ASN(100),ASW(100,EFSN(100),EFNS(1
         200),AWS(100),HNS(100),HSW(100),EFSW(100),HSN(100)
C         INPUT DATA FORMAT
      980 READ(5,1         ) RNI,GAP1,GAP2,LI,NODEN,RO
        1 FORMAT(4E10.3,I10,E10.3)
          READ(5,70)G
          READ(5,900)RNMAX,DRMAX,LMAX
      900 FORMAT(3E10.3)
          READ(5,904)DELDR,DELRN,DELL
      904 FORMAT(3E10.3)
          READ(5,70)DRI
       70 FORMAT(E10.3)
          READ(5,500)MAXIT
      500 FORMAT(I5)
          READ(5,2)SIGMA,Z1,Z2,Z3
        2 FORMAT(4E10.3)
          READ(5,40)ANKO,ANK1,ANK2,ANK3,AMAT1
       40 FORMAT(4E11.4,2A4)
          READ(5,40)ASKO,ASK1,ASK2,ASK3,AMAT2
          READ(5,40)AENO,AEN1,AEN2,AEN3,AMAT3
          READ(5,40)AESO,AES1,AES2,AES3,AMAT4
          READ(5,40)AEWO,AEW1,AEW2,AEW3,AMAT5
          READ(5,40)TW,TN1,TS1,QGENI
          READ(5,70)QGENS
          READ(5,2)QGENM,DELQG,GAPMAX,DELGAP
          READ(5,3)(TN(I,1),I=2,NODEN)
        3 FORMAT(7E11.4)
          READ(5,4)QCN(1),QCS(1)
        4 FORMAT(2E11.4)
          READ(5,3)(TS(I,1),I=2,NODEN)
          L=LI
          QGEN=QGENI
          DR=DRI
          RN=RNI
      903 RS=RN+GAP1
          RSN=RS+DR
          RW=RSN+GAP2
          M=1
          TN(1,1)=TN1
          TN(1,2)=TN1
          TS(1,1)=TS1
          TS(1,2)=TS1
          PI=3.1415
```

```
      WRITE(6,5)
    5 FORMAT(20X,'DATA',9X,'CONVERGENCE CRITERIA',6X,'GEOMETRY',//)
      WRITE(6,909)RNI
  909 FORMAT(57X,'RNI=',E10.3)
      WRITE(6,6)Z1,RS
    6 FORMAT(36X,'Z1=',E10.3,8X,'RS=',E10.3)
      WRITE(6,7)Z2,RN
    7 FORMAT(36X,'Z2=',E10.3,8X,'RN=',E10.3)
      WRITE(6,901)RSN
  901 FORMAT(57X,'RSN=',E10.3)
      WRITE(6,8) Z3,RW
    8 FORMAT(36X,'Z3=',E10.3,8X,'RW=',E10.3)
      WRITE(6,9)L,QGEN
    9 FORMAT(57X,'L='E10.3,/,1X,13X,'QGEN=',E10.3,//)
      WRITE(6,930)QGENI,DELQG,QGENM
  930 FORMAT(13X,'QGENI=',E10.3,2X,'DELQG=',E10.3,2X,'QGENM=',E10.3)
      WRITE(6,931)GAPMAX,DELGAP
  931 FORMAT(13X,'GAPMAX=',E10.3,2X,'DELGAP=',E10.3)
      WRITE(6,906)QGENS
  906 FORMAT(13X,'QGENS='E10.3)
      WRITE(6,907)DELDR,DELRN,DELL
  907 FORMAT(13X,'DELDR=',E10.3,2X,'DELRN=',E10.3,2X,'DELL=',E10.3)
      WRITE(6,908)DRMAX,RNMAX,LMAX
  908 FORMAT(13X,'DRMAX=',E10.3,2X,'RNMAX=',E10.3,2X,'LMAX=',E10.3)
      WRITE(6,604)ANKO,ANK1,ANK2,ANK3,AMAT1
  604 FORMAT(6X,'SUCCEPTOR THERMAL COND. DATA',//,6X,4E11.4,2X,2A4)
      WRITE(6,605)ASKO,ASK1,ASK2,ASK3,AMAT2
  605 FORMAT(6X,'SHIELD THERMAL COND. DATA',//,6X,4E11.4,2X,2A4)
      WRITE(6,606)AENO,AEN1,AEN2,AEN3,AMAT3
  606 FORMAT(6X,'SUCCEPTOR EMISSIVITY DATA',//,6X,4E11.4,2X,2A4)
      WRITE(6,607)AESO,AES1,AES2,AES3,AMAT4
  607 FORMAT(6X,'SHIELD EMISSIVITY DATA',//,6X,4E11.4,2X,2A4)
      WRITE(6,608)AEWO,AEW1,AEW2,AEW3,AMAT5
  608 FORMAT(6X,'WALL EMISSIVITY DATA',//,6X,4E11.4,2X,2A4)
      WRITE(6,609)DR
  609 FORMAT(6X,'DR=',E11.4)
      WRITE(6,910)DRI
  910 FORMAT(6X,'DRI=',E11.4)
      WRITE(6,905)GAP1,GAP2
  905 FORMAT(6X,'GAP1=',E11.4,3X,'GAP2=',E11.4)
      WRITE(6,10)
   10 FORMAT(20X,'N',1X,'INITIAL TEMP(N)',5X,'NS',1X,'INITIAL TEMP(NS)',
     1//)
      DO 12 I=1,NODEN
      WRITE(6,11) I,TN(I,1),I,TS(I,1)
   11 FORMAT(19X,I2,3X,E11.4,8X,I2,E11.4)
   12 CONTINUE
      WRITE(6,92)TW
   92 FORMAT(19X,'TW',3X,E10.3,//)
      JNODEN=NODEN-1
      RNODEN=NODEN
  602 CALL THMKN(ANKO,ANK1,ANK2,ANK3,TN1,NODEN)
      CALL THMKS(ASKO,ASK1,ASK2,ASK3,TS1,NODEN)
```

```
      CALL EMIS(AENO,AEN1,AEN2,AEN3,NODEN,AESO,AES1,AES2,AES3,
     1AEWO,AEW1,AEW2,AEW3,TW)
      CALL AREAS(PI,RN,RS,L,NODEN,DR,RW)
      CALL EXFCTR(NODEN)
      CALL HIGH(SIGMA,NODEN,TW)
      DO 601 I=1,JNODEN
      CN1(I)=L/((RNODEN-1.0)*PI*(KN(I)/12.0)*RN**2)
      CN2(I)=1.0/CN1(I)
  601 CONTINUE
      DO 13 I=2,JNODEN
      CN3(I)=(RNODEN-1.0)/(HNS(I)*2.0*PI*RN*L)
      CN4(I)=1.0/CN3(I)
   13 CONTINUE
      CN3(1)=(RNODEN-1.0)/(HNS(1)*PI*RN*L)
      CN3(NODEN)=(RNODEN-1.0)/(HNS(NODEN)*PI*RN*L)
      CN4(NODEN)=1.0/CN3(NODEN)
      QCN(2)=-((TN(2,1)-TN1)/CN1(1)+(TS1-TN1)/CN3(1)+QGEN*55.95*RO*
     1PI*(RN**2)*L/(2.0*(RNODEN-1.0)))
      DO 14 I=3,JNODEN
      TN(I,2)=(TN(I-1,1)/CN1(I-1)+TN(I+1,1)/CN1(I)+TS(I,1)/CN3(I)+
     1(QGEN*55.95*RO*PI*RN**2*(L/(RNODEN-1.0))))/(CN2(I-1)+CN2(I)+CN4(I)
     1)
   14 CONTINUE
      TN(2,2)=(TN1/CN1(1)+TN(3,1)/CN1(2)+TS(2,1)/CN3(2)+QGEN*55.95*RO
     1*(PI*RN**2)*(L/(RNODEN-1.0)))/(CN2(1)+CN2(2)+CN4(2))
      TN(NODEN,2)=(TN(JNODEN,1)/CN1(JNODEN)+TS(NODEN,1)/CN3(NODEN)+Q
     1GEN*55.95*RO*(PI*RN**2)*L/((RNODEN-1.0)*2.0))/(CN2(JNODEN)+CN4(N
     2ODEN))
      CALL EMIS2(AENO,AEN1,AEN2,AEN3,NODEN)
      CALL EXFCT2(NODEN)
      CALL HIGH2(NODEN,SIGMA)
      DO 15 I=1,JNODEN
      CS1(I)=L/((RNODEN-1.0)*(KS(I)12.0)*PI*((RS+DR)**2-RS**2))
      CS2(I)=1.0/CS1(I)
   15 CONTINUE
      DO 16 I=2,JNODEN
      CSW3(I)=(RNODEN-1.0)/(HSW(I)*2.0*PI*(RS+DR)*L)
      CSW4(I)=1.0/CSW3(I)
   16 CONTINUE
      CSW3(1)=(RNODEN-1.0)/(HSW(1)*PI*(RS+DR)*L)
      CSW3(NODEN)=(RNODEN-1.0)/(HSW(NODEN)*PI*(RS+DR)*L)
      CSW4(NODEN)=1.0/CSW3(NODEN)
      DO 17 I=2,JNODEN
      CSN3(I)=(RNODEN-1.0)/(HSN(I)*2.0*PI*RS*L)
      CSN4(I)=1.0/CSN3(I)
   17 CONTINUE
      CSN3(1)=(RNODEN-1.0)/(HSN(1)*PI*RS*L)
      CSN3(NODEN)=(RNODEN-1.0)/(HSN(NODEN)*PI*RS*L)
      CSN4(NODEN)=1.0/CSN3(NODEN)
      QCS(2)=-((TS(2,1)-TS1)/CS1(1)+(TW-TS1)/CSW3(1)+(TN1-TS1)/CSN3(1
     1)+QGENS*55.95*RO*(PI*((RS+DR)**2-RS**2)*L/(2.0*(RNODEN-1.0))))
      DO 18 I=3,JNODEN
      TS(I,2)=(TS(I-1,1)/CS1(I-1)+TS(I+1,1)/CS1(I)+TW/CSW3(I)+TN(I,2)
     1/CSN3(I)+QGENS*55.95*RO*PI*((RS+DR)**2 RS**2)*(L/(RNODEN-1.0)))/(C
     2S2(L-1)+CS2(I)+CSW4(I)+CSN4(I))
```

```
 18 CONTINUE
    TS(2,2)=(TS1/CS1(1)+TS(3,1)/CS1(2)+TW/CSW3(2)+TN(2,2)/CSN3(2)
   1+QGENS*55.95*RO*PI*((RS+DR)**2-RS**2)*(L/(RNODEN-1.0)))/(CS2(1)+C
   2S2(2)+CSW4(2)+CSN4(2))
    TS(NODEN,2)=(TS(JNODEN,1)/CS1(JNODEN)+TW/CSW3(NODEN)+TN(NODEN
   1,2)/CSN3(NODEN)+QGENS*55.95*RO*PI*(RS+DR)**2-RS**2)*(L/((RNODEN-
   21.0)*2.0)))/(CS2(JNODEN)+CSW4(NODEN)+CSN4(NODEN))
    IF(ABS(QCN(2)-QCN(1)).GT.Z1)GO TO 22
    DO 19 I=2,NODEN
    IF(ABS(TN(I,2)-TN(I,1)).GT.Z2) GO TO 22
 19 CONTINUE
    DO 20 I=2,NODEN
    IF(ABS(TS(I,2)-TS(I,1)).GT.Z3) GO TO 22
 20 CONTINUE
    QR=0.0
    SUM=HNS(1)*ANS(1)*(TN1-TS1)
    DO 21 I=2,NODEN
    QR=QR+HNS(I)*ANS(I)*(TN(I,1)-TS(I,1))
 21 CONTINUE
    QR=QR+SUM
    PCTRC=(QR/QCN(1)*100.
    VOL=(PI*RN**2)*L
    QGENT=QGEN*55.95*RO*VOL
    PCTRQG=(QR/QGENT)*100.
    QTOT=QR+ABS(QCN(1))
    DEVQS=QTOT-QGENT
    PCTRQT=(QR/QTOT)*100.
    ITERAT=M
    WRITE(6,23)
 23 FORMAT(53X,'CONCLUSIONS',/,20X,'N',7X,'HNS',10X,'TEMP(N)',11X,'NS'
   1,6X,'HSN',9X,'HSW',10X,'TEMP(NS)',//)
    DO 24 I=1,NODEN
    WRITE(6,25) I,HNS(I),TN(I,1),I,HSN(I),HSW(I),TS(I,1)
 25 FORMAT(19X,I2,2X,E10.3,5X,E11.4,10X,I2,2X,E10.3,2X,E10.3,5X,E11.4)
 24 CONTINUE
    WRITE(6,54)
 54 FORMAT(17X,'NODE',8X,'EN(I)',11X,'ES(I)',11X,'EW(I)')
    DO 50 I=1,NODEN
    WRITE(6,51)I,EN(I),ES(I),EW(I)
 51 FORMAT(19X,I2,2X,E11.4,5X,E11.4,5X,E11.4)
 50 CONTINUE
    WRITE(6,55)
 55 FORMAT(17X,'NODE',6X,'EFNS(I)',9X,'EFSN(I)',9X,'EFSW(I)')
    DO 52 I=1,NODEN
    WRITE(6,51)I,EFNS(I),EFSN(I),EFSW(I)
 52 CONTINUE
    WRITE(6,913)
913 FORMAT(17X,'NODE',8X,'KN(I)',11X,'KS(I)')
    DO 911 I=1,JNODEN
    WRITE(6,912)I,KN(I),KS(I)
912 FORMAT(19X,I2,2X,E11.4,5X,E11.4)
911 CONTINUE
    WRITE(6,26)QCN(1),QR
```

```
 26 FORMAT(1X,//,20X,'QCN=',E10.3,9X,'QR='E10.3)
    WRITE(6,27)PCTRC,PCTRQG,QTOT,DEVQS
 27 FORMAT(5X,'PCTRC=',E10.3,2X,'PCTRQG=',E10.3,2X,'QTOT=',E10.3,2X,'
   1DEVQS=',E10.3)
    WRITE(6,700)PCTRQT
700 FORMAT(38X,'PCTRQT=',E10.3)
    WRITE(6,800)QGENT
800 FORMAT(38X,'QGENT=',E10.3)
801 WRITE(6,28)ITERAT
 28 FORMAT(1X,//,5X,'ITERATIONS=',I10)
    DR=DR+DELDR
    DO 902 I=2,NODEN
    TN(I,1)=TN(I,2)
    TS(I,1)=TS(I,2)
902 CONTINUE
    IF(DR.LT.DRMAX) GO TO 903
    DR=DRI
    RN=RN+DELRN
    IF(RN.LT.RNMAX) GO TO 903
    DR=DRI
    RN=RNI
    L=L+DELL
    IF(L.LT.LMAX) GO TO 903
    QGEN=QGEN+DELQG
    IF(QGENS.LT..1E-20) GO TO 920
    QGENS=QGEN
920 CONTINUE
    L=LI
    DR=DRI
    RN=RNI
    IF(QGEN.LT.QGENM) GO TO 903
    IF(G.EQ.1.0) GO TO 922
    GO TO 29
922 QGEN=QGENI
    IF(QGENS.LT..1E-20) GO TO 921
    QGENS=QGEN
921 CONTINUE
    GAP1=GAP1+DELGAP
    GAP2=GAP1
    IF(GAP1.LT.GAPMAX) GO TO 903
    GO TO 980
950 CONTINUE
    GO TO 29
 22 IF(M.GT.MAXIT) GO TO 801
    M=M+1
    QCN(1)=QCN(2)
    DO 30 I=2,NODEN
    TN(I,1)=TN(I,2)
    TS(I,1)=TS(I,2)
 30 CONTINUE
    GO TO 602
 29 STOP
    END
    SUBROUTINE THMKN(ANKO,ANK1,ANK2,ANK3,TN1,NODEN)
```

```
      REAL KN,KS
      COMMON TN(100,2),KN(100),TNAVG(100),TS(100,2),KS(100),TSAVG(100),E
     1N(100),ES(100),EW(100),ANS(100),ASN(100),ASW(100),EFSN(100),EFNS(1
     200),AWS(100), HNS(100),HSW(100),EFSW(100),HSN(100)
      JNODEN=NODEN-1
      DO 1 I=1,JNODEN
      TNAVG(I)=(TN(I+1,1) + TN(I,1))/2.0
    1 CONTINUE
      DO 2 I=1,JNODEN
      KN(I)=ANKO + TNAVG(I)*(ANK1 + TNAVG(I)*(ANK2 + ANK3*TNAVG(I)))
    2 CONTINUE
      RETURN
      END
      SUBROUTINE THMKS(ASKO,ASK1,ASK2,ASK3,TS1,NODEN)
      REAL KN,KS
      COMMON TN(100,2),KN(100),TNAVG(100),TS(100,2),KS(100),TSAVG(100),E
     1N(100),ES(100),EW(100),ANS(100),ASN(100),ASW(100),EFSN(100),EFNS(1
     200),AWS(100),HNS(100),HSW(100),EFSW(100),HSN(100)
      JNODEN=NODEN-1
      DO 1 I=1,JNODEN
      TSAVG(I)=(TS(I+1,1) + TS(I,1))/2.0
      KS(I)=ASKO + TSAVG(I)*(ASK1 + TSAVG(I)*(ASK2 + ASK3*TSAVG(I)))
    1 CONTINUE
      RETURN
      END
      SUBROUTINE EMIS(AENO,AEN1,AEN2,AEN3,NODEN,AESO,AES1,AES2,
     1AES3,AEWO,AEW1,AEW2,AEW3,TW)
      REAL KN,KS
      COMMON TN(100,2),KN(100),TNAVG(100),TS(100,2),KS(100),TSAVG(100),E
     1N(100),ES(100),EW(100),ANS(100),ASN(100),ASW(100),EFSN(100),EFNS(1
     200),AWS(100),HNS(100),HSW(100),EFSW(100),HSN(100)
      DO 1 I=1,NODEN
      EN(I)=AENO + TN(I,1)*(AEN1 + TN(I,1)*(AEN2 + TN(I,1)*AEN3))
      ES(I)=AESO + TS(I,1)*(AES1 + TS(I,1)*(AEN2 + TS(I,1)*AES3))
      EW(I)=AEWO + TW*(AEW1 + TW*(AEW2 + TW*AEW3))
    1 CONTINUE
      RETURN
      END
      SUBROUTINE EXFCTR(NODEN)
      REAL KN,KS
      COMMON TN(100,2),KN(100),TNAVG(100),TS(100,2),KS(100),TSAVG(100),E
     1N(100),ES(100),EW(100),ANS(100),ASN(100),ASW(100),EFSN(100),EFNS(1
     200),AWS(100),HNS(100),HSW(100),EFSW(100),HSN(100)
      DO 1 I=1,NODEN
      EFNS(I)=(ASN(I)*ES(I)*EN(I))/(ASN(I)*ES(I)+ANS(I)*EN(I)*(1.0-ES(
     1I)))
      EFSW(I)=AWS(I)*EW(I)*ES(I)/(AWS(I)*EW(I)+ASW(I)*ES(I)*(1.0-EW(I)
     1))
    1 CONTINUE
      RETURN
      END
      SUBROUTINE AREAS(PI,RN,RS,L,NODEN,DR,RW)
```

```
      REAL KN,KS,L
      COMMON TN(100,2),KN(100),TNAVG(100),TS(100,2),KS(100),TSAVG(100),E
     1N(100),ES(100),EW(100),ANS(100),ASN(100),ASW(100),EFSN(100),EFNS(1
     200),AWS(100),HNS(100),HSW(100),EFSW(100),HSN(100)
      RNODEN=NODEN
      ANS(1)=2.0*PI*RN*L/(2.0*(RNODEN-1.0))
      ANS(NODEN)=ANS(1)
      JNODEN=NODEN-1
      ASN(1)=2.0*PI*RS*L/(2.0*(RNODEN-1.0))
      ASN(NODEN)=ASN(1)
      ASW(1)=2.0*PI*(RS+DR)*L/(2.0*(RNODEN-1.0))
      ASW(NODEN)=ASW(1)
      ASW(1)=2.0*PI*RW*L/(2.0*(RNODEN=1.0))
      ASW(NODEN)=AWS(1)
      DO 1 I=2,JNODEN
      ANS(I)=2.0*PI*RN*L/(RNODEN-1.0)
      ASN(I)=2.0*PI*RS*L/(RNODEN-1.0)
      ASW(I)=2.0*PI*(RS+DR)*L/(RNODEN-1.0)
      AWS(I)=2.0*PI*RW*L/(RNODEN-1.0)
    1 CONTINUE
      RETURN
      END
      SUBROUTINE HIGH(SIGMA,NODEN,TW)
      REAL KN,KS
      COMMON TN(100,2),KN(100),TNAVG(100),TS(100,2),KS(100),TSAVG(100),E
     1N(100),ES(100),EW(100),ANS(100),ASN(100),ASW(100),EFSN(100),EFNS(1
     200),AWS(100),HNS(100),HSW(100),EFSW(100),HSN(100)
      DO 1 I=1,NODEN
      HNS(I)=EFNS(I)*(SIGMA/144.)*((TN(I,1)+460.)**4-(TS(I,1)+460.)**4)
     1/(TN(I,1)-TS(I,1))
      HSW(I)=EFSW(I)*(SIGMA/144.)*((TS(I,1)+460.)**4-(TW+460.)**4)/(TS
     1(I,1)-TW)
    1 CONTINUE
      RETURN
      END
      SUBROUTINE EMIS2(AEN0,AEN1,AEN2,AEN3,NODEN)
      REAL KN,KS
      COMMON TN(100,2),KN(100),TNAVG(100),TS(100,2),KS(100),TSAVG(100),E
     1N(100),ES(100),EW(100),ANS(100),ASN(100),ASW(100),EFSN(100),EFNS(1
     200),AWS(100),HNS(100),HSW(100),EFSW(100),HSN(100)
      DO 1 I=1,NODEN
      EN(I)=AEN0 + TN(I,2)*(AEN1 + TN(I,2)*(AEN2 + TN(I,2)*AEN3))
    1 CONTINUE
      RETURN
      END
      SUBROUTINE EXFCT2(NODEN)
      REAL KN,KS
      COMMON TN(100,2),KN(100),TNAVG(100),TS(100,2)KS(100),TSAVG(100),E
     1N(100),ES(100),EW(100),ANS(100),ASN(100),ASW(100),EFSN(100),EFNS(1
     200),AWS(100),HNS(100),HSW(100),EFSW(100),HSN(100)
      DO 1 I=1,NODEN
```

```
      EFNS(I)=ASN(I)*ES(I)*EN(I)/(ASN(I)*ES(I)*ANS(I)*EN(I)*(1.0=ES(I))
     1)
      EFSN(I)=ANS(I)*EFNS(I)/ASN(I)
    1 CONTINUE
      RETURN
      END
      SUBROUTINE HIGH2(NODEN,SIGMA)
      REAL KN,KS
      COMMON TN(100,2),KN(100),TNAVG(100),TS(100,2),KS(100),TSAVG(100),E
     1N(100),ES(100),EW(100),ANS(100),ASN(100),ASW(100),EFSN(100),EFNS(1
     200),AWS(100),HNS(100),HSW(100),EFSW(100),HSN(100)
      DO 1 I=1,NODEN
      HSN(I)=EFSN(I)*(SIGMA/144.)*((TS(I,1)+460.)**4-(TN(I,2)+460.)**4)/
     1(TS(I,1)-TN(I,2))
    1 CONTINUE
      RETURN
      END
```

PH-4 Users Guide

Refer to Figure 2-4

A. Input Card 1 FORMAT(4E10.3,I10,E10.3)

1. RNI - minimum or initial susceptor radius to be evaluated (inches).
2. Gap 1 - width of annular gap between the inside wall of the containment tube and the outside of the heat shield (inches).
3. Gap 2 - width of annular gap between the inside wall of the heat shield and the susceptor (inches).
4. LI - minimum or initial susceptor length to be evaluated (inches).
5. NODEN - maximum number of susceptor or heat shield nodes.
6. RO - density of susceptor and heat shield material.

Input Card 2 FORMAT(E10.3)

1. G - control index with a value of 0 or 1. If G = 1, PH-4 does not increment internal heat generation rate values, if G = 0 then PH-4 does increment internal heat generation rate.

Input Card 3 FORMAT(3E10.3)

1. RNMAX - the maximum value of the susceptor radius, RN, for which calculations are made when incrementing the radius (inches).
2. DRMAX - the maximum value of the heat shield thickness, DR, for which calculations are made (inches).
3. LMAX - the maximum value of the susceptor length, L, for which calculations are made (inches).

Input Card 4 FORMAT(3E10.3)

1. DELDR - the amount by which the heat shield thickness, DR, is incremented when it is desirable to cycle calculations as a function of heat shield thickness (inches).
2. DELRN - the amount by which the susceptor radius, RN, is incremented when it is desirable to cycle calculations in terms of a variation in susceptor radius (inches).
3. DELL - the amount by which the susceptor length, L, is incremented when it is desirable to cycle calculations as a function of susceptor length (inches).

Input Card 5 FORMAT(E10.3)

1. DRI - the minimum or initial value for the heat shield thickness.

Input Card 6 FORMAT(I5)

1. MAXIT - the maximum number of iterations which the programmer allows for convergence to a given temperature profile during any one cycle.

Input Card 7 FORMAT(4E10.3)

1. SIGMA - Boltzman's constant equals .1714 x 10^{-8} BTU/hr-ft^2-°R^4.
2. Z1 - convergence criteria for the heat transfer rate at susceptor node 1.
3. Z2 - convergence criteria for the temperature at each susceptor node (See Chapter 3, Equation (3-36).
4. Z3 - convergence criteria for the temperature at each heat shield node.

Input Card 8 FORMAT(4E11.4,2A4)

$KN(T) = ANK0 + ANK1[T] + ANK2[T]^2 + ANK3[T]^3$

KN(T) = thermal conductivity of the susceptor material as a function of temperature, T (KN(T) is a least squares fit to experimental data).

1. ANK0 - zeroth order coefficient
2. ANK1 - 1st order coefficient
3. ANK2 - 2nd order coefficient

4. ANK3 - 3rd order coefficient

5. AMAT1 - signature for the material for which KN(T) is defined e.g. KFE implies thermal conductivity for iron.

Input Card 9 FORMAT(4E11.4,2A4)

$KS(T) = ASK0 + ASK1[T] + ASK2[T]^2 + ASK3[T]^3$

KS(T) = thermal conductivity of the heat shield material as a function of temperature, T.

1. ASK0
2. ASK1
3. ASK2 — definitions analogous to those on Input Card 8
4. ASK3
4. AMAT2

Input Card 10 FORMAT(4E11.4,2A4)

$EN(T) = AEN0 + AEN1[T] + AEN2[T]^2 + AEN3[T]^3$

EN(T) = the temperature dependent emissivity of the susceptor body surface.

1. AEN0
2. AEN1
3. AEN2
4. AEN3

See Input Card 8

5. AMAT3 - signature of the material for which EN(T) is defined e.g. EAU implies the thermal emissivity for stainless steel.

Input Card 11 FORMAT(4E11.4,2A4)

$ES(T) = AES0 + AES1[T] + AES2[T]^2 + AES3[T]^3$

ES(T) = the temperature dependent emissivity of the heat shield surface.

1. AES0
2. AES1
3. AES2 — See Input Card 10
4. AES3
5. AMAT4

Input Card 12 FORMAT(4E11.4,2A4)

$EW(T) = AEW0 + AEW1[T] + AEW2[T]^2 + AEW3[T]^3$

EW(T) = the temperature dependent emissivity of the containment tube wall surface.

1. AEW0
2. AEW1
3. AEW2 — See Input Card 10
4. AEW3
5. AMAT5

Input Card 13 FORMAT(4E11.4)

1. TW - containment tube wall temperature (°F).
2. TN1 - susceptor base node temperature (°F).
3. TS1 - heat shield base node temperature (°F).
4. QGENI - the initial or minimum value of the internal heat generation rate (watts/gm).

Input Card 14 FORMAT(E10.3)

1. QGENS - internal heat generation rate in the heat shield (watts/gm)

Input Card 15 FORMAT(4E10.3)

1. QGENM - the maximum value or upper limit of internal heat generation rates for which a calculation is made when incrementing the heat generation rate (watts/gm).
2. DELQG - the increment size by which changes are made in the internal heat generation rate (watts/gm).
3. GAPMAX - the maximum value of the annular gap spacings, GAP 1 and GAP 2 when incrementing the gap size between cycles (inches).
4. DELGAP - the increment size by which changes are made in the gap spacings (inches).

Input Card 16 FORMAT(7E11.4)

1. TN(I,1) - the initial temperature guess for each susceptor node, NODEN-1 in number, skips the first node (°F).

Input Card 17 FORMAT(2E11.4)

1. QCN(1) - the initial heat conduction guess for conduction from the first node at the susceptor base (BTU/hr).
2. QCS(1) - the initial guess for the heat conducted from node 1 in the heat shield (BTU/hr).

Input Card 18 FORMAT(7E11.4)

1. TS(I,1) - the initial temperature guess for each heat shield node, NODEN-1 in number, skips the first node (°F).

B. Output Characters

Output data is labeled for ease of interpretation. Output characters or symbols are identified in the following list.

1. RSN - outside radius of the heat shield.
2. RW - inside radius of the containment tube.
3. HNS(I) - the convection-like radiation heat transfer coefficient for heat transfer from the susceptor to the heat shield Equation (3-29).
4. HSN(I) - the convection-like radiation heat transfer coefficient for heat transfer from the heat shield to the susceptor.
5. HSW(I) - the convection-like radiation heat transfer coefficient for heat transfer from the heat shield to the containment tube wall.
6. EFNS(I) - the radiation "exchange factor" for radiation heat transfer from the susceptor to the heat shield, Equation (3-30).
7. EFSN(I) - the radiation "exchange factor" for radiation heat transfer from the heat shield to the susceptor, Equation (3-30).

8. EFSW(I) - the radiation "exchange factor" for radiation heat transfer from the heat shield to the containment tube wall, Equation (3-30).

9. QR - the total heat radiated from the susceptor (the summation overall body nodes) (BTU/hr).

10. PCTRC - the ratio of QR to QCN(1) times 100, the percent of total heat radiated from the susceptor body relative to the total heat conducted from the susceptor base.

11. PCTRQG - see PH-3 Users Guide B.8

12. QTOT - the sum of the absolute values of QR and QCN(1) (BTU/hr).

13. DEVQS - see PH-3 Users Guide B.6

14. PCTRQT - see PH-3 Users Guide B.9

15. QGENT - see PH-3 Users Guide B.10

16. ITERAT - the number of iterations required for convergence.

Generation III Program

Listing of PH-5

```
C         I-D HT. HFR IN A PIN FIN RADIATION CHARACTERIZED AS CONVECTION
C         TEMP PEPENDENT K AND ENISSIVITIES
          REAL L,K,MAXRN
          DIMENSION TN(100,2),AWR(100),ANR(100),EF(100),K(100),QC(2),EN(100)
         1,EW(100),C1(100),C2(100),C3(100),C4(100),HN(100),TAVG(100),AMAT1(2
         2),AMAT2(2),AMAT3(2)
          COMMON TN,AWR,ANR,EF,K,QC,EN,EW,C1,C2,C3,C4,HN,TAVG,AMAT2,AMAT1,
         1AMAT3,TB,AB,CII(21),C(21,21),E(21),R(21),EMAT(21),Q(11),
         2TT(22,22)
          READ(5,1) RNI,L,NODEN,MAXRN,RO
        1 FORMAT(2E10.3,I10,2E10.3)
          READ(5,914) QGENM,DELQG
      914 FORMAT(2E10.3)
          READ(5,500) MAXIT
      500 FORMAT(I5)
          READ(5,2) SIGMA,Z1,Z2
        2 FORMAT(3(E11.4))
          READ(5,40) AKO,AK1,AK2,AK3,AMAT1
       40 FORMAT(4E11.4,2A4)
          READ(5,40) AENO,AEN1,AEN2,AEN3,AMAT2
          READ(5,40) AEWO,AEW1,AEW2,AEW3,AMAT3
          READ(5,40) TF,T1,TB,QGEN
          READ(5,40) AB
      300 READ(5,3) (TN(I,1),I=2,NODEN)
        3 FORMAT(6E12.5)
          READ(5.41)QC(1)
       41 FORMAT(E11.4)
          READ(5,700)(CII(I),I=1,21)
      700 FORMAT(7E11.4)
          READ(5,705)((C(I,J),J=1,21),I=1,21)
      705 FORMAT(7E11.4)
          RN=RNI
      905 CONTINUE
          RW=RN+.020
          M=1
          TN(1,1)=T1
          TN(1,2)=T1
          PI=3.1415
          WRITE(6,4)
        4 FORMAT(16X,'DATA',9X,'CONVERGENCE CRITERIA',6X,'GEOMETRY',//)
          WRITE(6,913)RNI
      913 FORMAT(53X,'RNI=',E11.4)
          WRITE(6,5)Z1,RN
        5 FORMAT(33X,'Z1=',E11.4,7X,'RN=',E11.4)
          WRITE(6,6)Z2,RW
```

```
  6 FORMAT(33X,'Z2,E11.4,7X,'RW=',E11.4)
    WRITE(6,7)L,QGEN
  7 FORMAT(13X,'L=',E11.4,28X,'QGEN=',E11.4,///)
    WRITE(6,912)QGENM,DELQG
912 FORMAT(53X,'QGENM=',E11.4,2X,'DELQG=',E11.4)
    WRITE(6,8)T1
  8 FORMAT(28X,'N',1X,'INITIAL TEMP(N)',//28X,'1',3X,E10.3)
    DO 10 I=2,NODEN
    WRITE(6,9)I,TN(I,1)
  9 FORMAT(27X,I2,3X,E11.4)
 10 CONTINUE
    WRITE(6,11)TF
 11 FORMAT(27X,'TF',3X,E11.4,///)
    WRITE(6,603)AKO,AK1,AK2,AK3,AMAT1
603 FORMAT(6X,'THERMAL CONDUCTIVITY DATA',//,6X,4E11.4,2X,2A4)
    WRITE(6,604)AENO,AEN1,AEN2,AEN3,AMAT2
604 FORMAT(6X,'SUCCEPTOR EMISSIVITY DATA',//,6X,4E11.4,2X,2A4)
    WRITE(6,605)AEWO,AEW1,AEW2,AEW3,AMAT3
605 FORMAT(6X,'WALL EMISSIVITY DATA',//,6X,4E11.4,2X,2A4)
    JNODEN=NODEN-1
    RNODEN=NODEN
600 CALL THERMK(AKO,AK1,AK2,AK3,T1,TN,K,NODEN,TAVG)
    CALL SEMIS(AENO,AEN1,AEN2,T1,TN,EN,NODEN)
    CALL WEMIS(AEWO,AEW1,AEW2,TF,EW,NODEN)
    CALL AREARD(PI,RW,RN,L,AWR,ANR,NODEN)
    CALL EXFCTR(AWR,ANR,EN,EW,EF,NODEN)
    CALL HIGH(EF,SIGMA,TN,TF,HN,NODEN,T1)
    DO 601 I=1,JNODEN
    C1(I)=L/((RNODEN-1.)*(K(I)/12.0)*PI*RN**2)
    C2(I)=1.0/C1(I)
601 CONTINUE
    RADIATIVE RESISTANCE
    DO 12 I=2,JNODEN
    C3(I)=(RNODEN-1.0)/(HN(I)*2.0*PI*RN*L)
    C4(I)=1.0/C3(I)
 12 CONTINUE
    C3(1)=(RNODEN-1.0)/(HN(1)*PI*RN*L)
    C3(NODEN)=(RNODEN-1.0)/(HN(NODEN)*PI*RN*L)
    C4(NODEN)=1.0/C3(NODEN)
    QC(2)=-((TN(2,1)-T1(/C1(1)+(TF-T1)/C3(1)+(QGEN*55.95*RO*PI*RN
   1**2)*L/(2*(RNODEN-1.0)))
    DO 13 I=3,JNODEN
    TN(I,2)=(TN(I-1,1)/C1(I-1)+TN(I+1,1)/C1(I)+TF/C3(I)+QGEN*55.95*R
   10*PI*RN**2*L/(RNODEN-1.0))/(C2(I-1)+C2(I)+C4(I))
 13 CONTINUE
    TN(2,2)=(T1/C1(1)+TN(3,1)/C1(2)+TF/C3(2)+QGEN*55.95*RO*PI*RN**
   12*L/(RNODEN-1.0))/(C2(1)+C2(2)+C4(2))
    TN(NODEN,2)=(TN(JNODEN,1)/(C1(JNODEN)+TF/C3(NODEN)+QGEN*55.95*RO*
   1PI*RN**2*L/(2.0*(RNODEN-1.0)))/(C2(JNODEN)+C4(NODEN))
    IF(ABS(QC(2)-QC(1)).GT.Z1) GO TO 27
    DO 14 I=2,NODEN
    IF(ABS(TN(I,2)-TN(I,1)).GT.Z2) GO TO 27
 14 CONTINUE
    QR=0.0
```

```
      SUM=HN(1)*ANR(1)*(T1-TF)
      DO 15 I=2,NODEN
      QR=QR+HN(I)*ANR(I)*(TN(I,1)-TF)
   15 CONTINUE
      QR=QR+SUM
      QTOT=ABS(QR)+ABS(QC(1))
      PCTRC=(QR/QC(1))*100.
      VOL=PI*RN**2*L
      QGENT=QGEN*55.95*RO*VOL
      PCTRQG=(QR/QGENT)*100.
      PCTRQT=(QR/QTOT)*100.
      DEVQS=QTOT-(QGEN*VOL*55.95*RO)
      ITERAT=M
      WRITE(6,16)
   16 FORMAT(33X,'CONCLUSIONS',/,23X,'N',4X,'HN(N)',14X,'TEMP(N)',//)
      WRITE(6,17)HN(1),T1
   17 FORMAT(23X,'1',1X,E10.3,8X,E11.4)
      DO 19 I=2,NODEN
   18 FORMAT(22X,I2,1X,E10.3,8X,E11.4)
   19 CONTINUE
      WRITE(6,20)QC(1),QR
   20 FORMAT(1X,//,22X,'QC=',E10.3,6X,'QR=',E10.3)
      WRITE(6,21)QTOT,DEVQS
   21 FORMAT(20X,'QTOT=',E10.3,3X,'DEVQS=',E10.3)
      WRITE(6,22)RN,PCTRC,PCTRQG
   22 FORMAT(22X,'RN=',E10.3,3X,'PCTRC=',E10.3,3X,'PCTRQG=',E10.3)
      WRITE(6,610)PCTRQT
  610 FORMAT(38X,'PCTRQT=',E10.3)
      WRITE(6,800)QGENT
  800 FORMAT(38X,'QGENT=',E10.3)
      WRITE(6,26)M
   26 FORMAT(2X,'ITERATIONS=',I4)
      WRITE(6,900)MAXRN
  900 FORMAT(10X,'MAXRN=',E11.4)
      WRITE(6,803)(E(I),I=1,21)
  803 FORMAT(1H1,10X,'E(I)=',(7(E11.4,','),/1HO,10X))
      WRITE(6,801)(TT(I,1),I=2,22)
  801 FORMAT(1HO,10X,'TT(I+1,1)=',(7(E11.4,','),/1HO,10X))
      WRITE(6,802)(Q(I),I=1,11)
  802 FORMAT(1HO,10X,'Q(I)=',(6(E11.4,','),/1HO,10X))
      GO TO 24
   27 CONTINUE
      IF(M.GT.MAXIT) GO TO 25
      M=M+1
      QC(1)=QC(2)
      DO 100 I=2,NODEN
      TN(I,1)=TN(I,2)
  100 CONTINUE
      GO TO 600
   24 CONTINUE
      IF(RN.GT.MAXRN) GO TO 25
      RN=RN+.020
      DO 906 I=2,NODEN
      TN(I,1)=TN(I,2)
```

```
906 CONTINUE
    GO TO 905
 25 CONTINUE
    DO 910 I=2,NODEN
    TN(I,1)=TN(I,2)
910 CONTINUE
    RN=RNI
    QGEN=QGEN+DELQG
    IF(QGEN.LT.QGENM) GO TO 905
911 STOP
    END
    SUBROUTINE THERMK(AKO,AK1,AK2,AK3,T1,TN,K,NODEN,TAVG)
    DIMENSION TN(NODEN,1),K(NODEN),TAVG(NODEN)
    REAL K
    JNODEN=NODEN-1
    TAVG(1)=(TN(2,1)+T1)/2.0
    DO 1 I=2,JNODEN
    TAVG(I)=(TN(I+1,1)+TN(I,1))/2.0
  1 CONTINUE
    K(1)=AKO+TAVG(1)*(AK1+TAVG(1)*(AK2+AK3*TAVG(1)))
    DO 2 I=2,JNODEN
    K(I)=AKO,TAVG(I)*AK1+TAVG(I)*(AK2 + AK3*TAVG(I)))
  2 CONTINUE
    RETURN
    END
    SUBROUTINE SEMIS(AENO,AEN1,AEN2,T1,TN,EN,NODEN)
    DIMENSION TN(NODEN,1),EN(NODEN)
    EN(1)=AENO + T1*(AEN1 + T1*AEN2)
    DO 1 I=2,NODEN
    EN(I)=AENO + TN(1,1)*(AEN1 + TN(1,1)*AEN2)
  1 CONTINUE
    RETURN
    END
    SUBROUTINE WEMIS(AEWO,AEW1,AEW2,TF,EW,NODEN)
    DIMENSION EW(NODEN)
    EW(1)=AEWO + TF*(AEW1 + TF*AEW2)
    DO 1 I=2,NODEN
    EW(I)=EW(1)
  1 CONTINUE
    RETURN
    END
    SUBROUTINE AREARD(PI,RW,RN,L,AWR,ANR,NODEN)
    DIMENSION AWR(NODEN),ANR(NODEN)
    REAL L
    RNODEN=NODEN
    ANR(1)=2.0*PI*RN*L/(2.*(RNODEN-1.0))
    ANR(NODEN)=ANR(1)
    AWR(1)=2.0*PI*RW*L/(2.*(RNODEN-1.0))
    AWR(NODEN)=AWR(1)
    JNODEN=NODEN-1
    DO 1 I=2,JNODEN
    ANR(I)=2.0*PI*RN*L/(RNODEN-1.)
    AWR(I)=2.0*PI*RW*L/(RNODEN-1.0)
```

```
      1 CONTINUE
        RETURN
        END
        SUBROUTINE EXFCTR(AWR,ANR,EN,EW,EF,NODEN)
        DIMENSION EN(NODEN),EW(NODEN),EF(NODEN),AWR(NODEN),ANR(NODEN)
        DO 1 I=1,NODEN
        EF(I)=AWR(I)*EW(I)*EN(I)/(AWR(I)*EW(I)+ANR(I)*EN(I)*(1.0-EW(I))
       1)
      1 CONTINUE
        RETURN
        END
        SUBROUTINE HRAD(SIGMA,TF,NODEN,T1)
        DIMENSION TN(100,2),AWR(100),ANR(100),EF(100),K(100),QC(2),EN(100)
       1,EW(100),C1(100),C2(100),C3(100),C4(100),HN(100),TAVG(100),AMAT1(2
       2),AMAT2(2),AMAT3(2)
        COMMON TN,AWR,ANR,EF,K,QC,EN,EW,C1,C2,C3,C4,HN,TAVG,AMAT2,AMAT1,
       1AMAT3,TB,AB,CII(21),C(21,21),E(21),R(21),EMAT(21),Q(11),
       2TT(22,22)
C       CALCULATING THE BODY EMISSIVE POWER
        E(1)=(SIGMA/144.)*(TB+460.)**4
        E(2)=(SIGMA/144.)*(T1+460.)**4
        DO 1 I=3,11
        E(I)=(SIGMA/144.)*(TN(I-1,1)+460.)**4
      1 CONTINUE
        DO 2 I=12,21
        E(I)=(SIGMA/144.)*(TF+460.)**4
      2 CONTINUE
C       CALCULATION OF BODY RESISTANCE
        EB=EN(1)
        R(1)=(1.0-EN(1))/(AB*EN(1))
        R(2)=(1.0-EN(1))/(ANR(1)*EN(1))
        DO 3 I=3,11
        R(I)=(1.0-EN(I-1))/(ANR(I-1)*EN(I-1))
      3 CONTINUE
        DO 4 I=12,21
        R(I)=(1.0-EW(I-11))/(AWR(I-11)*EW(I-11))
      4 CONTINUE
C       CALCULATING COLUMN MATRIX EMAT
        DO 5 I=1,21
        EMAT(I)=-E(I)/R(1)
      5 CONTINUE
C       ADJUSTING MAIN DIAGONAL OF C MATRIX FOR TEMP VARIATION
        DO 6 I=1,21
        C(I,I)=CII(I)-1.0/R(I)
      6 CONTINUE
        CALL SIMEQ(C,EMAT,21,TT)
        DO 7 I=1,11
        Q(I)=(E(I)-TT(I+1,1))/R(I)
      7 CONTINUE
        HN(1)=Q(2)/(ANR(1)*(T1-TF))
        DO 8 I=2,10
        HN(I)=Q(I+1)/(ANR(I)*(TN(I,1)-TF))
```

```
    8 CONTINUE
      RETURN
      END
      SUBROUTINE SIMEQ(C,D,N,TT)
C     C=COEFFICIENT MATRIX OF ORDER N (SQUARE)
C     D=CONSTANT VECTOR
C     TT=SOLUTION MATRIX (SOLUTIONS IN FIRST COLUMN)
      DIMENSION C(21,21),D(21),CI(22,22),TN(22,22),T(22,22),TT(22,22)
      DO 10 I=1,22
      DO 10 J=1,22
      CI(I,J)=0.
   10 CONTINUE
C     GENERATE IDENTITY MATRIX CI
      NP=N+1
      DO 100 I=1,NP
  100 CI(I,1)=1.
      CALL MEQ(CI,T,NP,NP)
C     ASSEMBLING MATRIX T
      DO 200 I=1,N
      CALL MEQ(CI,TN,NP,NP)
      K=I+1
      DO 300 J=2,NP
  300 TN(K,J)=-C(I,(J-1))/C(I,I)
      TN(K,K)=0.
      TN(K,1)=D(I)/C(I,I)
      CALL MULT(TN,NP,NP,T,NP,NP,TT)
      CALL MEQ(TT,T,NP,NP)
  200 CONTINUE
C     MULTIPLICATIONS ARE ITERATED TO 2**NN
      NN=20
      DO 400 KM=1,NN
      KOUT=KM
      CALL MULT(T,NP,NP,T,NP,NP,TT)
C     USING A TOLERANCE OF 1.*10**-05
      SUM=0.0
      DO 500 K2=2,NP
      IF(ABS(T(K2,1)).LT.L.E-30) GO TO 500
      SUM=SUM+ABS((TT(K2,1)-T(K2,1)/T(K2,1)
  500 CONTINUE
      IF(SUM.LF.1.E-10) GO TO 600
      CALL MEQ(TT,T,NP,NP)
  400 CONTINUE
  600 CONTINUE
      WRITE(6,700)KOUT
  700 FORMAT(1HO,10X,'***** THE NUMBER OF ITERATIONS IS = ',I2)
      RETURN
      END
      SUBROUTINE MULT(A,NVA,NNA,B,NNB,NEB,C)
      DIMENSION A(22,22),B(22,22),C(22,22)
C     C=A*B
      IF(NNA.NE.NNB) GO TO 400
      DO 300 I=1,NVA
      DO 200 J=1,NEB
      CSUM=0.
      DO 100 K=1,NNA
```

```
      CSUM=CSUM+A(I,K)*B(K,J)
  100 CONTINUE
      C(I,J)=CSUM
  200 CONTINUE
  300 CONTINUE
      RETURN
  400 CONTINUE
      WRITE(6,6000)
 6000 FORMAT(1H,5X,'MATRIX A AND B ARE NOT CONFORMABLE')
      RETURN
      END
      SUBROUTINE MEQ(A,B,NV,NE)
      DIMENSION A(22,22),B(22,22)
C     B=A
      DO 200 J=1,NE
      DO 100 I=1,NV
      B(I,J)=A(I,J)
  100 CONTINUE
  200 CONTINUE
      RETURN
      END
```

PH-5 Users Guide

Refer to Figures 2-5 and 5-7

A. Input Data

Input Card 1 — PH-3 Users Guide

Input Card 2 — PH-3 Users Guide

Input Card 3 — PH-3 Users Guide

Input Card 4 — PH-3 Users Guide

Input Card 5 — PH-3 Users Guide

Input Card 6 — PH-3 Users Guide

Input Card 7 — PH-3 Users Guide

Input Card 8 — PH-3 Users Guide

Input Card 9 — FORMAT(E11.4)

1. AB - area of the base ring of the calorimeter (see Figure 2-3).

Input Card 10 — PH-3 Users Guide, Input Card 9

Input Card 11 — PH-3 Users Guide, Input Card 10

Input Card 12 — FORMAT(7E11.4)

1. CII(I) - the main diagonal terms from the coefficient matrix in Equation (5-7), see Equations (5-7.7) to (5-7.27).

Input Card 13 — FORMAT(7E11.4)

1. C(I,J) - the elements of the coefficient matrix in Equation (5-7), exclusive of the main diagonal terms (see Equations (5-7.1) to (5-7.6) and Input Card 12).

B. Output Characters

See the output characters and symbols of the PH-3 Users Guide.

1. E(I) - the radiation body emissive power (BTU/hr-in^2) where E(1) is the emissive power of the calorimeter base ring Figure 2-3, E(2) through E(11) are the emissive powers of the susceptor nodes, E(12) through E(21) are the emissive powers of the containment tube wall nodes.

2. TT(I,1) - the column and containment tube wall nodes radiosity values. See Equations (5-6) and (5-7). The first output radiosity is for the base ring node; the second through the eleventh are for the first ten susceptor nodes respectively; and the twelfth through twenty-first are for the first through tenth containment tube wall nodes respectively.

3. Q(I) - the heat radiation rate in each network branch joining a body node to a surface node in Figure 5-7. Q(1) is the radiation rate in the base ring branch; Q(2) through Q(11) is the radiation rate in the first through the tenth susceptor branches respectively, and Q(12) through Q(21) is

the radiation rate in the first through the tenth containment tube wall branches respectively. (BTU/hr) (See Equation 5-8, $\dot{q}_{rad}$).

APPENDIX F

Radiation Shape Factors and Properties[23]

The simplicity of the radiation exchange between parallel planes such that all of the radiation leaving one body strikes the other is seldom encountered in actual engineering applications. It is often necessary to consider the general case of finite surfaces which are not parallel and which are exchanging radiant energy. The surfaces are generally not plane and other surfaces may be present which can interfere with or aid the net exchange of energy.

The type of situation described above arises in the analysis of the modeling error, Chapter 5. The subroutine HRAD is generated from an analysis which requires shape factors for complex geometries.

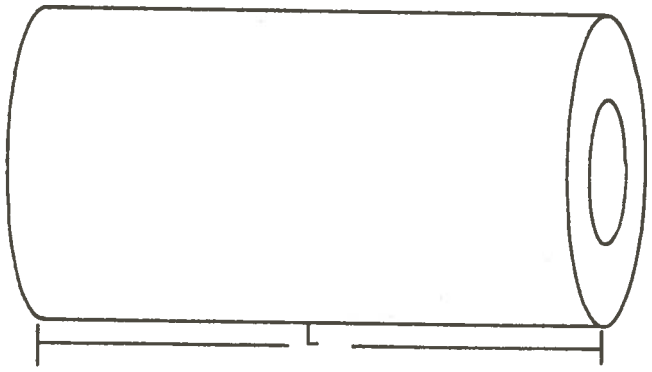

FIGURE F-1

Finite Length Cylinders

One such geometry is the one pictured in Figure F-1; there exists a closed form analytic expression for the shape factors relating the radiation exchange between two finite length cylinders with the smaller concentrically located within the larger. Radiation is exchanged between the outside wall of the inner cylinder and the inside wall of the outer cylinder. See reference 24. for the closed form analytic expression.

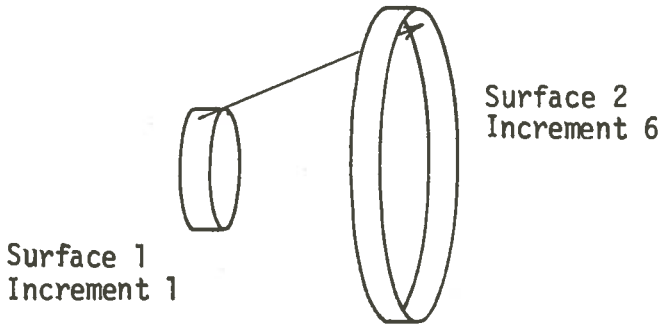

FIGURE F-2
Radiation Exchange Between Increment Length Cylinders

The other geometry encountered, Figure F-2 has no readily available closed form expression for generating the shape factors for radiation exchange between the outside of surface one and the inside of surface two. It is necessary to use the properties of shape factors, for example, the reciprocal property, the additive property, and the enclosure property, to derive the expressions needed. For simplicity the description of the opposing surfaces is of the form in Figure F-3, with reference to Figure F-2.

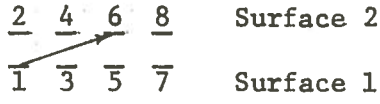

Figure F-3

The rings are depicted as one-dimensional opposing surfaces. Odd numbers 1, 3, 5, 7 .... denote adjacent inner rings on surface 1 and even numbers 2, 4, 6,.... denote the adjacent outer rings of surface 2. The shape factor F_{1-2}, Figure F-4, comes

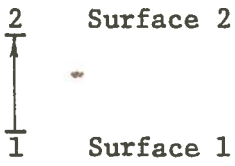

Figure F-4

from the closed form analytic expression previously referred to.

For the four body problem, Figure F-5:

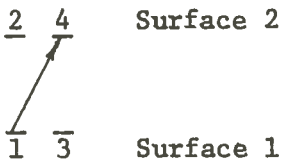

Figure F-5

$$F_{1-4} = \frac{F_{1,2-2,4} - 2F_{1-2}}{2},$$

where the presumption is that the areas of adjacent surfaces 1, 3, 5,.... are of equal size; that is body surfaces, one and two are divided into equal length increments.

Six body problem:

$$F_{1-6} = \frac{3F_{(1,3,5)-(2,4,6)} - 4F_{(1,3)-(2,4)} - F_{1-2}}{2}$$

Eight body problem:

$$F_{1-8} = \frac{1}{2}\left[2\,F_{(1,3,5,7)-(2,4,6,8)} - 3\,F_{(1,3,5)-(2,4,6)} + F_{(1,3)-(2,4)}\right]$$

Ten body problem:

$$F_{1-10} = \frac{1}{2}\left[5\,F_{(1,3,5,7,9)-(2,4,6,8,10)} - 8\,F_{(1,3,5,7)-(2,4,6,8)} + 3\,F_{(1,3,5)-(2,4,6)}\right]$$

n body problem:

$$F_{(1)-(2n)} = \frac{1}{2}\left[nF_{(1,3,5,\ldots.2n-1)-(2,4,6,\ldots.,2n)} - (2n-2)F_{(1,3,5,\ldots.,2n-3)-(2,4,6,\ldots.,2n-2)} + (n-2)F_{(1,3,5,\ldots.,2n-5)-(2,4,6,\ldots.,2n-4)}\right]$$

APPENDIX G

Parameter Tables

Table G-1

Limiting Case Comparison to Reduced Emissivities

Parameter	Symbol	PH-1	PH-2
Susceptor material	SS	Stainless steel	Stainless steel
Susceptor radius	RN	0.26"	0.11"
Heat shield inside radius	RS	--	0.22"
Heat shield thickness	DR	--	0.040"
Containment tube inside radius	RW	0.355"	0.355"
Susceptor length	L	1.0"	1.0"
Susceptor thermal conductivity	KN	13.5 BTU/hr ft°F	13.5 BTU/hr ft°F
Heat shield thermal conductivity	KS	13.5 BTU/hr ft°F	13.5 BTU/hr ft°F
Susceptor emissivity	EN	1.0×10^{-36}	1.0×10^{-36}
Heat shield emissivity	ES	--	1.0×10^{-36}
Containment tube emissivity	EW	1.0×10^{-36}	1.0×10^{-36}
Susceptor base temperature	TN1	752°F	752°F
Heat shield base temperature	TS1	--	750°F
Containment tube temperature	TW	740°F	740°F
Internal heat generation rate	QGEN	3.0 watts/gm	3.0 watts/gm
Number of node in geometry	NODEN	6 (axial)	6 (axial)

Table G-2

PH-1 Comparison to THTB
(Solid Susceptor Configuration)

Parameter	Symbol	PH-1	THTB
Susceptor internal	SS	stainless steel	stainless steel
Susceptor radius	RN	0.26"	0.26"
Containment tube inside radius	RW	0.355"	0.355"
Susceptor length	L	1.0"	1.0"
Susceptor thermal conductivity	KN	13.5 BTU/hr ft°F	See Appendix C
Susceptor emissivity	EN	.21	See Appendix C
Containment tube emissivity	EW	.21	See Appendix C
Susceptor base temperature	TN1	750°F	750°F
Containment tube temperature	TW	740°F	740°F
Internal heat generation rate	QGEN	3.0 watts/gm	3.0 watts/gm
Number of nodes used in analysis	NODEN	6 (axial) Fig. 3-6	20 (axial and 10 radial) (200 nodes)

Table G-3

PH-2 Comparison to THTB
(Heat Shielded Configuration)

Parameter	Symbol	PH-2	THTB
Susceptor material	SS	stainless steel	stainless steel
Susceptor radius	RN	0.11"	0.11"
Heat shield inside radius	RS	0.22"	0.22"
Heat shield thickness	DR	0.040"	0.040"
Susceptor length	L	1.0"	1.0"
Susceptor thermal conductivity	KN	13.5 BTU/hr ft°F	See Appendix C
Heat shield thermal conductivity	KS	13.5 BTU/hr ft°F	See Appendix C
Susceptor emissivity	EN	0.21	See Appendix C
Heat shield emissivity	ES	0.21	See Appendix C
Containment tube emissivity	EN	0.21	See Appendix C
Susceptor base temperature	TN1	752°F	752°F
Heat shield base temperature	TS1	750°F	750°F
Containment tube temperature	TW	740°F	740°F
Internal heat generation rate	QGEN	3.0 watts/gm	3.0 watts/gm
Number of nodes	NODEN	6 (axial) Fig. 3-7	20 axial and 10 radial (200 nodes)

Table G-4

Model Data for Comparison Run Number One
High vs. HRAD

Parameter	Value or description
Configuration A	solid susceptor
Material	stainless steel
Containment tube inside radius, RW	0.23"
Susceptor length, L	0.90"
Annular gap, Gap 1	0.02"
Susceptor radius, RN	0.21"
Susceptor thermal conductivity, KN	stainless steel (See Appendix C)
Susceptor emissivity, EN	stainless steel (See Appendix C)
Containment tube emissivity, EW	stainless steel (See Appendix C)
Susceptor base temperature, T1	752°F
Containment tube temperature, TW	740°F
Internal heat generation rate, QGEN	3.75 watts/gm

Table G-5

Model Data for Comparison Run Number Two
HIGH vs. HRAD

Parameter	Value or description
Configuration A	solid susceptor
Material	stainless steel
Containment tube inside radius, RW	0.23"
Susceptor length, L	0.90"
Annular gap, Gap 1	0.02"
Susceptor radius, RN	0.21"
Susceptor thermal conductivity, KN	stainless steel (See Appendix C)
Susceptor emissivity, EN	gold (See Appendix C)
Containment tube emissivity, EW	gold (See Appendix C)
Susceptor base temperature, T1	752°F
Containment tube temperature, TW	740°F
Internal heat generation rate, QGEN	3.75 watts/gm

Table G-6

Shape Factors and Areas for HRAD
(Figure 5-7)

$F_{1'-B} = .183$

$F_{2'-B} = .049$

$F_{1-B} = .153$

$F_{1-1'} = .694$

$F_{1-2'} = .150$

$F_{1-3'} = 0.0$

$F_{2-B} = .008$

$F_{2-1'} = .075$

$F_{2-2'} = .835$

$F_{2-3'} = .081$

$F_{2-4'} = .002$

$F_{3-1'} = .002$

$F_{3-5'} = F_{4-2'} = F_{5-3'} = F_{6-4'} = F_{7-5'} = F_{8-6'} = F_{9-7'}$
$= F_{4-6'} = F_{5-7'} = F_{6-8'} = F_{7-9'} = .002$

$F_{3-2'} = F_{3-4'} = F_{4-5'} = F_{5-6'} = F_{6-7'} = F_{7-8'} = F_{8-9'}$
$= F_{4-3'} = F_{5-4'} = F_{6-5'} = F_{7-6'} = F_{8-7'} = F_{9-8'} = .081$

$F_{3-3'} = F_{4-4'} = F_{5-5'} = F_{6-6'} = F_{7-7'} = F_{8-8'} = F_{9-9'} = .835$

$F_{8-10'} = .002$

$F_{9-10'} = .075$

$F_{9-10'm} = .006$

$F_{10-10'} = .694$

Table G-6 (Continued)

Shape Factors and Areas for HRAD

$F_{10-10'm} = .14$

$F_{10-9'm} = .009$

$F_{10-9'} = .15$

$F_{10-8'} = 0.0$

$A_B = .0276\ in^2$

$A_1 = A_{10} = A_{10m} = .0593$

$A_2 = A_3 = ...= A_9 = .1187$

VITA

P. Nelson English was born in Pasadena, Texas on June 27, 1943. He was raised in South Louisiana where he attended Buras High School. He graduated in 1961. He entered Louisiana State University in 1961 and finally received his Bachelor of Science in Engineering Science from LSU in December 1972. In 1974 he entered a Graduate program in the Department of Nuclear Science at Louisiana State University. At present he is a candidate for the degree of Master of Science in Nuclear Engineering.

P. Nelson English is married to the former Leslie H. Bloomenstiel, and is the father of a daughter, Jhan Elayne English.